WATERBORNE EPOXY RESIN MODIFIED BITUMEN EMULSION AS A HIGH-PERFORMANCE COLD PAVING BINDER: WORKING MECHANISM AND ENGINEERING PERFORMANCE

RUI LI

PhD

The Hong Kong Polytechnic University

2021

The Hong Kong Polytechnic University
Department of Civil and Environmental Engineering

Waterborne Epoxy Resin Modified Bitumen Emulsion as A High-Performance Cold Paving Binder: Working Mechanism and Engineering Performance

Rui Li

A thesis submitted in partial fulfilment of the requirements for the degree of Doctor of Philosophy

February, 2021

CERTIFICATE OF ORIGINALITY

I hereby declare that this thesis is my own work and that, to the best of my knowledge and belief, it reproduces no material previously published or written, nor material that has been accepted for the award of any other degree or diploma, except where due acknowledgement has been made in the text.

______________(Signed)
___Rui Li_____(Name of student)

To my parents

ABSTRACT

Asphalt pavement is the major type of pavement worldwide for its various advantages, such as driving comfortability, low noise and ease of maintenance. However, the production and construction of conventional hot-mix asphalt (HMA) must be conducted at high temperature, leading to significant energy consumption and potential hazardous emissions. To address the environmental concerns of HMA, bitumen emulsion can be applied as a cold binder in place of asphalt cement, because its viscosity is low enough at ambient temperature to achieve good workability. Nevertheless, bitumen emulsion faces the major concern of poor mechanical performance especially at high service temperatures. Recently, waterborne epoxy resin has emerged as a promising high-performance modifier which can significantly improve the mechanical performance of bitumen emulsion, while maintaining its advantage of ambient temperature construction. However, the modification mechanism of waterborne epoxy resin and its effects on the microstructure, rheology, aging, and fatigue of bitumen emulsion have not been fully understood yet. To fill this gap, this study aims to investigate the modification mechanism of waterborne epoxy resin and comprehensively evaluate its effects on the performances of bitumen emulsion.

To achieve the objectives of this study, a waterborne curing agent for epoxy resin was first synthesized in lab, which was then used to prepare the waterborne epoxy resin emulsion. The waterborne epoxy resin emulsion was subsequently mixed with bitumen emulsion in various percentages to produce the waterborne epoxy resin modified bitumen emulsions (WEMBEs), and the waterborne epoxy resin modified bitumen emulsion residues (WEBERs) were obtained after the drying process. Finally, comprehensive laboratory tests and constitutive modelling were conducted to characterize the properties of both WEMBEs and WEBERs, followed by a case study to demonstrate the performance of WEMBE as a tack coat material.

The characterization tests conducted on the WEMBEs mainly include the confocal laser scanning microscopy (CLSM) test, zeta potential test, and viscosity test, which evaluates the morphology, stability, and viscosity properties of the WEMBEs, respectively. It was found that stability of bitumen emulsion was not affected by waterborne epoxy resin. All bitumen emulsions showed shear-thinning behavior within the low shear rate range (0-10 s^{-1}). But within the high shear rate range (10-200 s^{-1}), the pure bitumen emulsion behaved like a Newtonian fluid, while WEMBE showed shear-thickening behavior.

To evaluate the performance of the WEBERs, the CLSM test, dynamic shear rheometer (DSR) test, pressure aging vessel (PAV) test, time-sweep and linear amplitude sweep (LAS) tests, boiling test, and bond strength test were conducted to characterize the distribution of waterborne epoxy resin in bitumen, the rheological properties, aging performance, fatigue performance and moisture susceptibility of the WEBERs, and the bonding between the WEMBEs and aggregate, respectively. The results indicated that the cured waterborne epoxy resin formed an inter-connected polymer-rich film when the waterborne epoxy resin content reached 3wt%. Such structure can dramatically improve the high temperature performance, fatigue resistance, aging resistance, adhesion with aggregate, and moisture damage resistance of the bitumen emulsion. Furthermore, it was found that the “2S2P1D” model can well describe the dynamic response of the WEBERs under loading in the frequency domain irrespective of the waterborne epoxy resin contents, and the Prony series can well fit the modulus data of the WEBERs in both the frequency and time domains.

Overall, the outcome of this study suggested that waterborne epoxy resin can effectively improve the mechanical performance of bitumen emulsion. Apart from the tack coat application which has been explored in this study, WEMBE is also a very promising high-performance cold binder for various other paving applications, such as pavement surface treatment, cold recycling, and cold mixes.

LIST OF PUBLICATIONS

Journal papers

R. Li, Z. Leng *, Y. Zhang, and X. Ma. (2019). Preparation and characterization of waterborne epoxy modified bitumen emulsion as a potential high-performance cold binder, *Journal of Cleaner Production*, vol. 235, pp. 1265-1275.

R. Li, Z. Leng *, J. Yang, G. Lu, et al. (2021). Innovative Application of Waste Polyethylene Terephthalate (PET) Derived Additive as An Antistripping Agent for Asphalt Mixture: Experimental Investigation and Molecular Dynamics Simulation, *Fuel*, vol. 300, p. 121015.

R. Li, Z. Leng *, Y. Wang, and F. Zou. (2020). Characterization and correlation analysis of mechanical properties and electrical resistance of asphalt emulsion cold-mix asphalt, *Construction and Building Materials*, vol. 263, p. 119974.

R. Li, Z. Leng *, M. N. Partl, and C. Raab. (2021). Characterization and Modelling of Creep and Recovery Behavior of Waterborne Epoxy Resin Modified Bitumen Emulsion, *Materials and Structures*, vol. 54, p. 8.

C. Hu, **R. Li**, J. Zhao, Z. Leng *, and W. Lin. (2020). Performance of Waterborne Epoxy Emulsion Sand Fog Seal as a Preventive Pavement Maintenance Method: From Laboratory to Field, *Advances in Materials Science and Engineering*, vol. 2020, p. 6425817.

C. Hu, J. Zhao, Z. Leng *, M. N. Partl, and **R. Li**. (2019). Laboratory evaluation of waterborne epoxy bitumen emulsion for pavement preventative maintenance application, *Construction and Building Materials*, vol. 197, pp. 220-227.

Conference Papers

R. Li, Z. Leng *, and Y. Zhang. (2019). Preparation and characterization of waterborne epoxy modified bitumen emulsion as a high-performance cold binder, *Transportation Research Board 98th Annual Meeting*.

R. Li, Z. Leng *. (2019). Creep and Recovery Behavior Modelling of Waterborne Epoxy Resin Modified Bitumen Emulsion, *The 8th International Transportation PhD Student Symposium*.

R. Li, Z. Leng *, Y. Wang, and F. Zou. (2020). Characterization and correlation analysis of mechanical properties and electrical resistance of asphalt emulsion cold-mix asphalt, *Transportation Research Board 99th Annual Meeting*.

R. Li, Z. Leng *, X. Xu, and J. Lan. (2021). Innovative Application of Waste Polyethylene Terephthalate (PET) Derived Additive as an Antistripping Agent for Asphalt, *Transportation Research Board 100th Annual Meeting*.

ACKNOWLEDGEMENTS

During this doctoral study, I have been supported and helped by many individuals. Their great support made the completion of this work possible. First of all, I would like to express my sincere appreciation to my chief supervisor Dr. Zhen Leng for his valuable guidance from the beginning to the completion of this research. His criticism and feedback at various stages through this research encouraged me to move ahead no matter what difficulties I encountered. The insightful discussions with him sharpened my thinking of doing research, which is invaluable for my doctoral study and beyond.

I would like to express my great gratitude to Prof. Manfred N. Partl. I benefited significantly from his guidance during my stay at EMPA (Swiss Federal Laboratories for Materials Science and Technology) as a visiting student. His ideas and suggestions on this thesis were very valuable. I would like to acknowledge Prof. Christiane Raab for providing me the opportunity to go to EMPA and her support for conducting experiments. The help from other staffs and PhD students in EMPA are also appreciated, Dr. Martin Hugener, Dr. Lily Poulikakos, Dr. Josef P. Kaufmann, Dr. Martin Arraigada, Dr. Moises Bueno, Mr. Farrokh Tarpoudi Baheri, and Mr. Zhengyin Piao.

I would like to extend my gratitude to the technicians in our transport laboratories, Mr. C.K. Chau, Mr. M.C. Choi, and Mr. W.L. Wong, for their technical support in preparing the equipment and assisting in experiment activities. My special thanks goes to Mr. W.K. Wong for helping with the specimens preparation using the Superpave gyratory compactor. I am also grateful to some technicians from other laboratories, Miss Celine Che, Miss Dorothy Chan, Dr. Dongxing Xuan, Mr. K.H. Leung, Mr. K.M. Leung, and Dr. Hardy Lui, for their kind support with equipment operations. Thanks Dr. Clara Hung greatly for her detailed guidance in operating the confocal laser scanning microscopy.

The support and daily help from my colleagues are truly appreciated. I am very grateful to Mr. Zhifei Tan, Mr. Bin Yang, Mr. Gaoyang Li, Mr. Yongli Wang, Mr. Ruiqi Chen, Mr. Fuliao Zou, Dr. Yuan Zhang, Dr. Kecheng Zhao, Dr. Huayang Yu, Dr. Jiwang Jiang, Dr. Guoyang Lu, Mr. Haopeng Wang, Dr. Xiong Xu, Dr. Ruijun Cao, Dr. Zongwu Cheng, Miss Jingting Lan, Mr. Danling Li, Mr. Gengreng Hao, Mr. Xingyu Chen, Mr. Xiaoxu Zhu, Miss Fangjing Li, Dr. Anand Sreeram, Mr. Feng Guo, and Dr. Yong Wen … They have all provided support and help in various ways.

I would like to thank my friends Mr. Wei Tian, Dr. Zhirong Liang, Dr. Jizhuang Wang, Dr. Weiqiang Feng, Dr. Tangtian He, and Dr. Yi Zhou. They made my life in Hong Kong more enjoyable.

My special gratitude goes to my wife, Xiyuan Wu, for her love, understanding, and encouragement during the four years of my doctoral study. Even though she is busy with her own job, she never hesitated to support me. I would like to sincerely thank my parents, for their endless love and support. They have taught me the importance of education and the spirit of hard working, which is a life-long treasure. This thesis is dedicated to them.

Last but not least, I would like to acknowledge the Department of Civil and Environmental Engineering of The Hong Kong Polytechnic University for providing the financial support of my doctoral study.

LIST OF TABLES

LIST OF FIGURES

LIST OF ABBREVIATIONS

AASHTO	American Association of State Highway and Transportation Officials
ASTM	American Society for Testing and Materials
ATR	Attenuated total reflection
CA	Christensen and Anderson
CV	Coefficient of variance
CAM	Cold mix asphalt
CIR	Cold in-place recycling
CLSM	Confocal laser scanning microscopy
DGEBA	Diglycidyl ether of bisphenol A
DLVO	Derjaguin-Landau-Verwey-Overbeek
DSR	Dynamic shear rheometer
DTG	Derivative thermogravimetry
EVA	Ethylene vinyl acetate
FM	Fluorescence microscopy
FTIR	Fourier transform infrared spectroscopy
GBM	Generalized Burgers model
GHG	Greenhouse gas
GMM	Generalized Maxwell model
GTCE	Glycidyl tertiary carboxylic ester
HB	Herschel-Bulkley
MHB	Modified Herschel-Buckley
MC	Modified Carreau
HMA	Hot mix asphalt
HS	Huet-Sayegh
HWMA	Half-Warm mix asphalt
LAS	Linear amplitude sweep
MHS	Modified Huet-Sayegh
MSCR	Multiple stress creep recovery

MTD	Mean texture depth
NR	Natural rubber
PAV	Pressure aging vessel
PG	Performance grade (Superpave)
PMB	Polymer modified bitumen
PMBE	Polymer modified bitumen emulsion
RAP	Reclaimed asphalt pavements
RDEC	Ratio of dissipated energy change
SARA	Saturates, aromatics, resins and asphaltenes
SBR	Styrene butadiene rubber
SIS	Styrene-isoprene-styrene
SBS	Styrene-butadiene-styrene
SGC	Superpave gyratory compactor
SHRP	Strategic Highway Research Program
TETA	Triethylenetetramine
TGA	Thermo-gravimetric analysis
TTSP	Time-temperature superposition principle
UTM	Universal testing machine
VECD	Viscoelastic continuum damage
VOC	Volatile organic compounds
WCA	Waterborne curing agent
WER	Waterborne epoxy resin
WEMBE	Waterborne epoxy modified bitumen emulsion
WEBER	Waterborne epoxy bitumen emulsion residue
WLF	Williams-Landel-Ferry
WMA	Warm Mix Asphalt

TABLE OF CONTENTS

CHAPTER 1 INTRODUCTION

1.1 Background

Over the past decades, Portland cement and bituminous materials have been extensively used as the bonding materials for rigid and flexible pavements, respectively [1]. Due to its various advantages, such as quick traffic opening, comfortable riding, and lower traffic noise, bituminous pavement has become the dominant type of pavement in most countries [2, 3]. As bitumen is a viscoelastic material, it behaves like an elastic solid at low temperatures, and acts as a viscous liquid at elevated temperatures [4]. Correspondingly, rutting, fatigue cracking, and low-temperature cracking are typical distresses for bituminous pavement at high, intermediate, and low service temperatures, respectively. To improve the performance of the raw bitumen, various polymers have been used as modifiers [5, 6].

Polymer modified asphalt binders have been successfully used in pavement construction, which provide increased resistance to permanent deformation and thermal cracking, improved fatigue performance, and decreased moisture susceptibility [7]. The commonly used polymers for bitumen modification include styrene-butadiene-styrene (SBS), styrene butadiene rubber (SBR), ethylene vinyl acetate (EVA), and crumb rubbers. However, these polymers must be mixed with bitumen and applied at high temperatures, leading to inevitable short-term aging of the binder due to the high production temperature [8]. In addition, the high-temperature mixing and application may produce significant amount of volatile organic compounds (VOC) and greenhouse gas (GHG) emissions, such as carbon dioxide (CO_2) and sulfur dioxide (SO_2) [9], which negatively affect the environment and personal health. The preparation and application of polymer modified asphalt binders also consumes large quantity of fossil fuels. Thus, from the environmental point of view, it is desirable that asphalt binder is applied at a lower temperature or even ambient temperature.

Bitumen emulsion, i.e., an emulsion of bitumen droplets dispersed in water, has been widely used in various paving applications, such as tack coat, pavement surface treatment, cold recycling, and cold mixes [10]. Since bitumen emulsion has water as the continuous phase, its viscosity is low enough to achieve good workability at ambient temperature [11], thereby eliminating the heating requirement and reducing the energy consumption and hazardous emissions during the manufacturing and construction. However, bitumen emulsion faces the major concern of low mechanical strength especially at high service temperatures [12-15]. To improve the mechanical performance of bitumen emulsion, it is desirable to modify the bitumen emulsion using polymers. Both solid polymers and polymer latexes have been applied for such purpose. However, the solid polymers must be mixed homogeneously with bitumen before emulsification. Such method still constitutes the preparation of polymer modified bitumen at high temperature, and the emulsification of the polymer modified bitumen is difficult because of the high viscosity. In contrast, polymer latexes are more favoured as they can be mixed with bitumen emulsion easily because of their liquid form, which represents a major advantage over the solid polymer method. In addition, the latex modification generally leads to similar performance benefits in bitumen emulsion residues as those obtained from solid polymer modified binders, such as higher resistance to load deformation and reduced thermal cracking [16]. Polymer latexes, such as SBS latex [17], SBR latex [18], and chloroprene rubber latex [19], have been commonly applied to modify bitumen emulsion, leading to improved mechanical performance of the bitumen emulsion. More recently, waterborne epoxy resin has emerged as a novel waterborne modifier for bitumen emulsion, which has shown significant effect in improving the performance of the bitumen emulsion [20-22].

1.2 Problem statement

Bitumen or asphalt cement is typically used as the binder for hot-mix asphalt (HMA). However, the production and construction of HMA are not environment friendly due to the generation of volatile organic compounds (VOCs) and greenhouse gases (GHGs) at high temperature. Bitumen emulsion, in contrast, is a greener material, since it can be applied at ambient temperature for its low viscosity. It has been widely used for various pavement construction and maintenance purposes, such as surface treatment, tack coat, cold recycling, and cold mixes [23-25]. However, the application of bitumen emulsion is limited by its relatively low mechanical strength. There lies a question on how to modify and improve the mechanical performance of bitumen emulsion. Polymer latex, which is partly soluble in water, can be used to prepare a homogeneous polymer modified bitumen emulsion by simply mixing the latex with bitumen emulsion. The latex will then disperse evenly in the aqueous phase, with the evaporation of water, the polymer latex can form the inter-connected networks, thereby improving the mechanical performance of bitumen emulsion.

Epoxy resin has been conventionally implemented to prepare epoxy modified asphalt by the hot-mix method, which showed excellent resistance to rutting and fatigue, and it is commonly used as a bridge deck paving material. However, the hot-mix process of epoxy asphalt generates significant amounts of hazardous emissions. In addition, the curing of epoxy resin proceeds rapidly at higher temperature. Thus, the pot life of epoxy asphalt is very short, making it rather challenging for the mixing, transportation, and paving of this material.

Waterborne epoxy resin is an epoxy in water emulsion system, within which the epoxy resin is stabilized by surfactant. The incorporation of waterborne epoxy resin into bitumen emulsion is a relatively new approach to modify bitumen emulsion, and the relevant research is very limited. The effects of waterborne epoxy resin on the microstructure and the performances of bitumen emulsion and emulsion residue need to be systematically investigated. In addition, better understanding on the strength formation mechanism of waterborne epoxy resin modified bitumen emulsion is desired for future research and applications.

1.3 Research objectives and scope

The main objectives of this research are to investigate the influences of waterborne epoxy resin on the microstructure of bitumen emulsion, and to explore the effects of waterborne epoxy resin on the properties of bitumen emulsion and emulsion residue. To achieve these objectives, the following research tasks were conducted in this study:

1. Literature review: to understand the current research and application status of bitumen emulsion, as well as the performances of the polymer latexes modified bitumen emulsion.
2. Synthesis of waterborne curing agent (WCA): to synthesize an appropriate WCA that can be used to emulsify the epoxy resin. The WCA can act as both an emulsifier for epoxy resin and a curing agent.
3. Evaluation of the waterborne epoxy resin modified bitumen emulsion (WEMBE): to investigate the effects of waterborne epoxy resin on the microstructure, stability, and rheological properties of bitumen emulsion.
4. Evaluation of the waterborne epoxy resin modified bitumen emulsion residue (WEBER): to evaluate the effects of waterborne epoxy resin on the microstructure, and properties of bitumen emulsion residues, including rheology, high temperature performance, aging, fatigue performance, bonding with aggregate, and resistance to moisture damage.
5. Constitutive modelling of WEBER: to investigate the constitutive relations of the WEBER based on frequency sweep and relaxation test results.
6. Evaluation of WEMBE as a tack coat material: to evaluate the performance of WEMBE on the interlayer bonding strength of asphalt mixtures.

1.4 Significance of this research

The original contributions of this research are listed below:

1. A better understanding about the modification mechanism of WEMBE has been achieved.

2. The overall performances of WEMBE and WEBER were thoroughly investigated. This thesis provides an enhanced understanding of the effect of waterborne epoxy resin on the properties of bitumen emulsion.

3. The WEMBE developed in this study represents a high-performance cold paving binder, which can potentially be applied in pavement surface treatment, tack coat, cold recycling and cold mixes, and significantly reduce the energy consumption and greenhouse gases emissions.

1.5 Organization of this thesis

This thesis is divided into seven chapters described as below.

Chapter 1 presents the general introduction of this thesis.

Chapter 2 presents a comprehensive literature review, including (1) modification of bitumen with polymers; (2) constitutes, stability, wetting on aggregate, and applications of bitumen emulsions; (3) modification of bitumen emulsions with polymer latexes and their properties; (4) application of epoxy resin in asphalt pavement; and (5) modification of bitumen emulsion with waterborne epoxy resin.

Chapter 3 presents the preparation and evaluation of waterborne epoxy resin modified bitumen emulsions (WEMBEs), including (1) synthesis of waterborne curing agent (WCA); (2) preparation and characterization of waterborne epoxy resin (WER) emulsion; and (3) characterization of WEMBEs, such as fluorescence microscopy images, zeta potential, shear-thinning and thixotropy properties.

Chapter 4 presents the performance evaluation of the waterborne epoxy resin modified bitumen emulsion residues (WEBERs), including (1) chemical analysis using the infrared spectra; (2) phase distribution of the waterborne epoxy resin and bitumen based on fluorescence microstructure; (3) rheological performance evaluation, such as temperature sweep and multiple stress creep recovery (MSCR) test; (4) aging effect on both the chemical and rheological properties of WEBERs; (5) fatigue evaluation employing the time-sweep test as well as the linear amplitude sweep (LAS) test; (6) bond strength between emulsion residues and aggregate; and (7) moisture susceptibility of bitumen emulsion aggregate mixture by boiling test.

Chapter 5 presents the constitutive modelling of the WEBERs. The data was fitted with both the “2S2P1D” model and the generalized Maxwell model.

Chapter 6 presents a case study of using WEMBEs as tack coat materials, and the inter-layer shear strength was compared for different contents of waterborne epoxy resin.

Chapter 7 presents the major findings and recommendations of this thesis study.

The overall research framework is depicted in Figure 1.1.

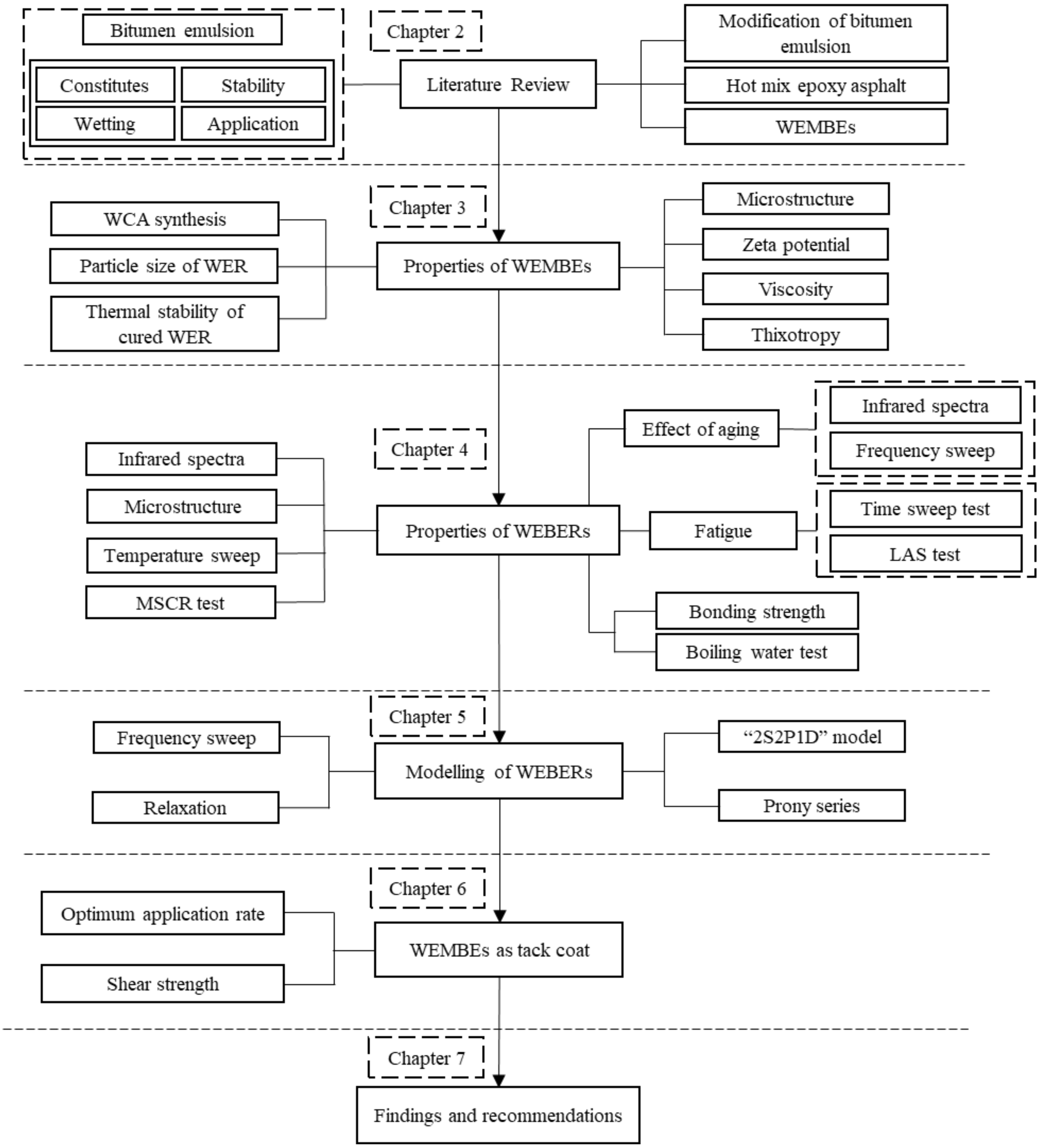

Figure 1.1 Research framework

CHAPTER 2 LITERATURE REVIEW

This chapter systematically reviewed the previous studies about bitumen emulsion and the polymer latexes modified bitumen emulsion. Section 2.1 presents the conventional method of bitumen modification and its drawbacks. Section 2.2 describes the constitutes, stability, wetting, and applications of bitumen emulsion. Section 2.3 and 2.4 describes the modification of bitumen emulsion with polymer latexes, and the properties, respectively. Section 2.5 presents the applications of epoxy resin in pavement construction, including the hot mix epoxy asphalt, and the waterborne epoxy resin modified bitumen emulsion.

2.1 Modification of bitumen

Neat asphalt binders generally cannot meet the requirements of high-level pavements, and thus polymers are commonly applied to improve the performance. The modification of bitumen using polymers has been extensively investigated in the past few decades. These polymers include styrene-butadiene-styrene (SBS), styrene-isoprene-styrene (SIS), styrene-ethylene/butylene-styrene (SEBS), polyethylene (PE), polypropylene (PP), ethylene-vinyl acetate (EVA), and crumb rubber, etc. [7, 26]. It is reported that these polymers generally lead to improved properties of the asphalt pavement, such as increased resistance to rutting and thermo-cracking, improved durability, and better moisture resistance [7]. Among all these polymers, SBS is recognized as the most appropriate polymer for bitumen modification, because of the excellent properties that can be achieved [26]. On the other hand, the addition of polymers increases the viscosity of bitumen binders, thus the polymer modified binders are usually used in hot-mix asphalt. However, concerns about the properties degradation and, particularly, environmental issues during the production and construction of hot-mix asphalt (HMA) are rising in recent years. When mixed with aggregate, asphalt binder will inevitably undergo the short-term aging induced by the high temperature [27, 28]. In addition, HMA produces significant amounts of volatile organic compounds (VOC) and greenhouse gas (GHG) emissions such as carbon dioxide (CO_2) and sulfur dioxide (SO_2) [9]. These emissions dramatically affect the environment and personal health. Furthermore, HMA consumes large quantity of fossil fuels to reach the required temperature. To implement greener and more sustainable approaches of pavement construction, this industry has been seeking alternative techniques to produce asphalt mixture at lower temperature such as warm-mix asphalt (WMA, 100~140℃), half-warm mix asphalt (HWMA, 60~100℃), and even cold-mix asphalt (CMA, 0~40℃) [29, 30]. Such techniques significantly reduce the consumption of fossil fuels and hazardous emissions [31]. It is reported that a 10℃ decrease in the production temperature of asphalt mixture contributes to the reduction of 1L fossil fuel consumption and 1 kg carbon dioxide emission per ton [32].

2.2 Bitumen emulsion

Bitumen emulsion is the most widely used cold construction material in the pavement industry at present. The main applications include pavement surface treating, tack coat, cold recycling, and cold mixes [10, 15, 23-25, 33-35]. With bitumen droplets dispersed in the aqueous phase, the viscosity of bitumen emulsion is low enough to achieve good workability at ambient temperature.

2.2.1 Constitutes of bitumen emulsion

2.2.1.1 Bitumen

Bitumen emulsions are mainly composed by bitumen, emulsifiers, and water. Bitumen is a semi-solid viscoelastic material with an extremely high viscosity (~7000 Pa·s) at ambient temperature [36, 37]. Owing to their pronounced waterproofing, adhesive, and rheological performance, bituminous materials are recognized as the most eligible materials for pavement construction. Bitumen is predominantly composed by carbon and hydrogen (>wt90 %), and the rest elements are mainly sulfur, nitrogen, and oxygen [4]. Generally, bitumen is divided into four fractions based on their polarity and aromaticity: saturates, aromatics, resins, and asphaltenes (SARA) [38]. The fractions with lower molecule weight: saturates, aromatics, and resins are defined as maltenes, while asphaltenes are the heaviest fraction in bitumen [39]. It is generally recognized that the SARA fractions form the so-called ‘colloid’ structure [4, 40], that the asphaltenes are surrounded by the maltenes, and the resins act as the interface layer between the solid-like asphaltenes and the liquid-like oily phase.

2.2.1.2 Emulsifiers

Typically, bitumen emulsion is characterized by high solid content (50~70%), and the average size of bitumen droplets generally falls in the range of 5-50 μm [10, 41, 42]. As the highly-dispersed droplets possess enormous interfacial energy, bitumen emulsion is a thermodynamically unstable system [43]. The bitumen droplets tend to coalescence and form larger bitumen particles, inducing phase separation of the bitumen emulsion [44, 45]. To increase the bitumen emulsion stability, emulsifiers are essentially an indispensable part. In general, emulsifiers are surfactant molecules with a hydrophilic head and a hydrophobic backbone [46]. When producing bitumen emulsions, emulsifiers are normally applied as stabilizer, which will then diffuse from water to the interface of bitumen and water, thereby reducing the interfacial energy and increasing the stability [47]. Based on the electric properties of the hydrophilic head, emulsifiers can be divided into three categories: cationic, anionic, and non-ionic [48-50]. Emulsifiers are generally used with a concentration no more than 3wt% of the emulsion system [51, 52]. As the non-ionic emulsifiers are rarely used in bitumen emulsion, only cationic and anionic emulsifiers are discussed here.

The cationic type emulsifiers are the most widely used emulsifiers in bitumen emulsions [3]. They are mainly composed by the fatty amines, alkyl-amide polyamines or lignin derivatives

[53]. The cationic emulsifiers are activated in acid conditions (e.g., addition of chlorine hydride) [10]. These emulsifiers then arrange themselves around the bitumen droplets, thus making the bitumen droplets positively charged. As most aggregates are of electronegative nature, the cationic type emulsifiers can effectively absorb to a wide variety of mineral aggregates, resulting in strong bitumen-aggregate adhesion. This is the reason why the cationic emulsifiers are more favoured in manufacturing bitumen emulsions [54]. Meanwhile, cationic emulsifiers are capable of reacting with both alkaline aggregates (e.g., limestone) and acid aggregates (e.g., basalt and granite). The salts (ammonium carbonates or ammonium silicates) formed following the chemical reaction can further enhance the adhesion between bitumen and aggregate [55].

The anionic emulsifiers, on the other hand, consist of long hydrocarbon chains terminated with a negatively charged head, mostly carboxylate ($R\text{-}COO^-$) and sulfonate ($R\text{-}SO_3^-$) [56]. The anionic bitumen emulsions can provide effective coating or bonding properties when mixed with alkaline aggregates (normally positively charged) [49]. However, the weak adhesion with acid aggregates (negatively charged) is the main drawback for anionic bitumen emulsions. Owing to this fact, the application of anionic emulsifiers is less common compared with the cationic emulsifiers.

2.2.2 Stability of bitumen emulsion

The stability of bitumen emulsion plays a significant role in the process from preparation to application [57]. One important requirement for bitumen emulsions is that the bitumen emulsion must remain stable during storage and transportation, and break in an appropriate speed upon application [58]. Various factors, creaming, sedimentation, flocculation, Ostwald ripening, and coalescence, may contribute to the destabilization of an emulsion [59]. It has been demonstrated that Ostwald ripening and coalescence are the main destabilizing mechanisms for nano-scale emulsion and micro-scale emulsion, respectively [60]. As the sizes of bitumen emulsion droplets are in the order of microns, coalescence is the key factor that influences the stability of bitumen emulsion. Researchers have found that the thinning and disruption of liquid film between bitumen droplets will lead to coalescence [61, 62], resulting in larger bitumen particles [63]. This process is energetically favourable, for larger bitumen particles possess lower surface energy.

When bitumen emulsions are stabilized by cationic or anionic surfactants, the surface of bitumen droplets becomes positively or negatively charged. Meanwhile, the bitumen droplets are surrounded by opposite electric ions dispersed in the aqueous phase. According to the classic Derjaguin-Landau-Verwey-Overbeek (DLVO) theory, both the repulsive and attractive forces between bitumen droplets appear simultaneously [39]. This theory assumes that the electrostatic double layer forces and the van der Waals forces are independent and therefore can be superimposed or added at each interacting distance for two particles. Figure 2.1 depicts the electrical double layer based on the DLVO theory [64]. For the cationic bitumen emulsion, the surface of bitumen particles is surrounded by the cationic emulsifiers, thus the surface is positively charged and provides the surface potential. A thin layer of ions of the opposite charge is then closely absorbed on the particle surface, making up the stern layer. The rest of ions, both positive and negative, are distributed in the outer diffuse layer. The so-called zeta potential is defined as the electric potential at the boundary of the double layer on the particle surface [64]. The zeta potential largely determines the stability of the system. In general, a solution is relatively stable if the magnitude of the zeta potential is larger than 30 mV [65].

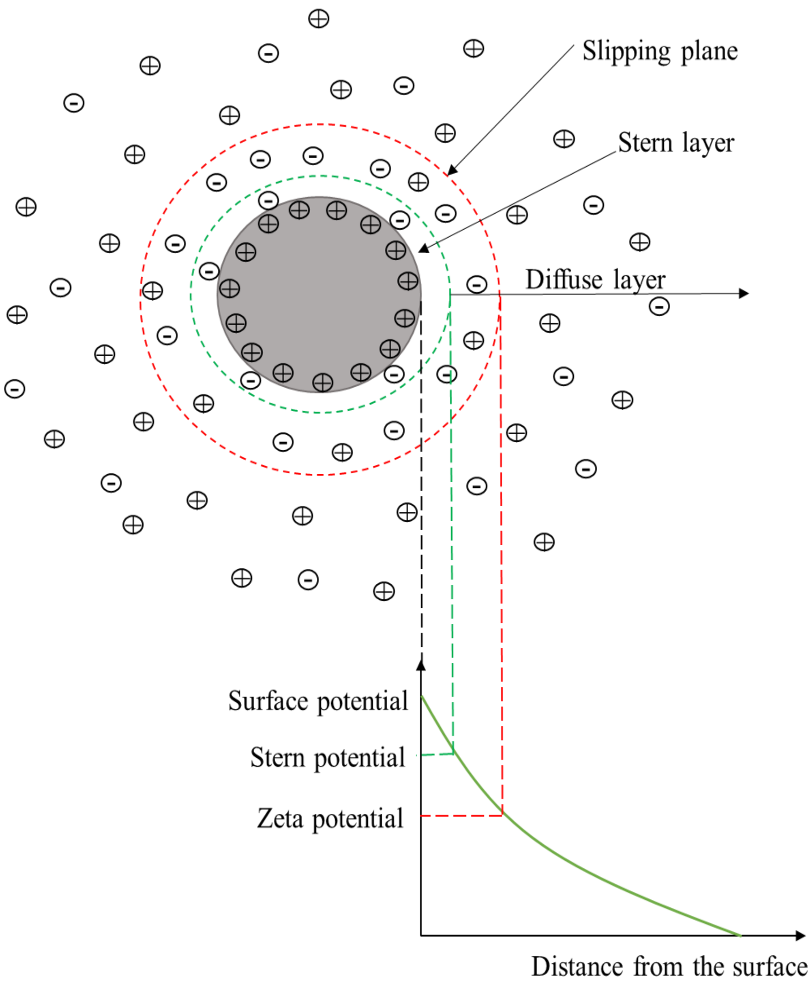

Figure 2.1 Electrical double layer of DLVO theory

According to the classical DLVO theory, the total interaction energy V_T is the sum of the attractive energy V_A and the repulsive V_R energy (Figure 2.2). The total interaction energy V_T results in a deep attractive well at the small distance, which is referred to as the primary minimum $V_{primary}$. At larger distances, the energy profile goes through a maximum, and subsequently decreases to a shallow minimum, which is referred to as the secondary minimum $V_{\sec}$. It is found that the secondary minimum can result in flocculation of the droplets, which is weak and reversible [66]. The stability of the particles depends on the balance of the attraction and the repulsion. When the repulsion overcomes the attraction, the particles are prevented from approaching and the emulsion is stable. Whereas when the attraction exceeds the repulsion, the particles tend to contact with each other, and this results in coalescence.

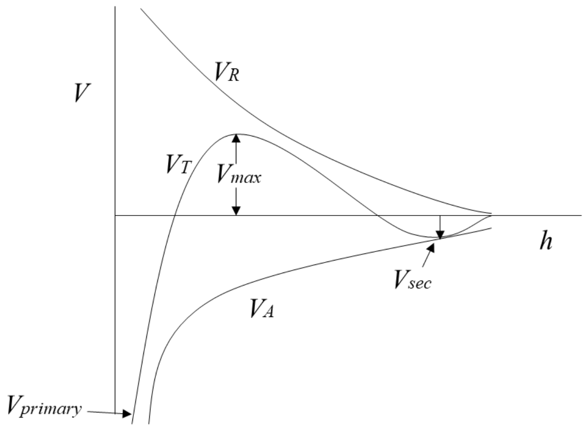

Figure 2.2 Total energy-distance curve according to the DLVO theory

Some previous studies [39, 67] have employed the zeta potential to evaluate the stability of the bitumen emulsions based on the chemical and interfacial properties of the bitumen. The zeta potential is positive for a cationic emulsion and negative for an anionic emulsion [68]. Jada, et al. [69] measured the zeta potentials for various cationic bitumen emulsions having different sizes and emulsifier contents, and concluded that zeta potential can be used to explain the emulsion behavior and predict the breaking mechanism in emulsion-aggregate mixes. Recently, Pinto and Buss [65] systematically investigated the effects of pH, emulsifier dosages, and temperature on the zeta potential of bitumen emulsion. The results indicate that zeta potential correlates well with the level of stability of the emulsion.

The zeta potential is calculated according to the Smoluchowski's equation,

$$\zeta = (\eta / \varepsilon) U_e \tag{2-1}$$

where U_e is the electrophoretic mobility, η and ε are the viscosity and permittivity of the aqueous phase, respectively.

The electrophoretic mobility U_e is then calculated as,

$$U_e = \frac{V_p}{E_x} \tag{2-2}$$

where V_p is the particle velocity, and E_x is the applied electrical field.

2.2.3 Bitumen emulsion wetting on aggregate

The bitumen droplets are stabilized within the emulsifier micelles, while some free emulsifier molecules can also be found in the aqueous phase (Figure 2.3(a)). When mixed with mineral aggregates, emulsifier molecules in the aqueous phase first absorb onto the solid surface and a monolayer of emulsifiers on the aggregate is formed (Figure 2.3(b)), which in turn changes the aggregate surface from hydrophilic to hydrophobic [70, 71]. The absorption of emulsifiers by aggregates decreases the concentration of emulsifiers in water. To restore equilibrium, emulsifiers will dissociate from the bitumen-water interface until a point that the remaining emulsifiers are unable to support the bitumen droplets, thereby decreasing the zeta potential of the bitumen droplets, and resulting in coalescence of bitumen droplets. Meanwhile, the evaporation and absorption of water on the porous aggregate surface would reduce the aqueous film thickness, thus the bitumen droplets become closer to each other. However, the repulsive force is insufficient to keep bitumen droplets from contacting, which further accelerates the bitumen coalescence [49]. As the aggregate surface has turned into hydrophobic, it becomes ideal for the wetting of bitumen. The strong physicochemical interactions between bitumen droplets and aggregate then initiate the bitumen emulsion breaking (Figure 2.3(c)). In the meantime, water is expelled out and then evaporates into air. Eventually, the bitumen adheres onto the solid surface and a bitumen film is formed around the aggregate (Figure 2.3(d)).

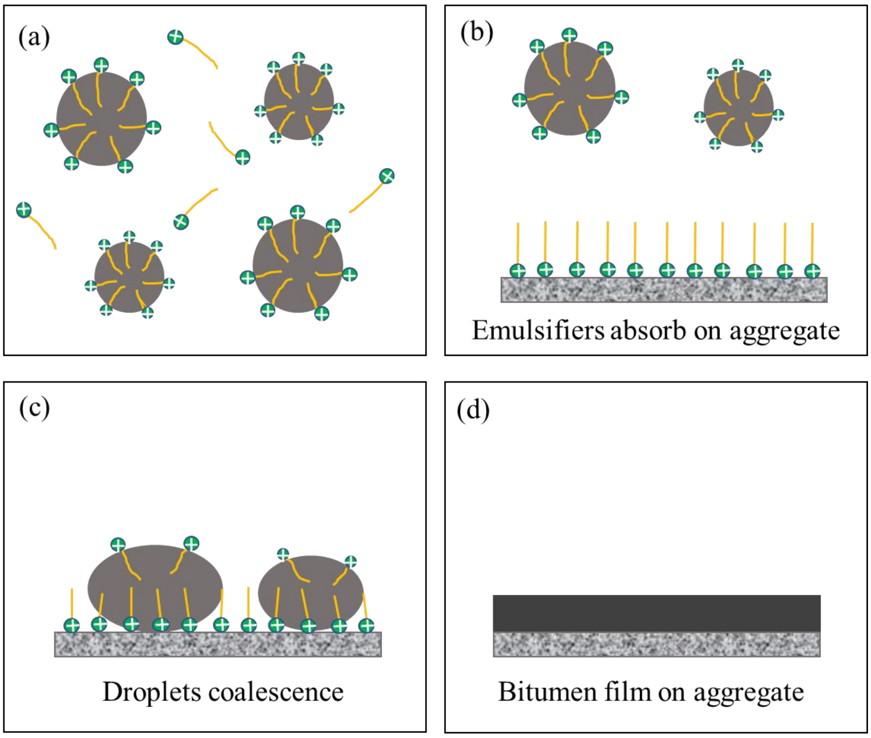

Figure 2.3 Process of bitumen emulsion wetting on aggregate

2.2.4 Applications of bitumen emulsion

Conventionally, bitumen emulsion was used in non-structural layers due to their weak strength, such as tack coat, surface treating, cold recycling or cold mixes [18, 72].

2.2.4.1 Tack coat

Weak interlayer bonding of different pavement layers usually leads to distresses like slippage [73, 74], especially at areas of frequent braking and accelerating [75]. Tack coat is generally used to enhance the interlayer bonding of different pavement layers [76]. A survey conducted by Mohammad et al. [77] shows that bitumen emulsion is the most commonly used material for tack coat. Collop et al. [78] found that bitumen emulsion improves the shear strength of different pavement layers in comparison with that without bitumen emulsion. Diakhaté et al. [79] compared the bonding fatigue performance of two asphalt concrete layers with and without tack coat, and the result indicated that bitumen emulsion tack coat increased the fatigue performance substantially. From these studies, it is concluded that the interlayer bonding strength of different pavement layers is rather important to reduce premature distresses, and bitumen emulsion plays a crucial role in improving the interlayer bonding.

2.2.4.2 Surface treatment

Due to the impact of weathering and repeated vehicle loadings [80], many different kinds of premature distresses will occur on asphalt pavements during their service life. These distresses, like rutting and cracking, must be treated in time to prevent further deterioration. To preserve pavement quality and functional performance, maintenance is necessary [81, 82]. Previous research has found that maintenance could minimize the development of distresses, leading to an extended service life, reduced life cycle cost of the pavements [83-85], and lower environmental impact [86]. Chip seal, slurry seal, fog seal, micro-surfacing and thin overlay have been proven to be effective maintenance methods [87-90]. However, it is worth noting that one maintenance method may not be universally applicable for all kinds of distresses. To determine the optimum maintenance method, the pavement conditions, climate, and budget must be carefully considered [90]. Bitumen emulsion is the major type of material used in pavement maintenance for ease of application, environmental benefits, and cost-effectiveness [82, 84, 91]. Table 2.1 lists the various surface treatment methods for different pavement distresses.

Table 2.1 Comparison between different surface treatment methods for pavement [82, 92]

Distress	Treatments						
	Micro-surfacing	Crack seal	Fog seal	Slurry seal	Cape seal	Chip seal	Thin overlay
Roughness (not associated with stability)	✓				✓		✓
Roughness (associated with stability)							✓
Rutting	✓						✓
Fatigue cracking (low severity)	✓		✓	✓	✓	✓	✓
Longitudinal and transverse cracking	✓	✓		✓	✓	✓	✓
Bitumen exudation	✓					✓	
Ravelling	✓	✓	✓	✓	✓	✓	

2.2.4.3 Cold recycling

Recycling of the reclaimed asphalt pavements (RAP) is becoming increasingly important for the sustainability of pavement industry. The aggregate and asphalt binder in RAP materials are still valuable resources which can partially replace the virgin aggregate and binder [93]. The recycling of RAP brings various benefits, like reduced energy consumption, less GHG emissions and lower costs [94, 95]. Cold in-place recycling (CIR) can further reduce the environmental footprint in comparison with other rehabilitation techniques as it is conducted at ambient temperature [96-98]. Moreover, the RAP mixture is recycled and reused right at the job site, which substantially decreases the energy consumption on haulage [99]. It is reported that the pavements with well-drained subbases that suffer from limited damages on the structure are the most suitable candidates for CIR [100, 101]. Both foamed asphalt and bitumen emulsion have been evaluated in CIR to bond RAP materials [102]. However, bitumen emulsion can be more successfully applied than foamed asphalt especially in wet conditions [103].

2.3 Modification of bitumen emulsion

To improve the performance of bitumen emulsion, polymers, including solid polymers and polymer latexes are used as modifiers to prepare polymer modified bitumen emulsion (PMBE). The solid polymers must be mixed homogeneously with bitumen to prepare polymer modified bitumen (PMB) prior to emulsification, which is known as the polymer pre-blending method. However, the emulsification of PMB is difficult because of the high viscosity. In addition, it was also noted that the polymer pre-blending method may not form the continuous polymer structure in the residue, which affects the final performance of the bitumen emulsion [104]. On the other hand, the polymer latexes can be directly added into bitumen emulsion by simply stirring (latex post-blending), in a plant or before application. It is reported by Forbes, et al.

[105] that an introduction of 3wt% of latex into bitumen emulsion is able to form a continuous polymer-rich phase for the latex modified bitumen emulsion. In contrast, at least 6wt% to 7wt% of solid polymers are needed in the PMB to form such polymer-rich continuous phase [4]. Takamura [106] from BASF investigated detailly about the SBR latex modified bitumen emulsion. Their findings showed that the SBR latex was dispersed in the aqueous phase and can form a continuous polymer film around the bitumen particles upon the curing of the emulsion (Figure 2.4). Takamura and Heckmann [107] further demonstrated that the formed polymer network remained intact even when reheated to “hot mix” temperatures. After removing of the bitumen by solvent, a honeycomb-like structure of the SBR polymer was then observed with a scanning electron microscope (Figure 2.5). The continuous polymer structure is deemed to be responsible for the performance improvement of the residual binder. Because of their various benefits, including improved stone retention, increased skid-resistance, and decreased temperature susceptibility, the latex modified bitumen emulsions are now increasingly used in surface treating, cold recycling, and cold mixes [19, 22, 108-110].

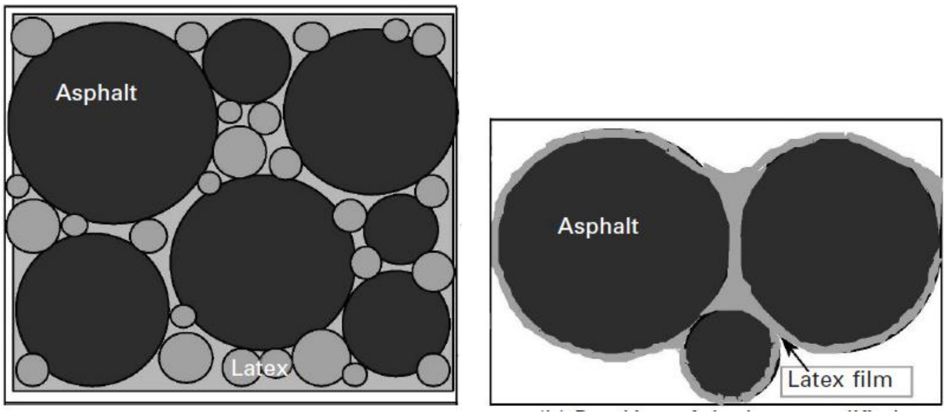

(a) (b)

Figure 2.4 Morphology of: (a) latex-modified bitumen emulsion and (b) continuous latex polymer phase after breaking [106]

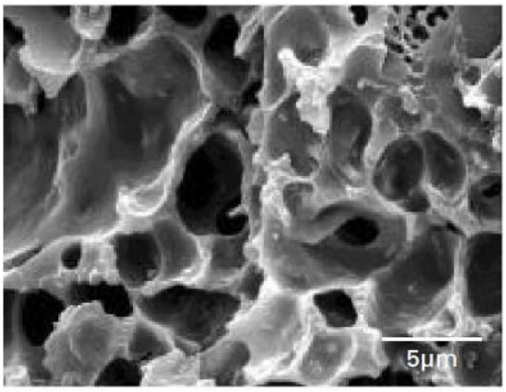

Figure 2.5 Scanning electron microscope image of latex modified bitumen emulsion (The bitumen has been removed by solvent) [107]

2.4 Properties of polymer latex modified bitumen emulsion

Styrene butadiene rubber (SBR) latex and natural rubber (NR) latex are among the most popular latexes used to modify bitumen emulsion at present [111]. SBR is a random copolymer of styrene and butadiene, while NR is made up by repeated isoprene monomers. Both SBR latex and NR latex are water-based dispersion of polymers, and thus can be easily mixed with bitumen emulsion to prepare the polymer modified bitumen emulsion. Khadivar and Kavussi [18] compared the effect of SBR latex and NR latex on the performance of bitumen emulsion, and found that both latexes can improve the high-temperature performance of the residual binders. In addition, their study also indicated that NR latex substantially increased the stiffness of the residual binder, while the elastic properties were poor compared with SBR latex bitumen emulsion. The authors explained that such difference may be related to the fact that the SBR latex can form a continuous polymer network, which is absent in the NR latex modified bitumen emulsion. Abedini, et al. [112] studied the residues of different percentages of SBR latex modified bitumen emulsion, which showed that the increase of SBR dosages led to increased softening point and decreased penetration. In addition, the rutting parameter $G^*/\sin\delta$ was also improved, indicating that the high temperature performance was increased with the incorporation of SBR latex. Other polymer latexes, like SBS latex [17] and polyurethane latex [113], were also investigated as modifiers for the bitumen emulsion, and the results demonstrated that both the softening point and ductility were increased, while the penetration was decreased. Xia and Luo [114] synthesized a poly(styrene-b-isoprene-b-styrene) (SIS) triblock copolymer latex, which was then used to modify bitumen emulsion. Their results showed that with an incorporation of 5wt% of SIS latex, the emulsion residue showed a significant increase in complex modulus at high temperature and a significant decrease in loss tangent, and the ductility at 5 ^{o}C also increased to some degree.

The incorporation of waterborne epoxy resin into bitumen emulsion is a relatively new approach to modify bitumen emulsion, and the relevant research is very limited. In one of the previous studies [115], waterborne epoxy resin and SBR latex were mixed with bitumen emulsion simultaneously as modifiers. The results showed that both the softening point and ductility of the bitumen emulsion residue increased slightly.

In summary, these studies indicated that the polymer latexes can be dispersed in the aqueous phase of bitumen emulsion, and a continuous polymer-rich network will be formed at a relatively small content of polymer latexes. Such continuous polymer-rich structure provides the residual binders with improved performances, such as increased stiffness, decreased temperature sensitivity, improved fatigue life, and enhanced elastic recovery.

2.5 Application of epoxy resin in pavement

Epoxy resin is a material that contains one or more epoxy groups (oxiranes) in the molecule structure. The epoxy groups are chemically active and can react with curing agents or hardeners, such as amines, amide, carboxy groups or anhydrides. A three-dimensional cross-linked polymer structure can be formed after the curing reaction. The cured epoxy resin will not dissolve in solvent or melt at elevated temperature.

The diglycidyl ether of bisphenol A (DGEBA)-based epoxy resin (Figure 2.6) is the most used epoxy resin at present. Epoxy resins can be cured with different types of hardeners to produce products with different mechanical properties [116-118]. During the curing process, the crosslink density increases and the epoxy-hardener system experiences gelation and vitrification stages, which leads to higher glass transition temperature (Tg) and mechanical properties [119, 120]. Amine-based hardeners can react with epoxy resins with relatively fast rate even at ambient temperature.

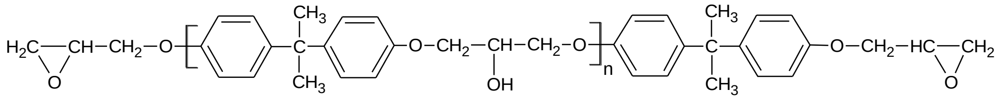

Figure 2.6 Molecule structure of DGEBA-based epoxy resin

The crosslink polymerization reaction between epoxy resin and amines involves a series of complicated processes as illustrated in Figure 2.7. Epoxy resin group first goes through a ring-opening process and the amino alcohols are formed subsequently (Figure 2.7(a)); the secondary amine then reacts with another epoxy group (Figure 2.7(b)); at the final stage, the hydroxyl groups react with epoxy to form a three-dimensional inter-connected structure (Figure 2.7(c)) [121, 122]. The hydroxyl obtained in the first stage has the ability to catalyse the curing reaction, which is typically an autocatalytic chemical reaction [123]. Epoxy curing reaction is characterized as polyaddition and will not produce any low-molecular weight products, which is quite important for the manufacturing of high-performance epoxy end products [122].

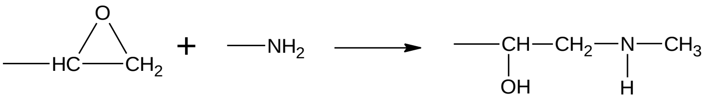

(a) Primary amine-epoxy reaction

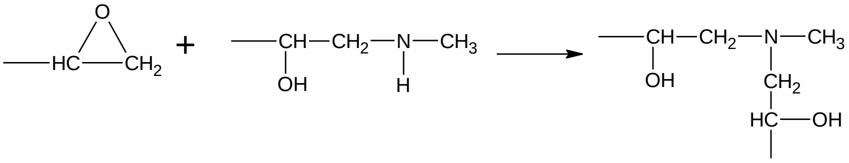

(b) Secondary amine-epoxy reaction

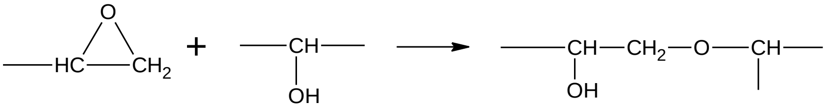

(c) Epoxy-alcohol reaction

Figure 2.7 Curing reaction process of epoxy resin and amine

2.5.1 Epoxy resin modified asphalt

The use of epoxy resin in pavement construction dates back to the late 1950s. Epoxy resin modified asphalt was first placed at airfields, which demonstrated outstanding resistance to permanent deformation and fuel spillage [124]. By mid-1960s, epoxy asphalt was applied to pave the steel bridge decks and performed extremely well [125]. Epoxy asphalt binder is a two-phase system in which the asphalt binder is dispersed in the thermosetting epoxy resin continuous phase, which changed the thermoplastic nature of asphalt binder. Unlike conventional asphalt, epoxy asphalt will not melt at high temperature, which results in superior performance at elevated temperature. Furthermore, epoxy asphalt provides high strength, prolonged fatigue stability, improved skid and chemical resistance [126, 127]. Consequently, epoxy asphalt concrete has been extensively used to pave orthotropic steel bridge decks worldwide. However, the application of epoxy asphalt is not solely limited to bridge decks surfacing. Over the years, researchers and engineers have successfully explored additional applications of epoxy asphalt in normal pavement, such as epoxy asphalt chip seals [128, 129], waterproofing layer [125], open-graded overlayers [130] and long-life wearing courses [131].

Nevertheless, the present epoxy asphalt is still hot mixing, which generates large amount of VOC or GHG. In addition, the epoxy resin cures rapidly at high temperature, making the working window rather limited [132]. Hence, it is desirable that epoxy resin be used at ambient temperature.

2.5.2 Waterborne epoxy resin bitumen emulsions

In recent years, waterborne epoxy resin has attracted considerable attention due to the ever-increasing restriction on environment protection. Waterborne epoxy resin is an epoxy in water system, within which the epoxy resin is stabilized by surfactant. Epoxy resin can be emulsified with external-surfactant or self-emulsified by attaching hydrophilic polar groups (e.g., carboxylate, sulfonate, quaternary ammonium salt or non-ionic groups) to epoxy resin backbones [133, 134]. The self-emulsifying method can produce droplets with smaller size, which is more stable and frequently used [133]. The two components of waterborne epoxy resin and hardener are mixed together before application. As water evaporates, the epoxy resin droplets coalesce, which initiates the curing reaction, resulting with the inter-connected polymer structure.

After curing with hardeners, epoxy resin become a highly crosslinked structure, providing the material with many useful properties, such as high strength, high adhesive ability, and low creep. The waterborne epoxy resin modified bitumen emulsion (WEMBE) can be prepared by mixing the waterborne epoxy resin with bitumen emulsion. The waterborne epoxy resin will disperse in the aqueous phase, and then cures upon water evaporation. The WEMBE has the following advantages: (1) ease of preparation, waterborne epoxy resin can be mixed with bitumen emulsion simply by stirring; (2) increase of mechanical strength; (3) low environmental footprint, the mixture constitutes no volatile solvents, and will not produce additional VOC since the mixing and construction are both conducted at ambient temperature; and (4) broader applications, such as surface treating, interlayer bonding, cold recycling, and cold mixes.

2.6 Summary

Bitumen emulsion represents a ‘greener’ construction material that can be used in the pavement industry. However, there is a research gap on how to effectively modify and improve the mechanical performance of bitumen emulsion. From the literature review in this chapter, it was found that the incorporation of polymer latexes can effectively improve the mechanical performance of bitumen emulsion. The following findings are summarized based on the literature review:

(1) Hot-mix asphalt generally leads to short-term aging of bitumen binder, which also produces significant amount of hazardous emissions (e.g., VOC, GHG), thereby increasing the environmental footprint.

(2) Zeta potential is a suitable indicator for the stability of bitumen emulsion.

(3) When mixed with bitumen emulsion, the polymer latexes can be homogeneously dispersed in the aqueous phase, and form a polymer-rich film around bitumen particles upon drying, which significantly increases the mechanical performance of bitumen emulsion residue.

(4) Waterborne epoxy resin is a novel material to modify bitumen emulsion. Waterborne epoxy resin cures in the drying process of bitumen emulsion, and can form thermosetting polymer-rich structures in the bitumen matrix. Such structure can potentially provide substantial improvement in terms of the mechanical performance of the emulsion residue.

CHAPTER 3 PREPARATION AND EVALUATION OF WEMBEs

This chapter presents the experimental evaluations of both the waterborne epoxy resin and the waterborne epoxy resin modified bitumen emulsions (WEMBEs). Section 3.1 describes the experiments and characterization methods, including the synthesis of the waterborne curing agent, preparation of waterborne epoxy resin and the corresponding modified bitumen emulsion, and the characterizations of these materials. Section 3.2 presents the experimental results, including the particle size measurements of the waterborne curing agent (WCA) and the waterborne epoxy resin, and the thermal stability of the waterborne epoxy resin; the microstructure, zeta potential, shear-thinning, and thixotropy properties of the WEMBEs were also analysed.

3.1 Experiments and methods

3.1.1 Materials

Bisphenol-A type epoxy resin with an epoxy equivalent mass of 196 was supplied by Nantong Xingchen Synthetic Material Co., Ltd. Triethylenetetramine (TETA), acetic acid (HAc) and hydrochloric acid (HCl) were all purchased from Sigma-Aldrich. Glycidyl tertiary carboxylic ester (GTCE) was obtained from HEXION (Netherland). Propylene glycol methyl ether (PGME) was obtained from Sinopharm Chemical Reagent Co., Ltd. All materials were used without any further purification.

A base bitumen with a penetration grade of 60/70 (Pen 60/70), commonly used in Hong Kong, was used in this study. The bitumen emulsifier was provided by Ingevity under the trade name of INDULIN® W-5. The basic properties of the base bitumen and the emulsifier are listed in Table 3.1 and Table 3.2, respectively.

Table 3.1 Properties of base bitumen

Property		Value	Specification
Penetration (25 °C, 0.1 mm)		64.5	ASTM D5
Softening point (°C)		48.5	ASTM D36
Viscosity at 135 °C (mPa·s)		477.5	ASTM D4402
Ductility at 25 °C (cm)		78.5	ASTM D113
SARA fraction	Saturate	17.58 wt %	ASTM D4124
	Aromatic	46.85 wt %	
	Resin	26.20 wt %	
	Asphaltene	9.37 wt %	

Table 3.2 Properties of INDULIN® W-5 emulsifier

Property	Result
Physical state	Liquid
Color	Dark brown
Odor	Fish amine-like
pH	11.9
Density (25 °C, g/cm^3)	1.09
Solid content (wt %)	40.0
Viscosity (25 °C, mPa·s)	1200

3.1.2 Synthesis of waterborne curing agent (WCA)

In this study, the waterborne curing agent (WCA) was synthesized in lab. The obtained WCA has a linear molecular structure, and there are amine groups at both ends of the WCA molecules, which is hydrophilic after ionization. On the other hand, the middle part of the WCA molecule is hydrophobic. Therefore, the WCA can be used as a surfactant for epoxy resin. The epoxy resin was then emulsified by WCA to prepare the waterborne epoxy emulsion. With the evaporation of water, the curing reaction between the two parts proceeds. What interesting is that the synthesized WCA can act as a surfactant for epoxy resin as well as a hardener. The prepared waterborne epoxy resin emulsion can be then used to modify bitumen emulsion by simply stirring. Some previous studies have used commercial waterborne epoxy resins in bitumen emulsions [135, 136]. Though these products are readily available, their compositions or molecular structures are generally unknow to the users. To have a better understanding and control of the material composition and performance, the waterborne epoxy resin was synthesized in lab. The detailed procedure is described as below.

The synthesis procedure of the WCA is shown in Figure 3.1 [137]: 1) a 250ml four-necked flask equipped with a stirrer, reflux condenser and nitrogen gas, was heated by a water bath and charged with TETA; 2) the epoxy dissolved in PGME was added dropwise and reacted for 4 h at 65 °C; 3) followed by the incorporation of GTCE, the temperature was then increased to 70 °C and kept constant for 3 h; 4) the reactant product was vacuum distilled to remove the solvent; 5) acetic acid (HAc) was added to protonate the curing agent. The mole ratio of epoxy resin, TETA and GTCE was 1:2.2:1. Figure 3.2 depicts the equipment set-up for WCA synthesis. The light yellow WCA with a solid content of 60% was obtained by adding deionized water dropwise with stirring (Figure 3.3 (a)).

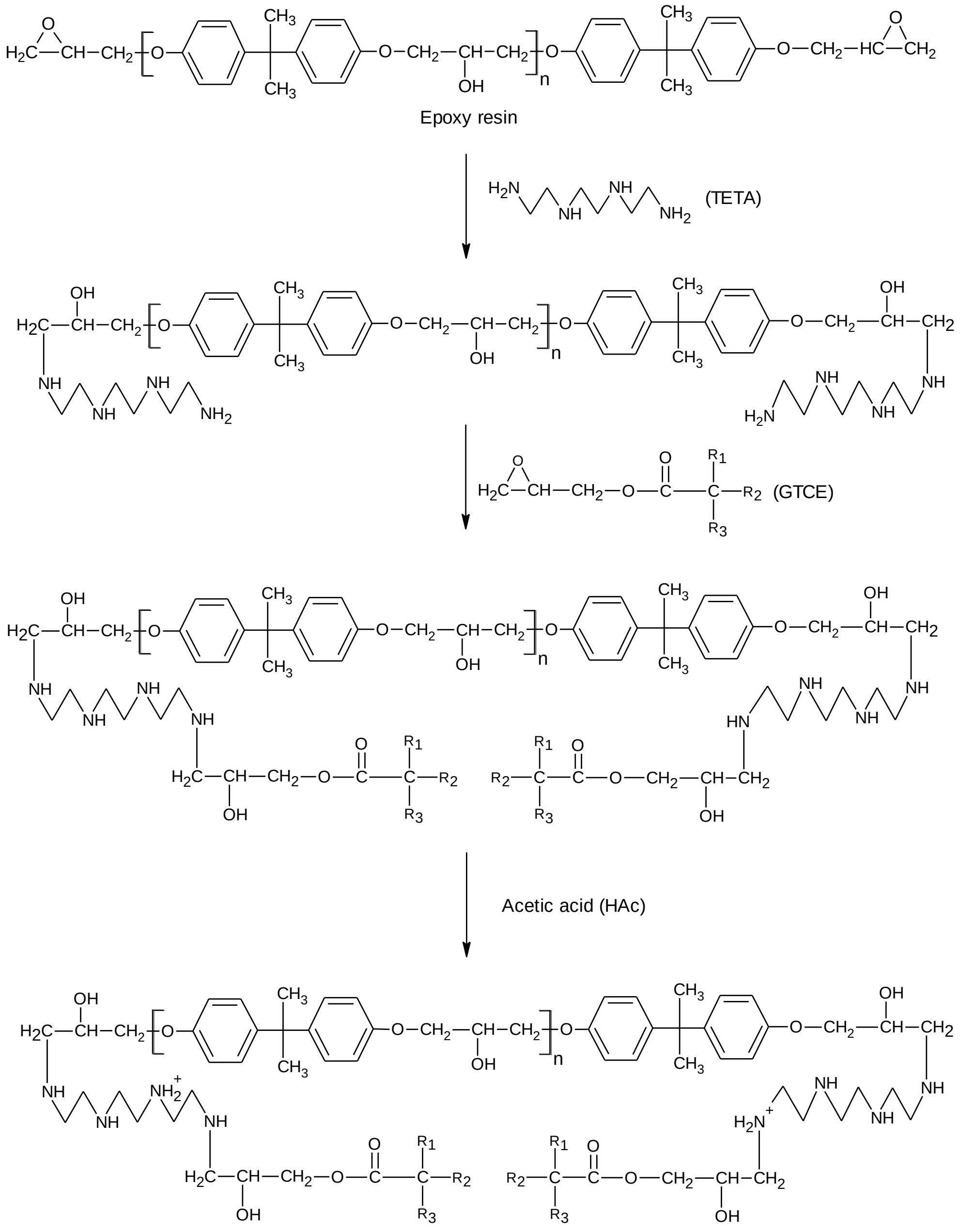

Figure 3.1 Synthesis procedure of waterborne curing agent

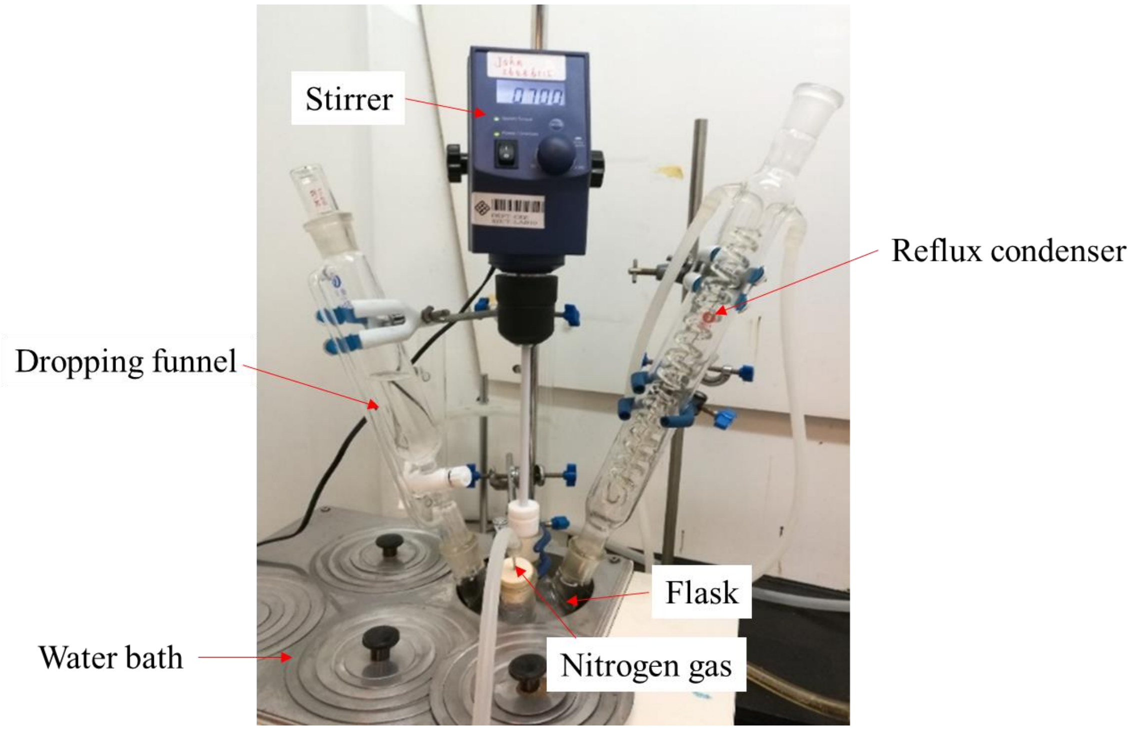

Figure 3.2 Equipment set-up for WCA synthesis

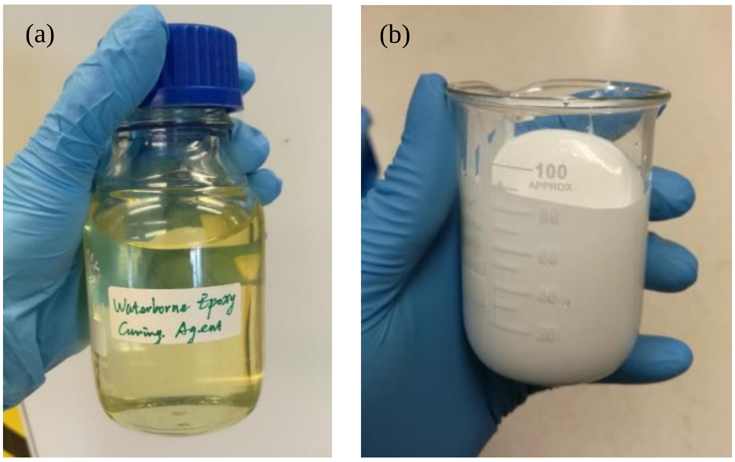

Figure 3.3 The synthesized (a) waterborne curing agent and (b) waterborne epoxy emulsion

3.1.3 Preparation of waterborne epoxy emulsion

The WCA was mixed with epoxy resin in a three-necked flask to produce the epoxy emulsion with a solid content of 60% by weight. Based on the stoichiometric calculation, the weight ratio of epoxy resin and WCA was determined to be 4:3. Deionized water was dropped slowly using a dropping funnel during the stirring of the two parts of epoxy emulsion. This process was continued by stirring at a speed of 700-800 rpm for 5 min at the ambient temperature. The obtained milky white waterborne epoxy emulsion is shown in Figure 3.3 (b).

3.1.4 Preparation of waterborne epoxy modified bitumen emulsion

To prepare bitumen emulsion, base bitumen was preheated to 150 °C. Meanwhile, by mixing emulsifier and deionized water at 60 °C, and with the addition of hydrochloric acid solution to a pH value of 2.0-2.5, the so-called "soap water" was prepared. The amount of emulsifier was 3% by weight of bitumen as suggested by the supplier. The preheated bitumen and “soap water” were then emulsified in a colloid mill (Jiaxing Mide Machinery Co., Ltd.) at a speed of 2,840 rpm to produce the bitumen emulsion with a solid content of ~63.0% by weight.

The bitumen emulsion and epoxy resin emulsion were mixed and stirred at a speed of 200-300 rpm for about 10 min to prepare a homogeneous WEMBE (Figure 3.4). Figure 3.5 represents a schematic structure of the WEMBE, where the bitumen particles are stabilized by cationic emulsifier, while the waterborne epoxy emulsion is distributed in the aqueous phase. Epoxy resin emulsion were added into bitumen emulsion in three different percentages: 1wt%, 3wt%, and 5wt%, and the corresponding WEMBEs were denoted as WEMBE-1, WEMBE-3, and WEMBE-5, respectively. All the percentages were based on the solid weight of emulsions. The bitumen emulsion without waterborne epoxy resin was also evaluated as a control material and denoted as WEMBE-0.

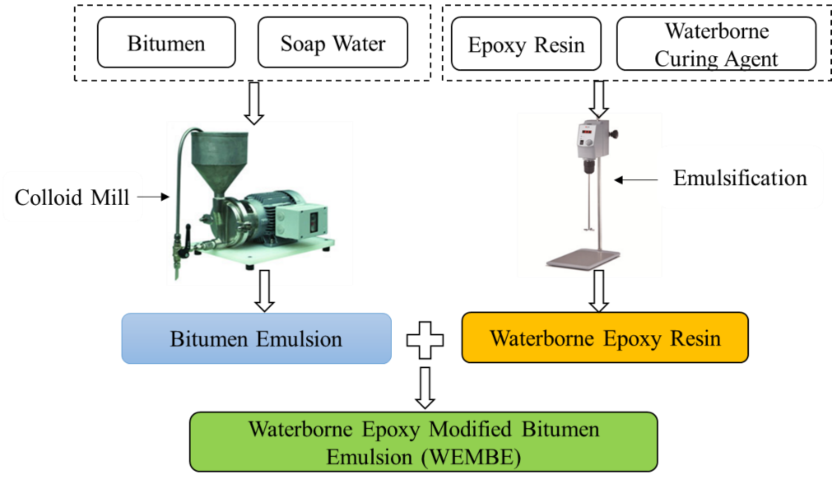

Figure 3.4 Procedure of waterborne epoxy bitumen emulsion preparation

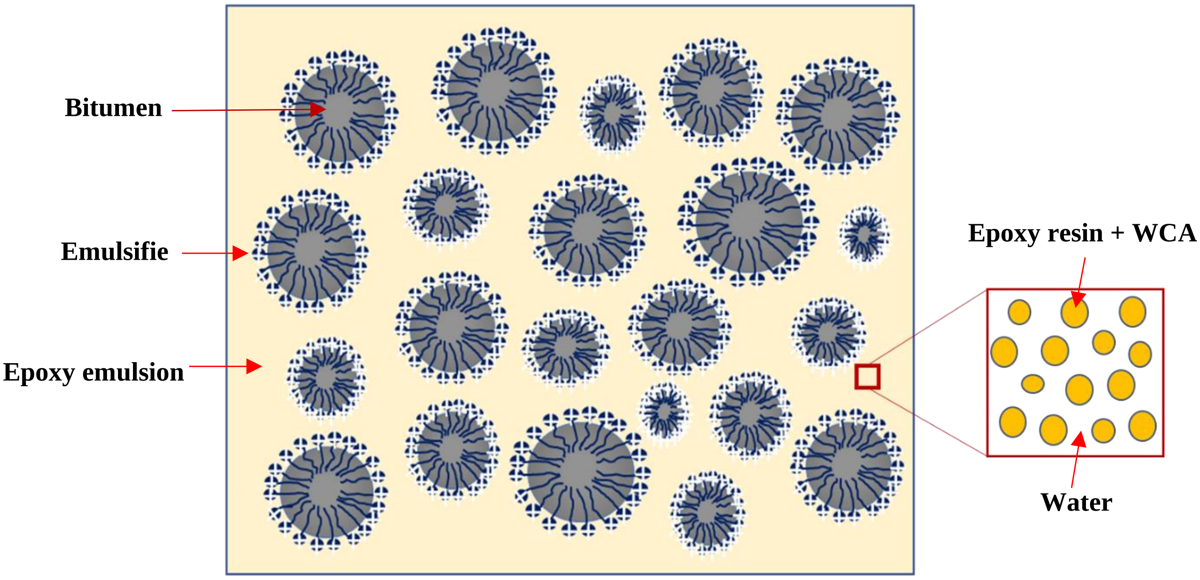

Figure 3.5 Schematic structure of waterborne epoxy bitumen emulsion

3.1.5 Characterization

Fourier transform infrared spectroscopy (FTIR)

An infrared spectrometer (Spectrum Two, PerkinElmer, Figure 3.6) was used to analyse the FTIR spectra of WCA in the synthesis procedure with a 4 cm^{-1} resolution between 400 and 4,000 cm^{-1}. Three replicates were measured for each specimen.

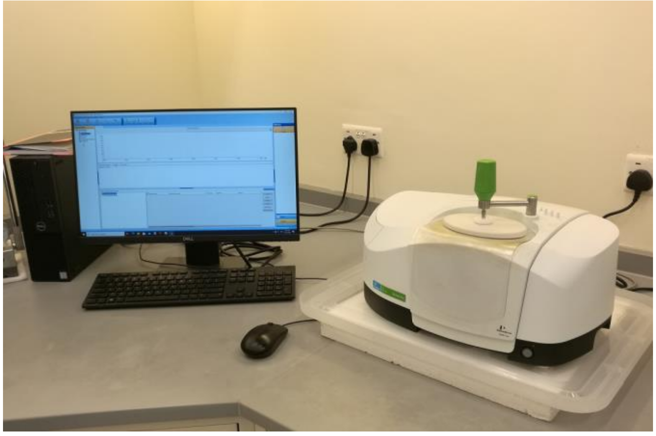

Figure 3.6 FTIR spectrometer

Particle size distribution measurement

The particle size distributions of WCA and waterborne epoxy emulsion were measured using the Zetasizer (Nano ZS90, Malvern, Figure 3.7). All the samples were 1000-fold diluted with deionized water prior to test. At least two measurements were performed for each specimen.

Figure 3.7 Zetasizer

Zeta potential

Zeta potential was also measured with the Zetasizer (Nano ZS90, Malvern). The equipment first measures the electrophoretic mobility of the droplets dispersed in aqueous solutions by applying a certain electric field, and then automatically calculates the zeta potential. Three replicates were measured for each specimen.

Thermogravimetric analysis (TGA)

The TGA of the epoxy resin, WCA, as well as the cured waterborne epoxy resin was carried out on a TGA/DSC 3+ instrument (METTLER TOLEDO, Figure 3.8) at a heating rate of 10 °C/min from 30 °C to 800 °C. The sample weight was approximately 5 mg and the measurement was performed under nitrogen atmosphere at a purge rate of 40 ml/min.

Figure 3.8 Thermogravimetric analysis (TGA)

Confocal laser scanning microscopy (CLSM)

A Leica TCS SPE Confocal Microscope (Figure 3.9) was used to examine the microstructures of WEMBEs. The images were captured in fluorescent mode using an argon-krypton laser with a wavelength of 488 nm (blue light). To prepare the WEMBE samples, the emulsion was first slightly stirred, and then 2 μL of the emulsion was dropped on a microscope glass slide with a pipette, which was then covered with a glass. The specimens were observed under the CLSM within 5 min to ensure that the emulsions stay in liquid state.

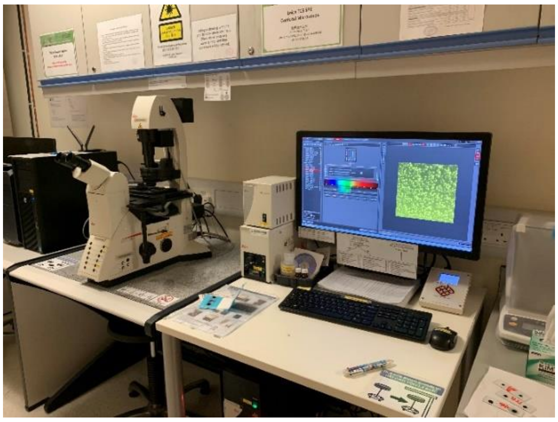

Figure 3.9 Confocal laser scanning microscopy (CLSM)

Shear viscosity

The shear viscosity of WEMBEs was measured with the dynamic shear rheometer (DSR, model MCR702 produced by Anton Paar, Figure 3.10). Because of the liquid state of the emulsion, the concentric-cylinder measuring system was used. The inner diameter of the cylinder was measured to be 18.8 mm, and the diameter of the rotator was measured to be 16.6 mm. Thus, the gap between the cylinder and the rotator was 0.6 mm during testing. The emulsion was slightly stirred prior to measurement. Approximately 5 ml of emulsion was added into the cylinder with a pipette. The shear viscosity was measured by increasing the shear rate from 0.01 s^{-1} to 200 s^{-1} at 23 ± 0.5 °C. Each measurement would take around 10 min. The shear rate was then decreased from 200 s^{-1} to 0.01 s^{-1} without rest, and the viscosity was recorded. At least two replicates were measured for each emulsion.

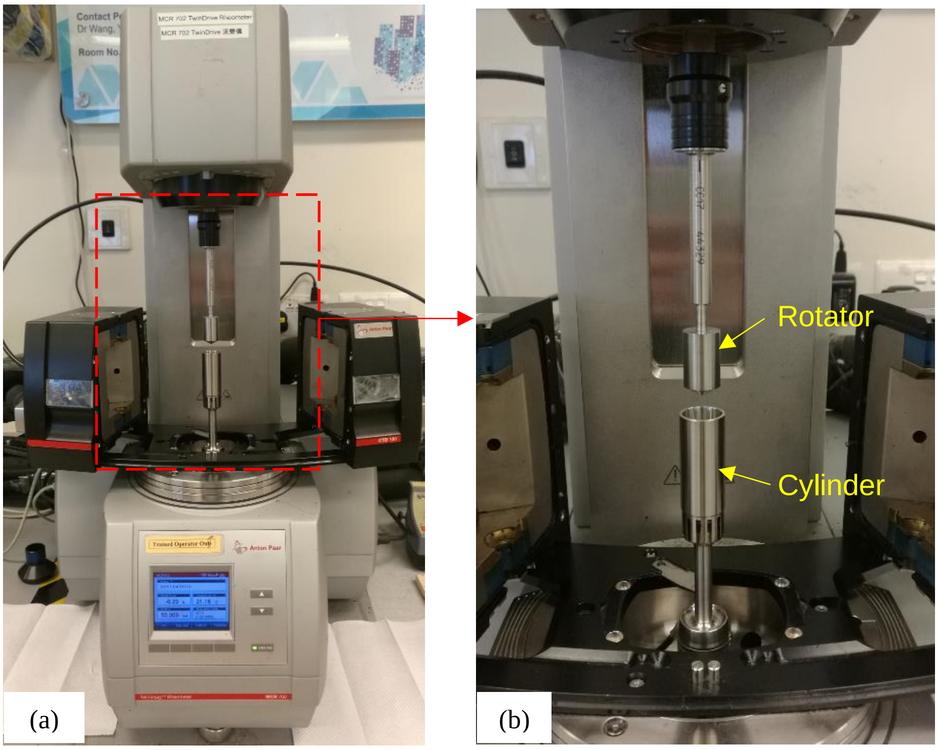

Figure 3.10 Shear viscosity equipment set-up: (a) MCR 702 concentric-cylinder measuring system, and (b) a closer look-up of the cylinder and the rotator

3.2 Results and discussion

3.2.1 Synthesis of waterborne curing agent

In the first step of WCA synthesis, epoxy resin reacted with TETA. Ring-opening reaction took place at both end oxirane groups and TETA was attached to the epoxy resin backbone. Then, the oxirane group in GTCE reacted with the primary amines. Finally, the product was neutralized with HAc to obtain the self-emulsifying WCA. The hydrophilic amines at both ends of the molecules can provide emulsifying ability and react with epoxy resin to form an inter-connected polymer network.

Figure 3.11 presents the FTIR spectra of Epoxy resin, Epoxy-TETA and Epoxy-TETA-GTCE, which illustrate the chemical reactions during the synthesis of WCA. Table 3.3 further details the FTIR band assignment of these materials. The peak at 917 cm^{-1} corresponding to the characteristic stretching absorption of the oxirane ring in epoxy resin could hardly be seen in the FTIR spectra of (b) and (c), indicating that the ring-opening reaction between epoxy resin and TETA had taken place. The presence of the broad peak located at 3,290 cm^{-1} in spectrum (b) ascribed to the absorption of N-H bonding also confirms such reaction. In addition, the distinct peak at 1,724 cm^{-1} in spectrum (c) is attributed to the absorption of ester carbonyl group of Epoxy-TETA-GTCE, revealing the reaction of GTCE with $-NH_2$ in Epoxy-TETA. It can therefore be inferred that the waterborne curing agent was successfully synthesized.

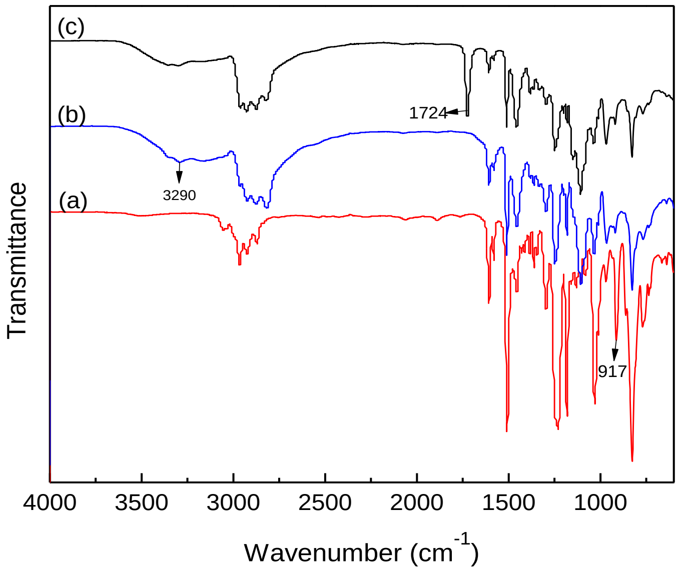

Figure 3.11 FTIR spectra of: (a)Epoxy, (b)Epoxy-TETA and (c)Epoxy-TETA-GTCE

Table 3.3 Characteristic FTIR Band Assignments of Epoxy, Epoxy-TETA and Epoxy-TETA-GTCE

Wavenumber (cm^{-1})	Band assignment
3,362	O−H stretching
3,290	N−H stretching
2,927	methyl groups
2,873	methylene groups
1,724	C=O stretch
1,606, 1,507, 1,454	C−C stretch in aromatic ring
1,230, 1,107, 1,032	C−O−C stretch (ether groups)
1,182	O−H bend
917	oxirane ring

3.2.2 Particle size measurement

Figure 3.12 (a) and (b) present the particle size distributions of the prepared WCA and waterborne epoxy emulsion, respectively. As shown in Figure 3.12 (a), the diameter of WCA particles distributed in the range of 24-120 nm with a mean value of 55 nm. The small particle size evidenced the strong hydrophilic property and emulsifying ability of the synthesized WCA. While the particle size distribution of waterborne epoxy emulsion was in the range of 140-400 nm, with a mean particle size of 247 nm.

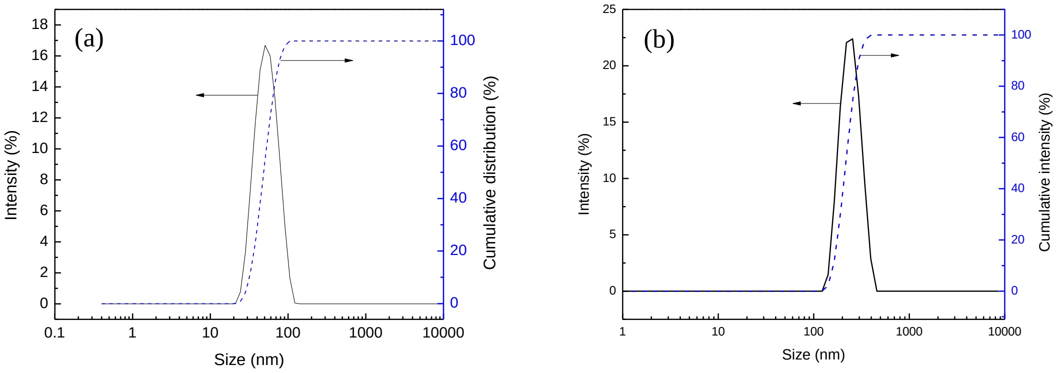

Figure 3.12 Particle size distribution of: (a) waterborne curing agent and (b) waterborne epoxy resin

3.2.3 Thermal stability

The TGA tests were performed to evaluate the thermal stability of the epoxy resin before and after curing. Figure 3.13 (a) shows the TGA as well as the DTG (derivative of TGA) curves for both epoxy resin and WCA, and Figure 3.13 (b) shows the TGA and DTG curves of the cured epoxy resin. Table 3.4 presents the initial decomposition temperature (T_i, corresponding to the temperature of the first 5% weight loss) and the maximum decomposition temperature (T_{max}, corresponding to the peak temperature in the DTG curve).

It can be seen that the T_i of epoxy resin was 273 °C, and it degraded rapidly with temperature increased beyond that. The epoxy resin DTG curve has only one peak, and the maximum decomposition temperature (T_{max}) was determined to be 338 °C. On the other hand, the WCA showed a three-stage weight loss profile from the TGA curve, and the corresponding DTG curve shows three peaks. It is noted that the first peak in the DTG curve of WCA is located around 139 °C, which may result from the evaporation of the residual solvent. The boiling point of the solvent PGME is around 120 °C, while the decomposition of polymers normally takes place at much higher temperatures. In addition, the primary decomposition temperature (the third peak) of WCA is 360 °C, which is higher than that of the epoxy resin, indicating that the molecular weight of WCA is larger than epoxy resin. Furthermore, the maximum decomposition temperature of the cured epoxy resin was 364 °C, which is higher than that of the uncured epoxy resin and WCA, indicating that the molecular weight increased after curing reaction of epoxy resin and WCA, and thus the cured epoxy resin become more thermally stable.

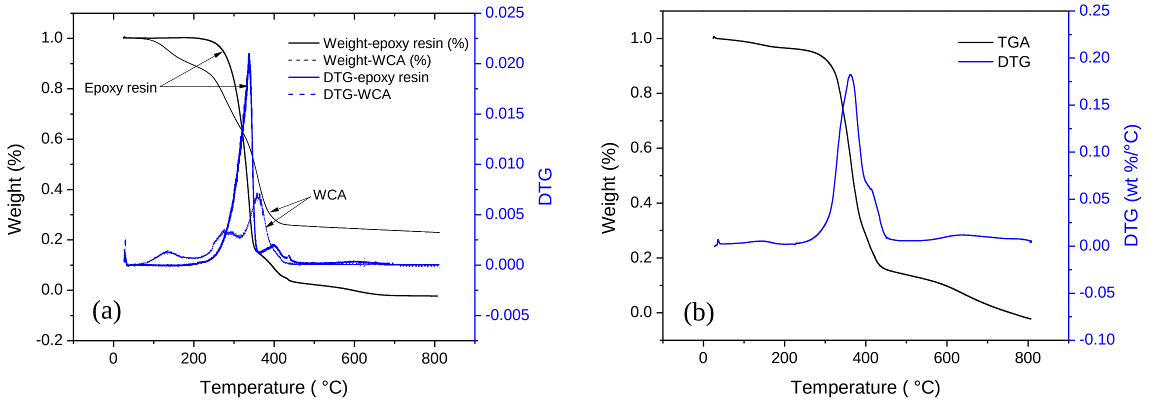

Figure 3.13 TGA and DTG curves of: (a) epoxy resin and WCA, and (b) the cured epoxy resin

Table 3.4 Thermal stability of epoxy resin, WCA, and the cured epoxy resin

Sample	T_i (°C)	T_{max} (°C)
Epoxy resin	273	338
WCA	139	135, 280, 360
Cured epoxy resin	271	364

3.2.4 Confocal laser scanning microscopy analysis

There has been quite a lot of studies on the microstructure of polymer modified bitumen (PMB) employing the fluorescence microscopy (FM) [138-142]. Polymers generally show strong fluorescence emissions, while bitumen lacks such effect [105]. Hence, the FM is able to distinguish the polymer phase and the bitumen phase in PMB, and thus the microstructure of the polymer distribution in PMB can be obtained. CLSM offers several distinct advantages over traditional FM, such as the ability to control depth of field and reduction of background information from the focal plane [143]. As a result, the CLSM technique has been widely used to assess the microstructure of polymer modified bitumen [138, 144, 145].

This study employs the CLSM to characterize the microstructures of WEMBEs. Figure 3.14 compares the CLSM images of WEMBE-0 and WEMBE-3 (the images of WEMBE-1 and

WEMBE-5 are not presented for simplicity, as they are very similar with WEMBE-0 and WEMBE-3). It can be seen that both emulsions show identical microstructure, and the presence of waterborne epoxy resin cannot be identified from the images. The bright yellow particles represent the bitumen droplets. It can be observed that the bitumen droplets are very close to each other, and they are separated by thin films of aqueous phase. Note that the size of the waterborne epoxy resin droplets is in the range of a few hundred nano meters, which may be too small to be observed. On the other hand, the epoxy resin could also show fluorescence emissions, which cannot be distinguished from the fluorescence emissions of the bitumen particles.

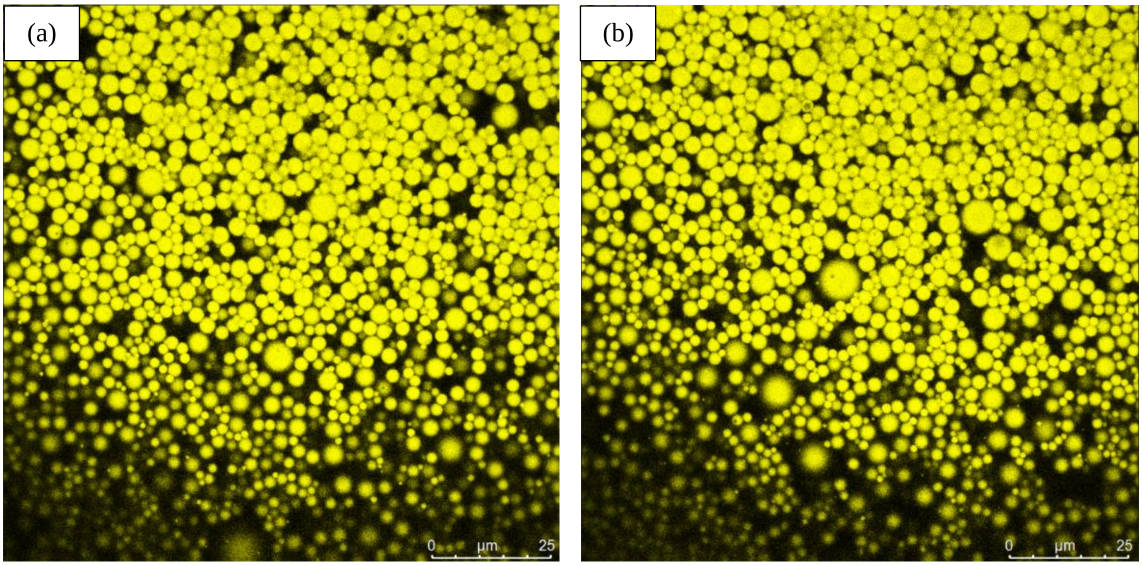

Figure 3.14 CLSM of: (a) WEMBE-0 and (b) WEMBE-3 (scale bar: 25 µm)

Generally, bitumen has very few fluorescence effects, but the bitumen particles were observed under CLSM. The reason may be that all the bitumen particles are surrounded and stabilized by emulsifier in bitumen emulsion, and the emulsifier, coming from the lignin derivatives, may induce this fluorescence effect. To confirm this hypothesis, the emulsifier was then evaluated by the CLSM. From the image of the emulsifier in Figure 3.15, it is clear that emulsifier shows the fluorescence effect. Thus, the fluorescence effect in bitumen emulsion is mainly induced by the emulsifier.

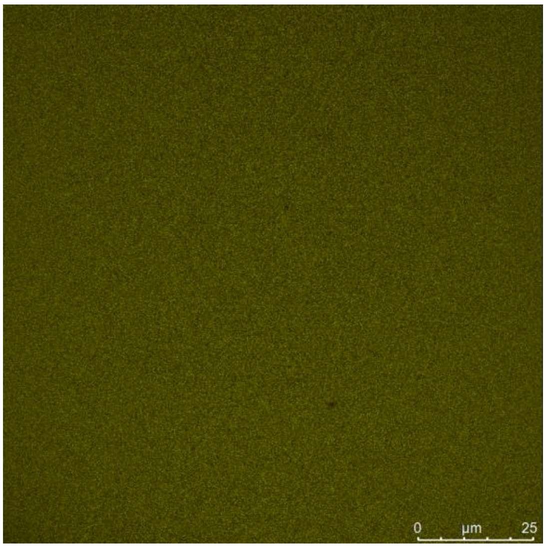

Figure 3.15 CLSM of emulsifier (scale bar: 25 µm)

The bitumen particles in Figure 3.14 are too concentrated and difficult to analyse. Thus, the bitumen emulsions were 10-times diluted with deionized water. The CLSM images of the diluted bitumen emulsions are shown in Figure 3.16, which indicates that the bitumen droplets became more dispersed after dilution. It can be noticed that most of the bitumen particles are within the size of 10 µm.

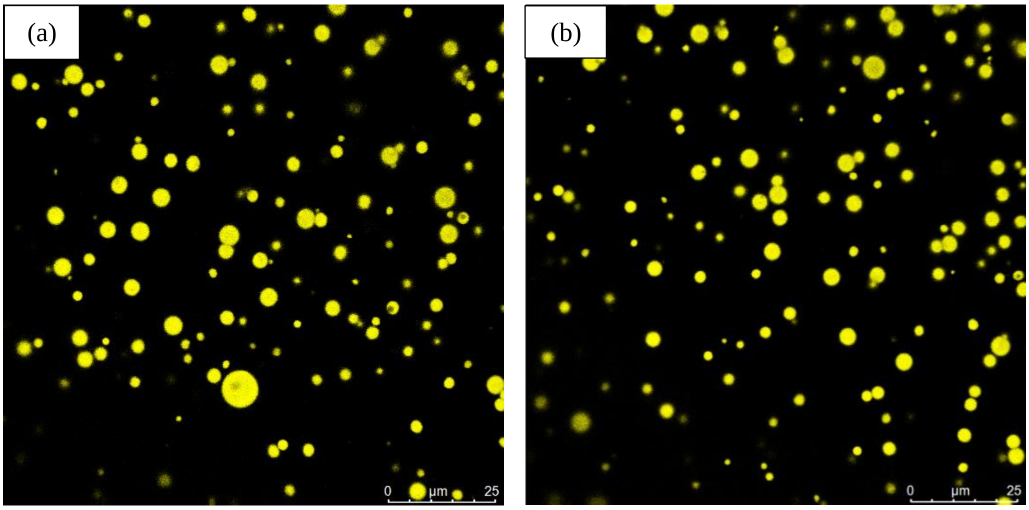

Figure 3.16 CLSM of the 10-times diluted bitumen emulsion: (a) WEBMBE-0, (b) WEMBE-1, (c) WEMBE-3, (d) WEMBE-5 (scale bar: 25 µm)

Continued

Figure 3.16 Continued

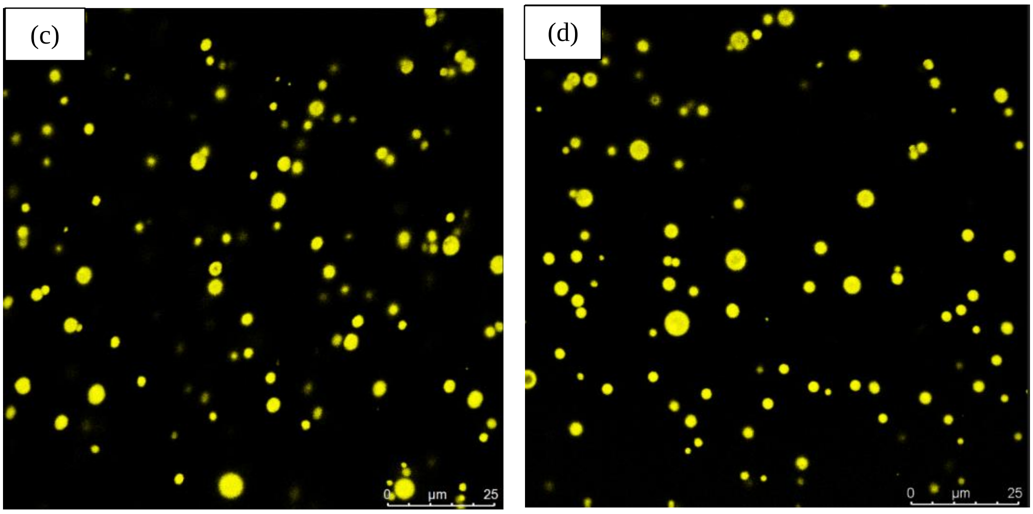

Bitumen emulsion is a thermodynamically unstable system [44], and the bitumen droplets would generally flocculate and coalescence to form bigger particles, thus reduce the interfacial energy. To evaluate such effect, the four groups of bitumen emulsions with different amounts of waterborne epoxy resin were stored at ambient room conditions for 5 days. The emulsions were then 10-times diluted with deionized water, and the CLSM images were subsequently taken as shown in Figure 3.17.

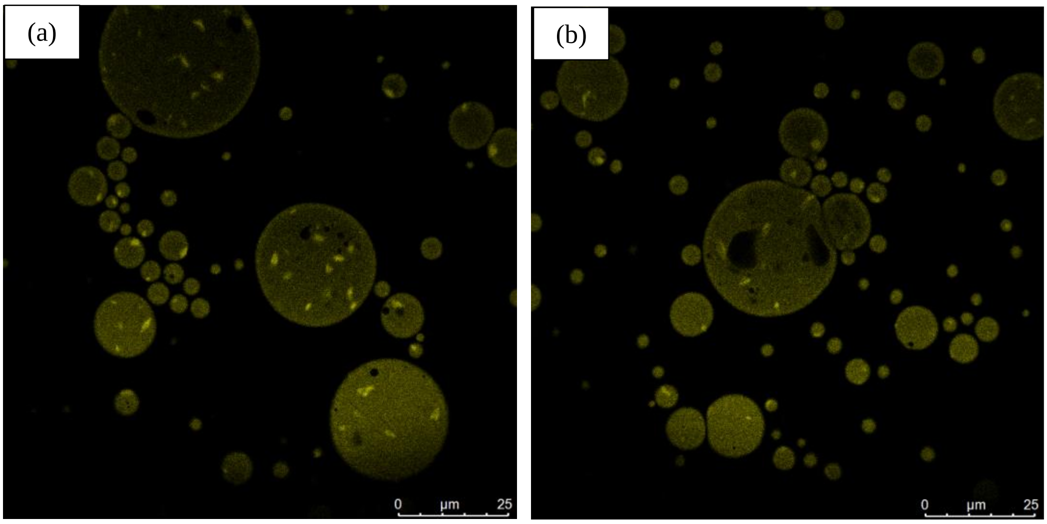

Figure 3.17 CLSM of bitumen emulsion after 5 days: (a) WEBMBE-0, (b) WEMBE-1, (c) WEMBE-3, (d) WEMBE-5 (scale bar: 25 μm)

Continued

Figure 3.17 Continued

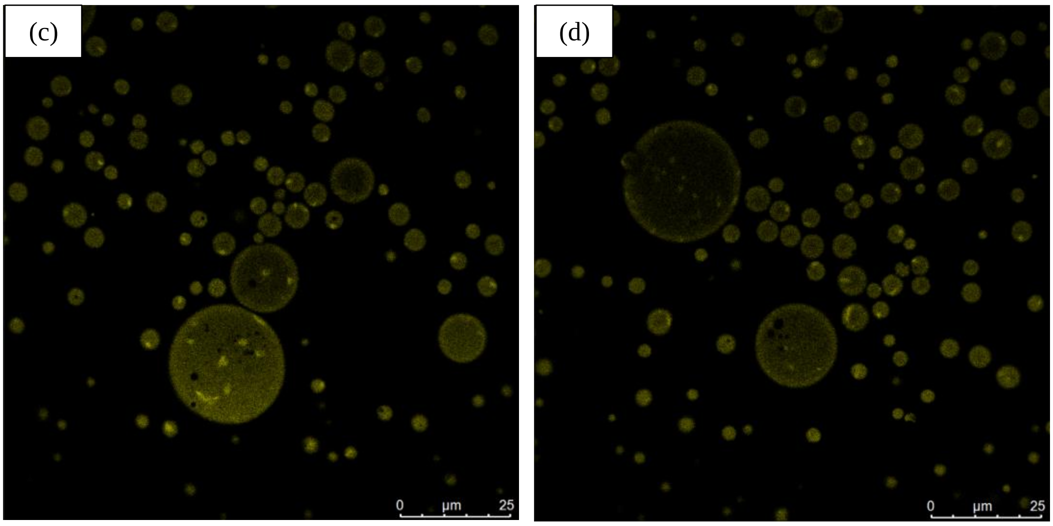

It can be seen that the bitumen particles generally become larger after storing for 5 days, and flocculation of particles is also observed. It is interesting to note in Figure 3.17 that WEMBE-0 and WEMBE-1 have larger bitumen particles compared with WEMBE-3 and WEMBE-5. The presence of waterborne epoxy resin increased the viscosity of the aqueous phase. On the other hand, the waterborne epoxy resin acted as a barrier between the bitumen droplets, thereby reducing the possibility of the bitumen droplets flocculation. Hence, less large particles in WEMBE-3 and WEMBE-5 were observed after 5 days of storage in comparison with those of the WEMBE-0 and WEMBE-1.

Flocculation of emulsions may occur when the van der Waals attractive energy exceeds the repulsive energy [146], and coalescence mainly results from the thinning and disruption of the liquid film between the droplets, with the ultimate joining of these droplets [147]. Generally, the flocculation of bitumen droplets takes place first, when the droplets become close enough, coalescence happens subsequently (Figure 3.18). Figure 3.19 shows the flocculation and coalescence of the bitumen emulsion. The flocculation is weak and reversable. Thus, the particles can dissociate with each other by slightly shearing. However, the coalescence is not reversable. As a result, the size of the bitumen particles would increase with time during the storage of bitumen emulsion.

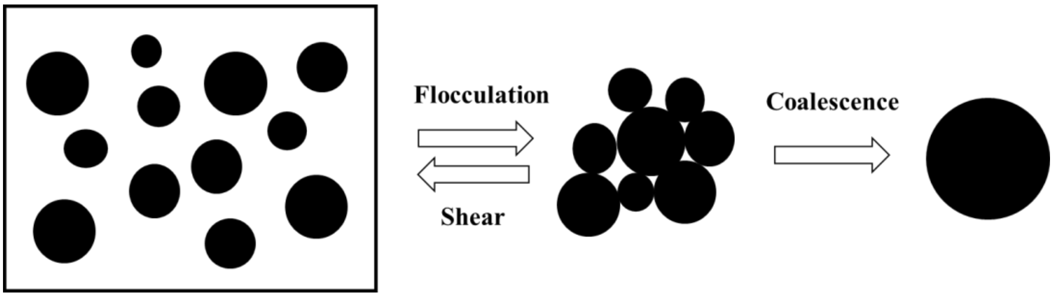

Figure 3.18 Schematic of bitumen emulsion flocculation and coalescence

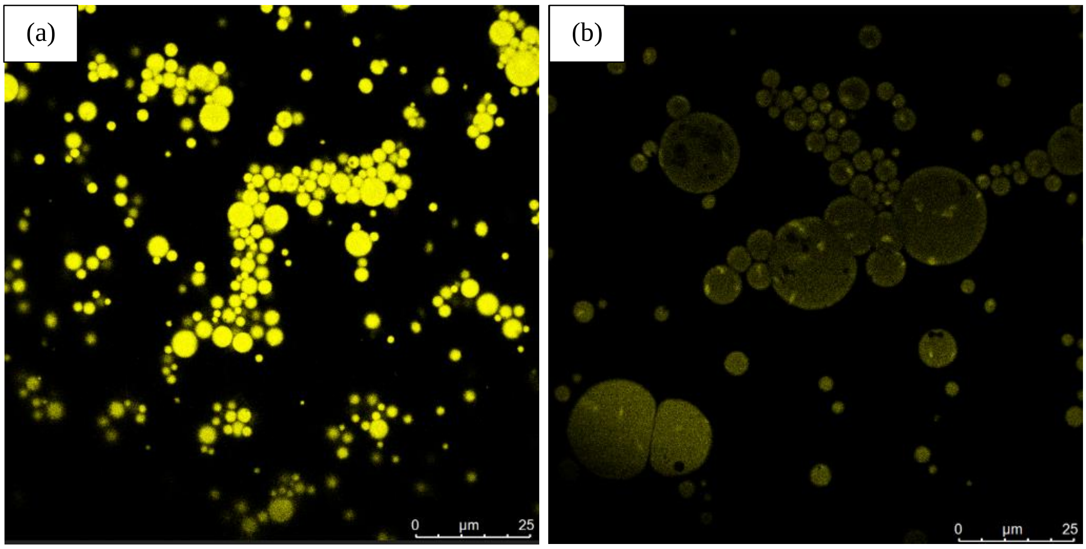

Figure 3.19 Flocculation (a) and coalescence (b) of bitumen droplets (scale bar: 25 µm)

3.2.5 Zeta potential of WEMBEs

Figure 3.20 shows the zeta potentials of WEMBEs. Three measurements were performed on each specimen. It can be found that the zeta potential of the pure bitumen emulsion was around 50 mV. The zeta potentials of the waterborne epoxy resin modified bitumen emulsions were similar with that of the pure bitumen emulsion, indicating that the stability of the bitumen emulsion was not affected by the incorporation of waterborne epoxy resin. As both the bitumen emulsion and waterborne epoxy resin were of cationic type in this study, and the particle size of the waterborne epoxy resin missiles were smaller than that of the bitumen emulsion particles, the waterborne epoxy resin has good compatibility with bitumen emulsion. The good compatibility between waterborne epoxy resin and bitumen emulsion plays an important role in the manufacturing and application of this novel material. This result indicates that the waterborne epoxy resin and bitumen emulsion can be simply mixed prior to application.

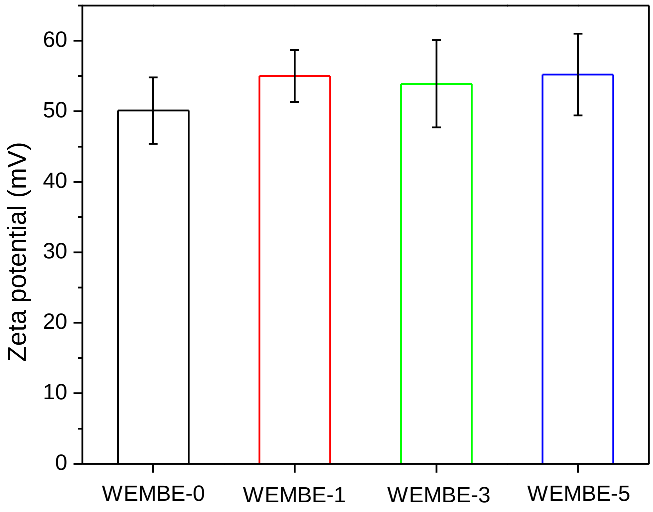

Figure 3.20 Zeta potential of bitumen emulsions

3.2.6 Shear-rate dependence of viscosity

Figure 3.21 shows the shear-rate dependence of viscosity for the bitumen emulsions, which demonstrates the typical shear-thinning behavior of the bitumen emulsions. The viscosity of bitumen emulsion generally decreases with increasing of shear rate at lower shear rate, which represents pseudoplastic behavior below 10 s^{-1}. Such viscosity profile can be attributed to the interaction between the bitumen droplets in bitumen emulsion. As can be seen from Figure 3.14, the closely packed bitumen droplets would form certain flocs at rest, which are weak and reversable upon shearing. The interactions between the bitumen droplets are disrupted when subjected to shear stress, resulting in a reduction in the viscosity of bitumen emulsion. With further increasing of the shear rate, the bitumen emulsions with different amount of waterborne epoxy resin emulsions showed quite different behaviors. For WEMBE-0, the viscosity dropped to a constant value at higher shear rate, which demonstrated typical Newtonian behavior. The shear-thinning effect of bitumen emulsion was also reported by Mercado and Fuentes [148], however, the Newtonian region was not observed in their study presumably because the shear rate they applied was not high enough.

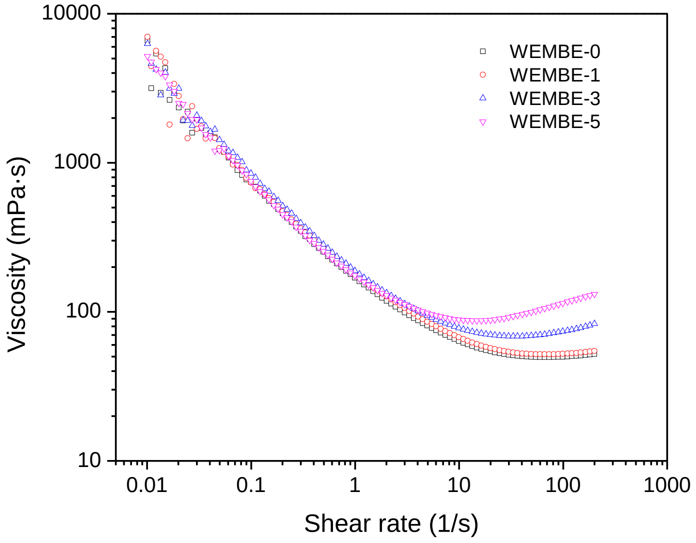

Figure 3.21 Shear rate dependence of viscosity for bitumen emulsion

On the other hand, the viscosity profile of waterborne epoxy modified bitumen emulsions is quite different, which shows a shear-thinning region at lower shear rate, followed by a shear-thickening region at higher shear rate. The shear-thickening behavior is also called dilatancy. The dilatancy effect becomes more pronounced with higher contents of waterborne epoxy resin, indicating that indeed the waterborne epoxy resin is responsible for the dilatancy effect at higher shear rate. The reason may be that the epoxy resin is stabilized by WCA, and the molecular structure of WCA is very long. Thus, at higher shear rate, the WCA emulsifiers began to get entangled with each other, which contributed to the increase of the overall viscosity. Figure 3.22 represents a schematic structure of the waterborne epoxy resin modified bitumen emulsion. Similar effect was also reported by Otsubo and Prud'homme [149] in a paraffin oil-in-water emulsion, which also showed pseudoplastic behavior at lower shear rate and dilatancy at higher shear rate.

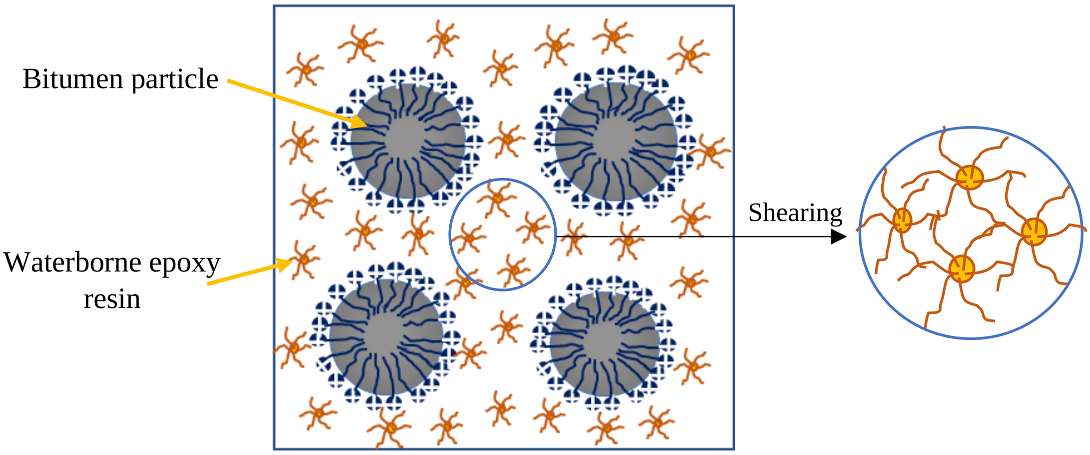

Figure 3.22 Schematic structure of the waterborne epoxy resin modified bitumen emulsion

To simulate the shear-rate dependence of the viscosity of emulsions or polymer melts, the Carreau model described by the following equation is generally applied [150].

$$\eta = \eta_\infty + \frac{\eta_0 - \eta_\infty}{(1+(\beta\dot{\gamma})^2)^\alpha} \tag{3-1}$$

where η_0 is the zero-shear viscosity, η_∞ is the viscosity at infinite shear rate, α is a dimensionless parameter, β is a time constant, and $\dot{\gamma}$ is the shear rate.

The fitting error is given as,

$$Error = \frac{1}{n}\sum_{i=1}^{n}\frac{|\eta_{e\_i} - \eta_{m\_i}|}{\eta_{e\_i}} \cdot 100\% \tag{3-2}$$

where η_{e_i} is the *i*th experiment data, η_{m_i} is the *i*th modelled data, and *n* is the total number of experiment data.

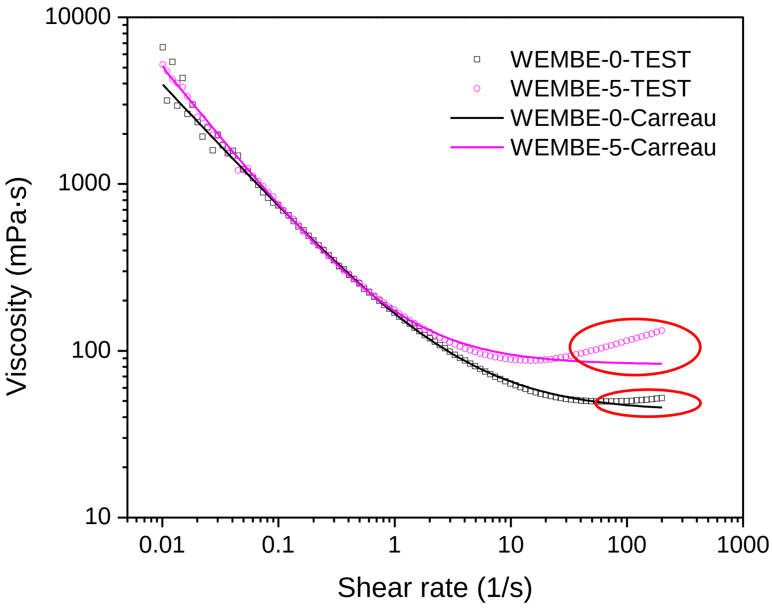

Figure 3.23 Viscosity simulation using Carreau model

Table 3.5 Fitting parameters of the Carreau model

Bitumen emulsion	η_0 (mPa·s)	η_∞ (mPa·s)	α	β	Fitting error (%)
WEMBE-0	60,253	43.3	0.37	3,811.9	4.17
WEMBE-1	55,520	45.0	0.37	3,534.8	5.78
WEMBE-3	86,178	60.6	0.40	3,776.9	5.14
WEMBE-5	1,083,954	82.7	0.43	48,699.4	7.14

Figure 3.23 shows the viscosity simulation of the bitumen emulsion with the Carreau model. For simplicity, only the viscosity simulations for WEMBE-0 and WEMBE-5 are presented. It can be seen that viscosity profile at the lower shear rate was simulated fairly well. However, significant deviation occurred at the higher shear rate, and the discrepancy increased for the bitumen emulsion modified by waterborne epoxy resin. The fitting parameters are shown in Table 3.5, and it is found that the fitting error increased with increasing concentrations of waterborne epoxy resin, which reached to 7.14% for WEMBE-5. The reason is that the Carreau model is a decreasing function. While the viscosity of WEMBE-0 demonstrates Newtonian behavior at higher shear rate. Regarding the waterborne epoxy resin modified bitumen emulsion, the dilatancy behavior at higher shear rate is observed. Both the Newtonian and the

dilatancy behavior cannot be simulated with the Carreau model. To solve this limitation, a power law model is added to the original Carreau model, which is referred to here as a "modified-Carreau" (MC) model given as below,

$$\eta = \eta_\infty + \frac{\eta_0 - \eta_\infty}{(1 + (\beta\dot{\gamma})^2)^\alpha} + m\dot{\gamma}^n \tag{3-3}$$

where m and n are the fitting parameters.

Figure 3.24 shows the bitumen emulsion viscosity simulated using the modified-Carreau model. It is clear that the viscosity of both WEMBE-0 and WEMBE-5 was well simulated with high accuracy. With respect to WEMBE-0, the modified-Carreau model can not only simulate the shear-thinning behavior at lower shear rate, but also the Newtonian behavior at higher shear rate. In addition, the dilatancy region of the waterborne epoxy resin modified bitumen emulsion at the higher shear rate was also successfully simulated.

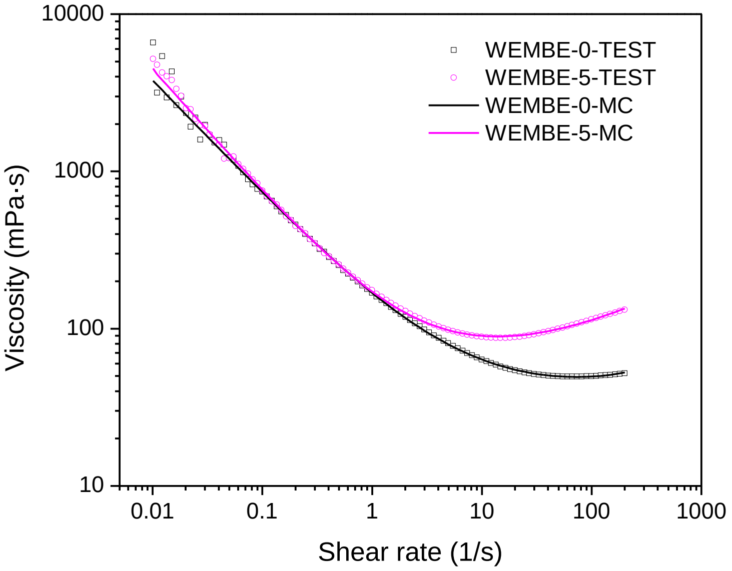

Figure 3.24 Viscosity simulation using the modified-Carreau model

Table 3.6 shows the fitting parameters of the modified-Carreau model. It can be seen that the fitting errors decreased significantly compared with the original Carreau model, which are all lower than 5%. The results indicate that the fitting accuracy of modified-Carreau model increased significantly compared with that of the original Carreau model. The original Carreau model can only simulate the shear-thinning behavior, while the modified-Carreau model can also simulate the Newtonian behavior as well as the dilatancy behavior. Thus, the modified-Carreau model can be more widely used.

Table 3.6 Fitting parameters of the modified-Carreau model

Bitumen emulsion	η_0 (mPa·s)	η_∞ (mPa·s)	α	β	m	n	Fitting error (%)
WEMBE-0	30,912.0	38.0	0.36	1,794.8	0.2	0.74	3.18
WEMBE-1	85,859.3	34.7	0.35	9,856.2	0.9	0.55	4.83
WEMBE-3	438,087.3	47.0	0.38	43,340.1	1.5	0.58	2.60
WEMBE-5	405,121.6	49.9	0.40	29,519.6	7.8	0.45	2.27

Figure 3.25 shows the shear-rate dependence of the stress for WEMBEs. The stress data at the shear rate of 0.01~200 s^{-1} were obtained simultaneously with the viscosity described above. It can be seen that the stress was similar in the shearing rate range of 0.01~10 s^{-1} and was very close for different WEMBEs. The stress of the waterborne epoxy resin modified bitumen emulsions increased more rapidly with shearing rate larger than 10 s^{-1}, because of the dilatancy effect at higher shearing rate.

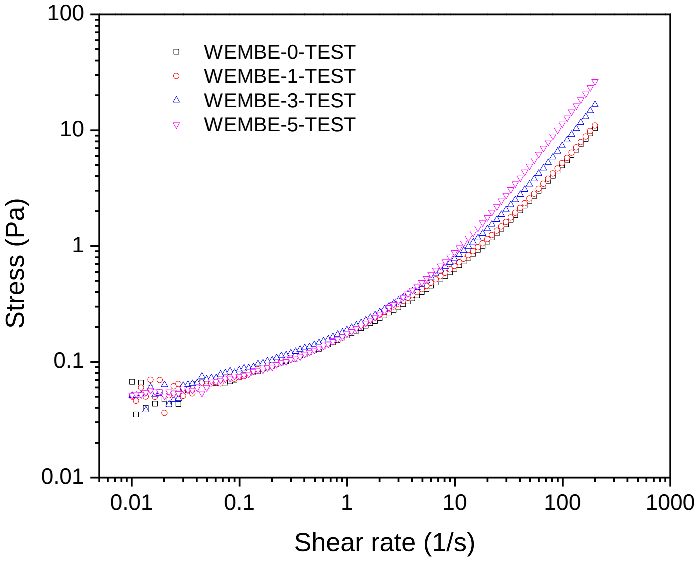

Figure 3.25 Shear-rate dependence of stress

The Herschel-Bulkley model as shown below is generally applied to simulate the shear-rate dependence of the stress [151].

$$\sigma = \sigma_{\beta} + k\dot{\gamma}^{n} \tag{3-4}$$

where σ_{β} is extrapolated yield value, *k* is a dimensionless parameter, and *n* is the power index.

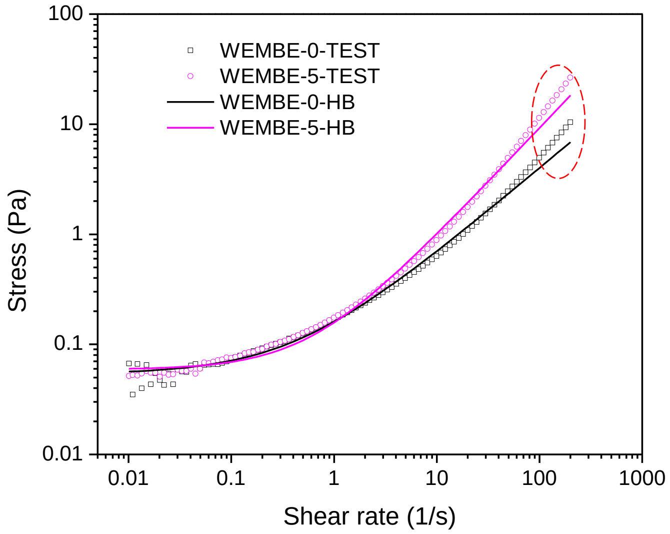

Figure 3.26 Shear stress fitted by Herschel-Bulkley model

It can be seen in Figure 3.26 that the HB model can well simulate the low shear rate stress, however, significant deviation was observed at higher shear rate region. The fitting parameters are presented in Table 3.7, which shows that the fitting errors are all larger than 9%.

Table 3.7 Fitting parameters of the Herschel-Bulkley model

Bitumen emulsion	σ_{β} (Pa)	k	n	Fitting error (%)
WEMBE-0	0.05	0.11	0.78	10.16
WEMBE-1	0.05	0.12	0.77	9.49
WEMBE-3	0.06	0.12	0.84	12.21
WEMBE-5	0.06	0.10	0.98	11.15

To solve this problem, one more power series is added into the original Herschel-Bulkley model, which gives the following modified Herschel-Bulkley (MHB) model,

$$\sigma = \sigma_{\beta} + k_1\dot{\gamma}^{n_1} + k_2\dot{\gamma}^{n_2} \tag{3-4}$$

where σ_{β} is extrapolated yield value, k_1 and k_2 are dimensionless parameter, and n_1 and n_2 are the power indexes.

Figure 3.27 shows the shear-rate dependence of the stress simulated by the MHB model. It can be seen that the model agrees very well with the test data for all the WEMBEs, and the fitting errors are all less than 3% (Table 3.8), which represents a significant decrease in comparison with the original Herschel-Bulkley model. It is noted that the σ_β for the bitumen emulsions was very small, which also indicates that the bitumen particles in the emulsion are only slightly contacted, and they disassociate easily when subjected to shearing.

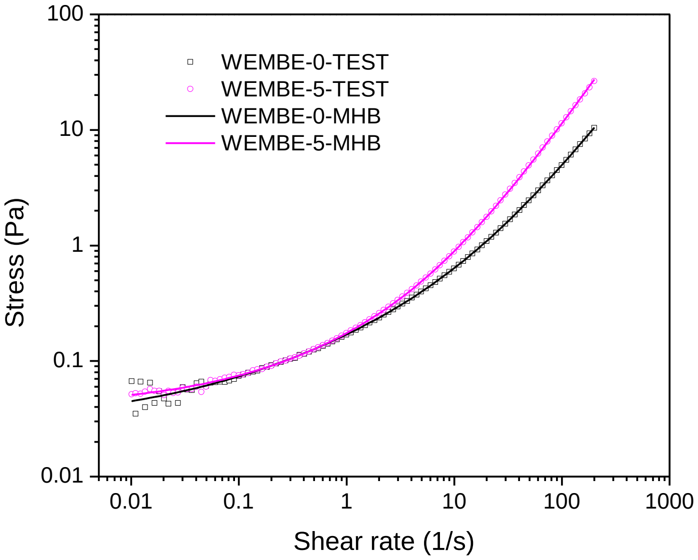

Figure 3.27 Shear stress fitted by modified Herschel-Bulkley (MHB) model

Table 3.8 Fitting parameters of the modified Herschel-Bulkley model

Bitumen emulsion	σ_β (Pa)	k_1	n_1	k_2	n_2	Fitting error (%)
WEMBE-0	0.03	0.01	1.21	0.12	0.47	2.95
WEMBE-1	0.03	0.01	1.26	0.13	0.51	2.49
WEMBE-3	0.03	0.02	1.25	0.14	0.45	2.43
WEMBE-5	0.04	0.02	1.33	0.11	0.53	1.44

3.2.7 Thixotropy of WEBMEs

For some emulsions, the viscosity decreases with increasing shear rate, and recovers to its original value with decreasing shear rate. Such reversible behavior of viscosity is referred to as the so-called thixotropy [152]. As figure 3.28 shows, all WEMBEs exhibited strong thixotropy. The viscosity at the decreasing shear rate curve (red dots) overlaps with that at the increasing shear rate (black dots). As shown in Figure 2.2, the secondary minimum depth becomes significant at intermediate zeta potential. Thus, weak flocculation of the bitumen emulsions could occur at static situation. Such flocculation is reversible, i.e., the flocs are disrupted by shearing, which can then reform on decreasing shear force or shear rate. In addition, the presence of waterborne epoxy resin did not affect the thixotropy of the bitumen emulsion.

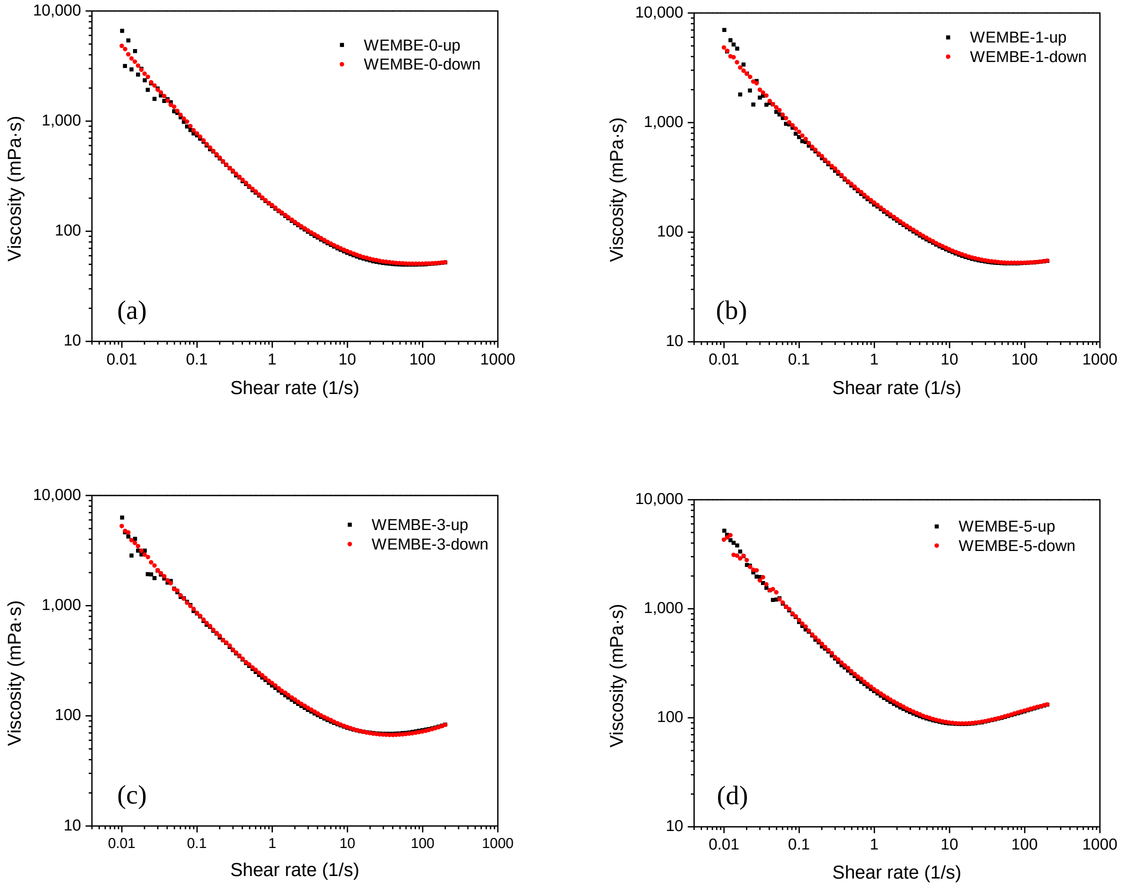

Figure 3.28 Thixotropy of emulsions: (a) WEMBE-0, (b) WEMBE-1, (c) WEMBE-3, and (d) WEMBE-5

(Note: ‘up’ indicates increasing of shear rate, and ‘down’ indicates decreasing of shear rate)

3.3 Summary

In this chapter, the waterborne curing agent (WCA) was synthesized and used to prepare the waterborne epoxy emulsion. The waterborne epoxy resin was subsequently used to modify bitumen emulsion. As the waterborne epoxy resin was a hydrophilic emulsion, it can be mixed with bitumen emulsion directly to prepare the WEMBE. In addition, both the waterborne epoxy resin emulsion and the bitumen emulsion were cationic type emulsions, thus they were compatible with each other. Therefore, the stability of the bitumen emulsion was preserved. The microstructure and rheological properties of the modified bitumen emulsion was then evaluated. The main findings of the study presented in this chapter are summarized below:

(1) The WCA synthesized in this study was dispersed in water with a very small mean particle size of 55 nm, indicating strong self-emulsifying ability. In addition, the WCA can effectively emulsify the epoxy resin, and the average diameter of the obtained epoxy resin droplets is 247 nm.

(2) The cured waterborne epoxy resin showed good thermal stability, which was generally stable below 270 °C.

(3) The zeta potential of the bitumen emulsion containing waterborne epoxy resin were similar with that of the pure bitumen emulsion, indicating the stability of bitumen emulsion was not affected by waterborne epoxy resin.

(4) The bitumen particles in the manufactured bitumen emulsion are mostly smaller than 10 μm, and become larger after storing for 5 days. However, the bitumen particles in bitumen emulsion with waterborne epoxy resin was smaller than the pure bitumen emulsion, indicating that the waterborne epoxy resin acts as a barrier between bitumen particles, thus hindered the bitumen particles from coalescence.

(5) Bitumen emulsion showed significant shear-thinning behavior at the lower shear rate region (0-10 s^{-1}). The pure bitumen emulsion then behaved like a Newtonian fluid at higher shear rate, while the waterborne epoxy resin modified bitumen emulsion showed shear-thickening behavior. The difference may be caused by the waterborne epoxy resin, which could become entangled with each other at higher shear rate, thus increasing the viscosity. Such phenomenon about the waterborne epoxy resin modified bitumen emulsion has not been reported previously.

(6) The bitumen emulsion demonstrated strong thixotropy effect. The interactions between bitumen particles in the emulsion can be disrupted by shear stress, and, when decreasing the shear rate, such interactions can reform subsequently.

CHAPTER 4 PERFORMANCE EVALUATION OF WEBERs

This chapter presents the overall evaluations of the waterborne epoxy resin modified bitumen emulsion residues (WEBERs). Section 4.1 describes the experiments conducted, including the infrared spectra, confocal laser scanning microscopy, dynamic shear test, aging, bond strength, and boiling test. Section 4.2 presents the results and discussions, including the microstructures of the emulsion residues, the temperature sweep and the multiple stress creep and recovery of the emulsion residues, the chemical and rheological analysis of the emulsion residues before and after being aged in the pressure aging vessel (PAV), the fatigue life characterization of WEBERs based on both time-sweep test and linear amplitude sweep (LAS) test, the bond strength with aggregate, and the resistance to moisture damage using the boiling water test.

4.1 Experiments and methods

Attenuated total reflection - Fourier transform infrared spectroscopy

ATR-FTIR (Spectrum Two, PerkinElmer) was used to analyse the FTIR spectra WEBERs (both the unaged and PAV aged specimens) with a 4 cm^{-1} resolution between 400 and 4,000 cm^{-1}. Each spectrum represents the accumulation of 32 spectra. The emulsion residues with 0wt%, 1wt%, 3wt%, and 5wt% of waterborne epoxy resin are denoted as WEBER-0, WEBER-1, WEBER-3, and WEBER-5, respectively. Three measurements were performed for each specimen.

Confocal laser scanning microscopy (CLSM)

A Leica TCS SPE Confocal Microscope was used to examine the fluorescence images of the emulsion residues. The images were recorded in fluorescent mode using an argon-krypton laser with a wavelength of 488 nm (blue light). The emulsion residue was obtained by placing a drop of emulsion on a microscope slide and dried at ambient temperature for 3 h, the cover glass was then placed on the specimen, and finally the specimen was put into a forced air oven at 60 °C for 3-4 h to fully evaporate the water.

Temperature sweep test

The rheological properties of WEBERs were characterized through dynamic shear tests using a DSR (model MCR702, Anton Paar, Figure 4.1). A thin layer of waterborne epoxy resin bitumen emulsion was spread on a silicone paper and kept at room temperature for 3 days, followed by 24 h conditioning in oven at 60 °C. Such a procedure was adopted to ensure the evaporation of water and fully curing of epoxy resin. Temperature sweep from 40 to 94 °C at 6 °C increments was applied with a testing frequency of 10 rad/s. All tests were conducted within the linear viscoelastic region. The complex modulus (G*) and phase angle (δ) of each sample were determined. Two measurements were performed for each specimen.

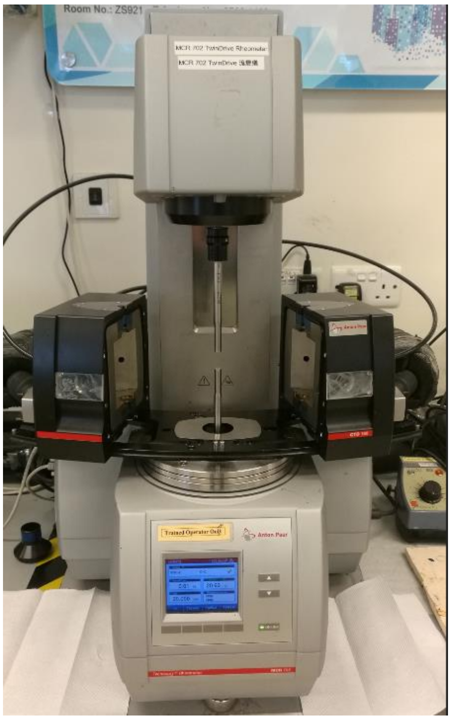

Figure 4.1 Dynamic shear rheometer (MCR 702, Anton Paar)

Frequency sweep test

Bulk rheological properties of the WEBERs were tested employing a dynamic shear rheometer (DSR, MCR 702, Anton Paar). Frequency sweeps over the range of 0.1-30 Hz at -10 °C, 0 °C, 10 °C, 20 °C, 30 °C, 40 °C, 50 °C, and 60 °C were conducted in the linear viscoelastic domain on all the specimens. The master curves of complex modulus were then constructed using the time-temperature superposition principle (TTSP) at the reference temperature of 10 °C. Two measurements were performed for each specimen.

Multiple stress creep and recovery (MSCR) test

The MSCR tests were conducted at 50 °C, 60 °C, and 70 °C according to ASTM D7405. During the MSCR test, constant stress was applied to the sample for 1 s followed by a recovery period of 9 s at zero stress. Ten cycles of creep and recovery were applied at the two stress levels of 0.1 kPa and 3.2 kPa. The 0.1 kPa shear stress level reflects the linear viscoelastic response of the bitumen binder, while the 3.2 kPa shear stress level was adopted to evaluate the non-linear viscoelastic behavior of the bitumen binder [153]. Two important parameters, the average strain recovery (R) and nonrecoverable creep compliance (Jnr), were calculated to analyse the binder response to shear stress. Two replicates were measured for each specimen.

PAV aging of WEBERs

Since bitumen emulsions are generally applied at ambient temperature without heating, no short-term aging is experienced. Thus, aging in the pressure aging vessel (PAV), was performed directly on the WEBERs according to ASTM D6521 to simulate the long-term in-service aging.

Time-sweep fatigue test

The fatigue tests were conducted using the dynamic shear rheometer (DSR) with an 8 mm diameter parallel plates and a 2 mm gap. All the fatigue tests were carried out at 20 °C on the PAV aged WEBERs. For the time sweep tests, three stress levels were evaluated, i.e., 300 kPa, 400 kPa, and 500 kPa, at a frequency of 10 Hz. The time sweep tests were continued until complete failure of the materials. At least two measurements were performed for each specimen.

Linear amplitude sweep test

The linear amplitude sweep (LAS) test was conducted at 20 °C using the PAV aged samples following the AASHTO TP-101 [154]. During the LAS test, the frequency sweep from 0.2 - 30 Hz was first applied at a constant shear strain of 0.1% to capture the material’s response in the linear viscoelastic domain, followed by the amplitude sweep from 0.1% - 30% at the frequency of 10 Hz. Two replicates were measured for each specimen.

Test on bond strength between WEMBEs and aggregate

To evaluate the bond strength between WEMBEs and aggregate, the pull-off test was conducted. The granite stone, which was used as the substrate, was slightly abraded with the 80-mesh size grinding wheel to create a rough surface (Figure 4.2). A small amount of bitumen emulsion was dropped on the cleaned surface subsequently. The upper pull-off stub was carefully put on the emulsion after the breaking of bitumen emulsion. The specimens were then allowed to cure at ambient room conditions for 24 h, followed by 24 h of oven heating at 60 °C. The test was then performed at two temperatures: 23 °C and 50 °C. In addition, the strength of WEMBEs evolves with the breaking of the emulsions and the curing of waterborne epoxy resin. To measure the strength improvement with time, WEMBE-0 and WEMBE-5 were selected for comparison. After preparation of the specimens, they were allowed to cure at ambient room conditions for up to 14 days, and the pull-off test was conducted after 1day, 3 days, 7 days and 14 days. All the pull-off tests were conducted at ambient room temperature using a dynamic testing system (DTS-30, PAVETEST) with a loading rate of 5 mm/min. At least two replicates were tested and averaged to characterize the bond strength.

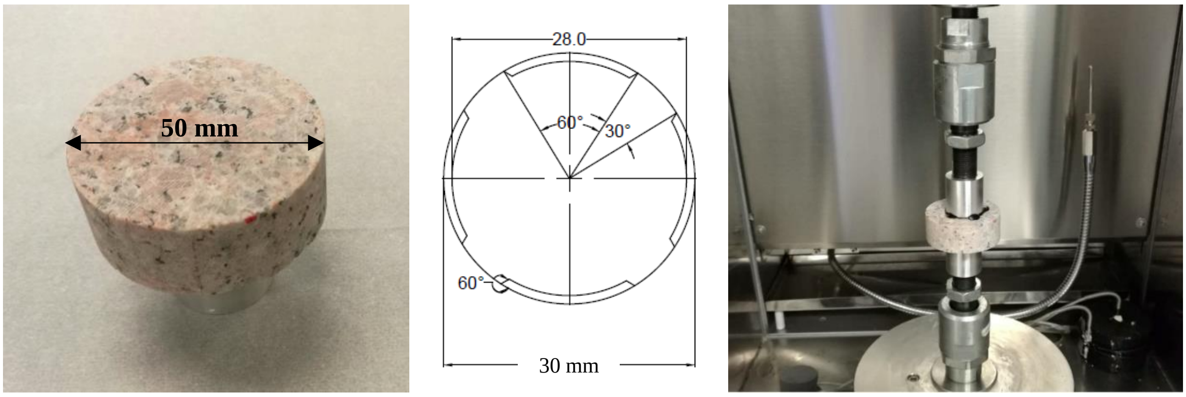

(a) (b) (c)

Figure 4.2 Pull-off test: (a) granite substrate, (b) pull-off stub, and (c) test setup

Moisture sensitivity test

The adhesion between bitumen emulsion and aggregate under water was evaluated through the boiling water tests in accordance with ASTM D3625. Granite, commonly used in Hong Kong, was used as the testing aggregate. In each test, 465 g of coarse aggregate and 35 g of bitumen emulsion were first manually mixed for 1 min. The coated aggregate was then cured at ambient temperature for 1 day and 3 days. The cured mixture was subsequently boiled for 10 min in a container. Finally, the boiled mixtures were visually inspected to determine the moisture sensitivity of the mixtures.

4.2 Results and discussion

4.2.1 Infrared spectra of WEBERs

After waterborne epoxy resin emulsion was mixed into bitumen emulsion, it would disperse evenly in the aqueous phase. The cross-link curing reaction would proceed as water evaporates. The molecular structure of the cured epoxy resin is shown in Figure 4.3. Epoxy groups at the other end of R^1 can then react with another WCA, leading to an inter-connected polymer structure. Figure 4.4 demonstrates the FTIR spectra of all the WEBERs. As the dosages of waterborne epoxy resin were small, no significant difference between the WEBERs was observed. However, it can be seen that the peak intensity at 1250 cm^{-1} corresponding to the ether group (-C-O-) increased with increasing dosages of waterborne epoxy resin.

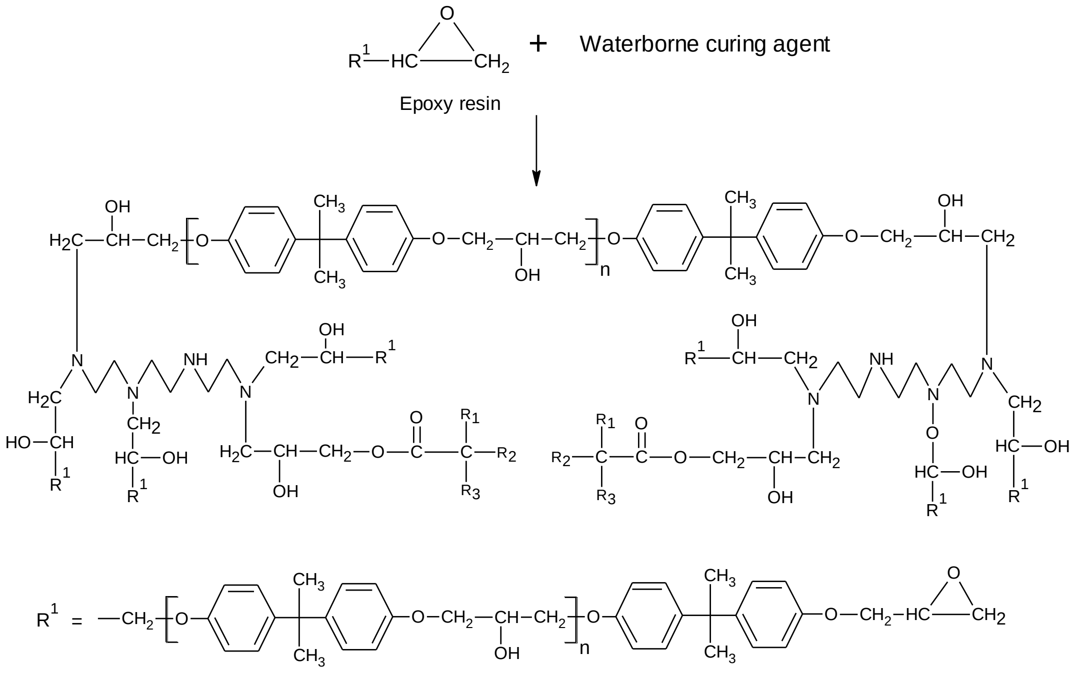

Figure 4.3 Curing reaction of epoxy with waterborne curing agent

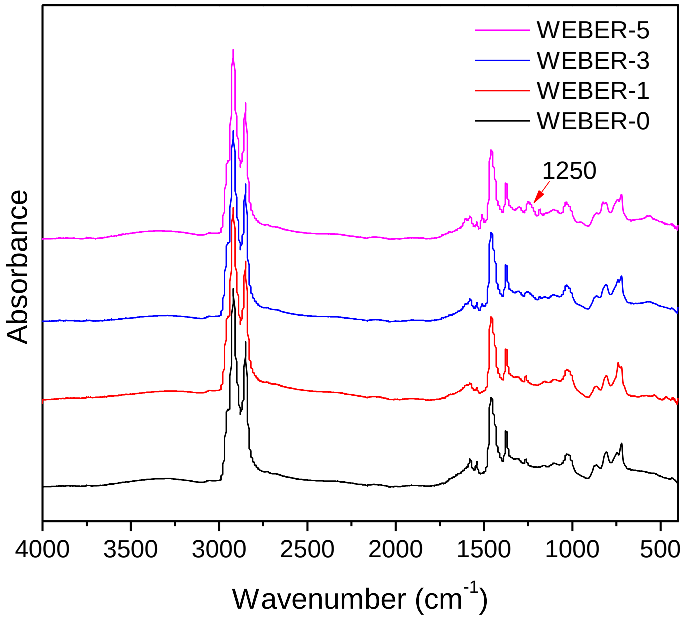

Figure 4.4 FTIR spectra of WEBERs

4.2.2 Microstructure of WEBERs

Figure 4.5 demonstrates the fluorescence images of the cured WEBERs. The dark phase corresponds to bitumen, and the yellow phase corresponds to epoxy resin. With the increase of waterborne epoxy resin dosages, the area of the yellow phase increased as shown in the figure. What is interesting in the figure is that the cured epoxy resin forms an inter-connected polymer (or honeycomb-like) structure when the dosages of the waterborne epoxy resin reached 3wt%, and the bitumen particles were encapsulated in the epoxy film. In a previous study by Liu, et al. [135], a commercial waterborne epoxy resin was used to modify bitumen emulsion. However, such polymer-rich film structure was not observed even when 40wt% waterborne epoxy resin was added. Gu, et al. [155] evaluated the microstructure of a non-ionic based waterborne epoxy resin modified bitumen emulsion employing FM and SEM. Their findings indicated that the polymer-rich film structure can only be formed with the dosages of the waterborne epoxy resin larger than 20wt%, while 3wt% of waterborne epoxy resin has already been able to form such structure in this study based on the CLSM test results. The reason may lie in the different compositions of the waterborne epoxy resin. The cationic type of waterborne epoxy resin is more compatible with the cationic bitumen emulsion compared with the non-ionic type, thus the waterborne epoxy resin can be more homogeneously mixed with the bitumen emulsion in this study. As a result, less quantity of cationic waterborne epoxy resin is required to form the polymer-rich film structure in the bitumen emulsion residue.

The waterborne epoxy resin was initially dispersed in the aqueous phase after mixing with bitumen emulsion, as water evaporates and the bitumen droplets become closer, the epoxy resin particles are squeezed to form a thin layer around the bitumen particles. After the curing process of the epoxy resin, a continuous epoxy film will be formed around the bitumen particles. It can be further noticed that the bitumen particles are generally smaller than 10 μm. Recall that most of the bitumen droplets in the bitumen emulsion were smaller than 10 μm as shown in Figure 3.14, indicating that the majority of the bitumen droplets did not merge to form bigger particles during the curing process because of the barrier formed by the waterborne epoxy resin. Such inter-connected epoxy structure may dramatically change the overall performances of the emulsion residues, which will be investigated in the rest parts of this chapter.

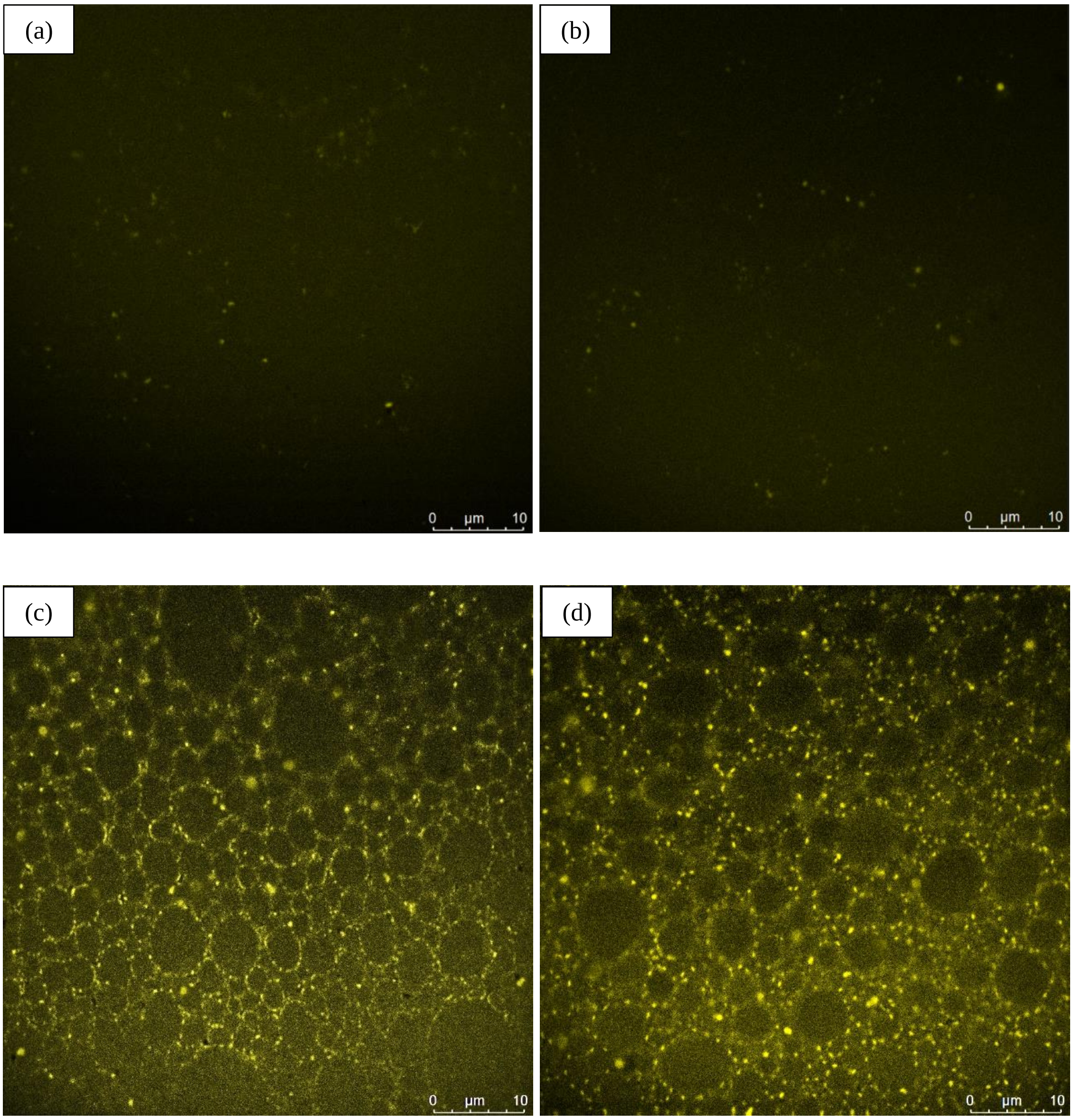

Figure 4.5 CLSM images of WEBERs: (a) WEBER-0, (b) WEBER-1, (c) WEBER-3 and (d) WEBER-5 (scale bar: 10 μm)

4.2.3 Temperature sweep of WEBERs

The results of the temperature sweep tests are presented in Figure 4.6. From Figure 4.6 (a), it can be seen that the WEBERs containing waterborne epoxy resin had much larger complex modulus |G*| than that of the pure bitumen emulsion residue. With the increase of waterborne epoxy resin content, the complex modulus of the emulsion residues increased considerably within the entire tested temperature range. This increment was more significant at higher temperature than at lower temperatures. The improvement of the complex modulus indicates the formation of epoxy resin networks within the bitumen matrix. Particularly, the |G*| of WEBER-5 is one order greater than that of WEBER-0 at 40 °C, and over two orders larger at 70 °C. The substantial increase of |G*| for WEBER-5 reveals that a denser inter-connected polymer network was formed, which turned the bitumen into a more elastic material.

Previous research has suggested that phase angle can better reflect the chemical and physical structure of bitumen [156]. Figure 4.6 (b) shows that the phase angle of WEBER-0 increased continuously with the increasing temperature and approached 90° when the temperature reached 70 °C, indicating dominant viscous behavior. However, the addition of epoxy resin significantly decreased the phase angle, especially at higher temperatures, which also confirmed the presence of inter-connected polymer networks within bitumen. It is interesting to notice that the phase angle of the emulsion residues containing waterborne epoxy resin showed an upward trend until 60 °C and then declined. At lower temperatures, bitumen is stiffer and plays an important role on the viscoelastic properties, while at higher temperatures, bitumen becomes viscous, thus the viscoelastic properties are dominated by the epoxy resin. These results further support the formation of the inter-connected polymer structure observed in Figure 4.5.

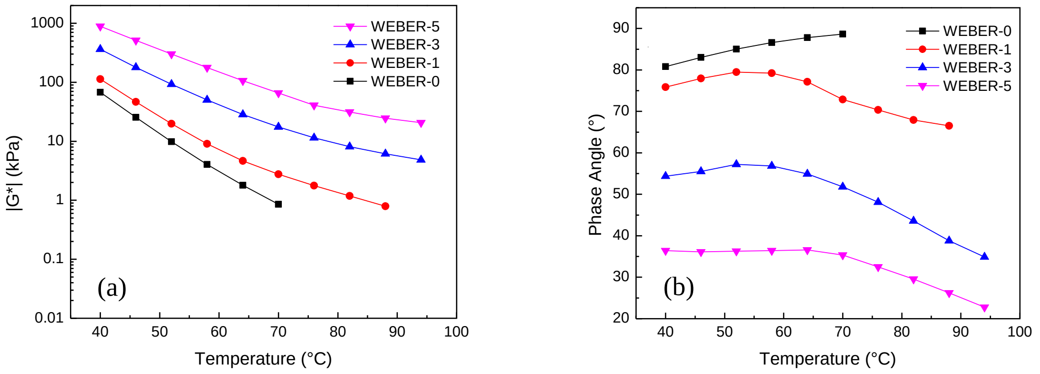

Figure 4.6 Isochronal plots of: (a) | G*| vs temperature, and (b) phase angle vs temperature (at 10 rad/s)

In the Strategic Highway Research Program (SHRP) specifications, $|G^*|/\sin\delta$ is defined as the rutting parameter, which can be used to characterize a binder's resistance to permanent deformation. The minimum requirement for $|G^*|/\sin\delta$ is 1 kPa at the highest service temperature. Figure 4.7 presents the isochronal plots of the rutting parameter versus temperature. It is evident that the incorporation of waterborne epoxy resin significantly increased the rutting parameter. The effects of waterborne epoxy resin on binders' high-temperature performance are shown in Table 4.1. It can be seen that $T_{(G^*/\sin\delta=1\ \mathrm{kPa})}$ (temperature corresponding to a $|G^*|/\sin\delta$ of 1 kPa) reached 86 °C with only 1wt% of epoxy resin, and it became larger than 94 °C for both WEBER-3 and WEBER-5. Considering the low content of epoxy resin, the modification effect is rather surprising. To achieve a similar modification effect for high temperature performance achieved by 1wt% of epoxy resin, the required amount of SBS is about 3-5wt% [157].

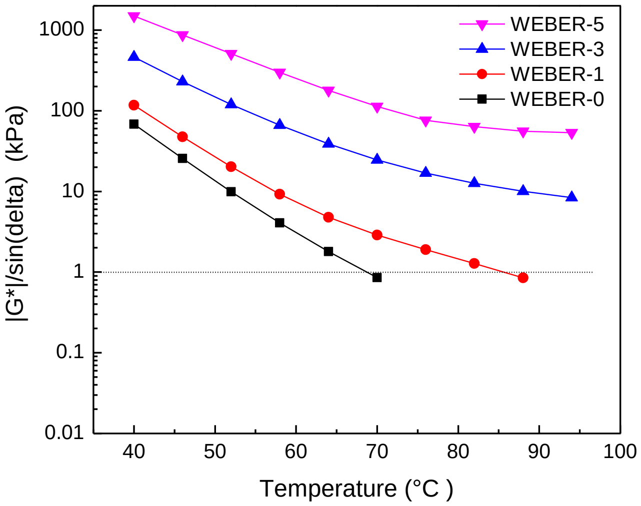

Figure 4.7 Isochronal plots of rutting parameter versus temperature at 10 rad/s

Table 4.1 High temperature performance of WEBERs

Sample ID	$T_{G^*/\sin\delta=1\ \mathrm{kPa}}$ (°C)
WEBER-0	68.7
WEBER-1	86.0
WEBER-3	>94
WEBER-5	>94

4.2.4 Frequency sweep of WEBERs

Figure 4.8 shows the master curves of complex modulus $|G^*|$ and phase angle of the original WEBERs at the reference temperature of 10 °C. According to the time-temperature superposition principle (TTSP), lower frequency corresponds to higher temperature, while higher frequency corresponds to lower temperature. As shown in Figure 4.8 (a), the complex modulus $|G^*|$ for all the WEBERs was very close at higher frequency, while larger quantities of waterborne epoxy resin led to dramatic improvement of the $|G^*|$ at lower frequency. This result indicated that the addition of waterborne epoxy substantially decreased the temperature susceptibility of the WEBERs. On the other hand, the phase angle in Figure 4.8 (b) showed a reverse trend, which decreased with larger dosages of waterborne epoxy resin, revealing that the waterborne epoxy resin increased the elasticity of the emulsion residues. It is worth noting that δ of WEBER-0 approached close to 90 ° at lower frequency, demonstrating essentially Newtonian liquid response at high temperature. What stands out in the figure is that the phase angle of WEBER-3 and WEBER-5 first increased and then decreased with decreasing frequency. Such phenomenon is typically associated with the presence of interconnected polymer structure in polymer modified bitumen [158, 159]. It is also interesting to note that the phase angle of WEBER-5 was always smaller than 45°, which indicates that WEBER-5 demonstrates elastic-dominated response in the whole frequency spectra. Recall the fluorescence micro-structure of the WEBERs, the inter-connected structure was identified in WEBER-3 and WEBER-5. Such distinct structure significantly improved the elasticity of the emulsion residues. At very low temperature (high frequency) the bitumen is very stiff, and the overall performance of the polymer modified bitumen is mainly dominated by the bitumen, thus the difference between different WEBERs was insignificant. Upon increasing the temperature, both the bitumen and the polymer structure soften to some extent. Thus, the phase angle increased. With further increasing of temperature, the bitumen transfers to a viscous state, however, the polymer structure will not melt at this stage, and the overall performance of the mixture is dominated by the epoxy resin networks. As a result, the phase angle decreased at higher temperature (lower frequency).

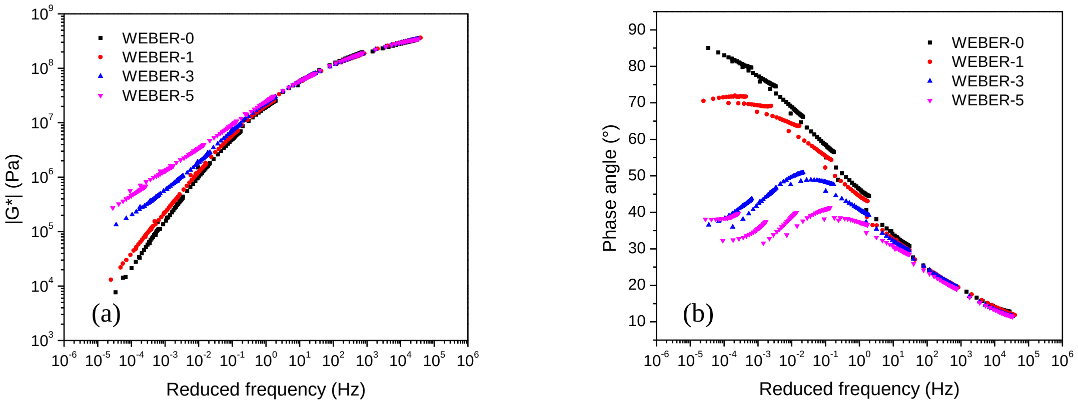

Figure 4.8 Master curves of: (a) complex modulus, and (b) phase angle for the original WEBERs (reference temperature: 10 °C)

4.2.5 Multiple stress creep and recovery (MSCR) test

4.2.5.1 High-temperature performance based on MSCR test

Rutting is one of the main distresses of asphalt pavements affecting pavement service life, driving comfort and safety. To characterize the rutting potential of bituminous binders, the Superpave rutting parameter |G*|/sinδ has been developed and used in the US binder grading system. However, many studies have indicated that this parameter is not always adequate in representing the rutting potential of bituminous binders, especially the polymer modified binders [160-163]. This is because that polymer modified binders possess substantial delayed elastic response [162]. Correspondingly, the MSCR test has been proposed as an alternative approach to characterize the rutting potential of bitumen and polymer modified binders [164, 165]. This test is now listed in the standard specification of AASHTO MP 19. The non-recoverable creep compliance (J_{nr}) derived from this test has been reported to correlate well with the performance of ordinary asphalt pavement mixtures [166-168].

Figure 4.9 depicts the average percent recovery (R) calculated at the stress levels of 0.1 kPa and 3.2 kPa. The data were the average of 10 cycles of percent recovery, and the standard deviation was within 5% of the mean values. It can be seen that the percent recovery generally increased with increasing of the waterborne epoxy resin content. In addition, the percent recovery showed a decreasing trend with the increasing temperature, except for those of WEBER-3 and WEBER-5 at 0.1 kPa. In fact, at the stress level of 0.1 kPa, the percent recovery for WEBER-0 was less than 15% even at 50 °C, while those of WEBER-3 and WEBER-5 reached more than 90% at the same temperature. The recovery difference between different temperatures indicates temperature susceptibilities. It is apparent that the recovery difference was much lower when larger amount of waterborne epoxy resin was used. Thus, the addition of waterborne epoxy resin in bitumen emulsion can decrease the temperature susceptibility of the binder.

Moreover, it was found in Figure 4.9 that the strain recovery at 3.2 kPa decreased compared with that at 0.1 kPa. The larger difference of recovery between different stresses means higher stress sensitivity. However, the percent recoveries for WEBER-3 and WEBER-5 did not change much at the two stress levels, while those of WEBER-0 and WEBER-1 decreased significantly. Thus, it can be inferred that larger quantities of waterborne epoxy could lead to lower stress sensitivity of the emulsion residues. As larger quantities of waterborne epoxy can result in more crosslinks of epoxy polymers, those WEBERs with more epoxy crosslinks will be more damage resistant than those with less epoxy crosslinks.

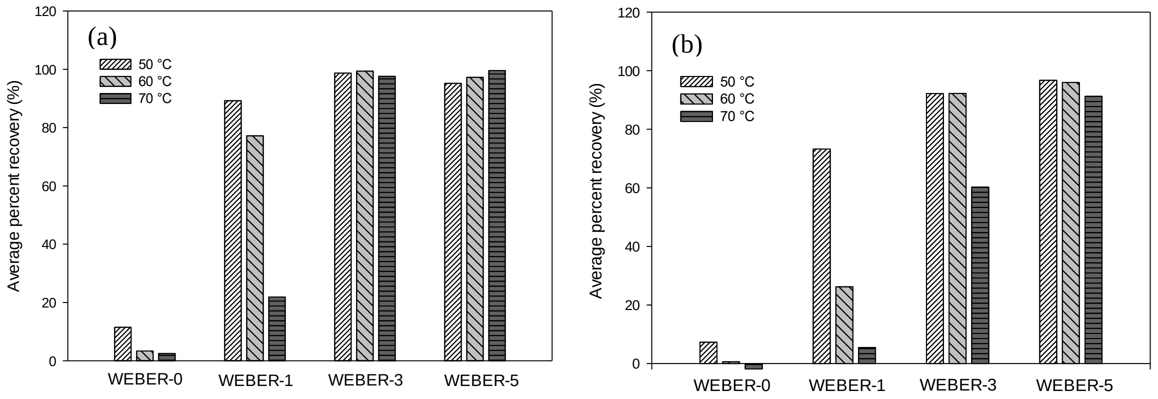

Figure 4.9 Average percent recovery of MSCR test: (a) 0.1 kPa, and (b) 3.2 kPa

The non-recoverable creep compliance (J_{nr}) results are shown in Figure 4.10. It is clear that J_{nr} decreased dramatically with the increasing waterborne epoxy resin content. The most distinct decrease of J_{nr} was observed in WEBER-3 and WEBER-5 at all test temperatures and stress levels. In addition, J_{nr} generally increased with the increase of temperature and stress. The non-recoverable compliance J_{nr} has been used as an important indicator for the rutting sensitivity. Lower J_{nr} indicates stronger resistance to rutting. It is suggested that a value of J_{nr} below 0.5 kPa^{-1} at a stress level of 3.2 kPa represent good resistance to permanent deformation [166]. A closer look at Figure 4.10 reveals that the values of J_{nr} of WEBER-3 and WEBER-5 were both less than 0.02 kPa^{-1} even at the stress of 3.2 kPa, substantially lower than that of WEBER-0. Therefore, it can be concluded that waterborne epoxy resin remarkably improved the rutting resistance of bitumen emulsion residues, and a minimum of 3wt% waterborne epoxy resin is a reasonable requirement for obtaining good rutting resistance. Such finding is consistent with the microstructure of the WEBERs. The waterborne epoxy resin has formed the polymer-rich film structure within the emulsion residue when the dosages reached 3wt%, which dramatically increased the elasticity of the material, thereby improving the resistant to rutting potential.

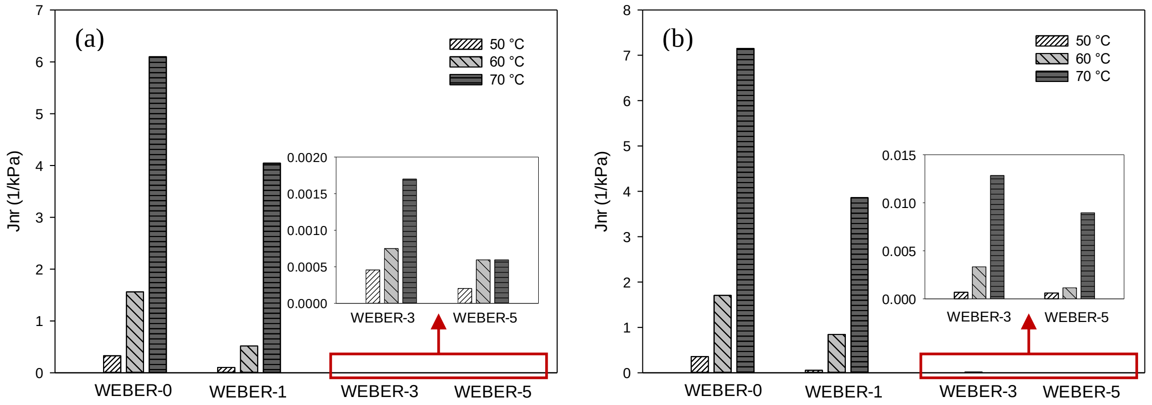

Figure 4.10 Non-recoverable creep compliance J$_{nr}$ of MSCR test ((a) 0.1 kPa, (b) 3.2 kPa, a close up was shown for WEBER-3 and WEBER-5)

4.2.5.2 Creep and recovery modelling

In the MSCR test, the lower stress of 0.1 kPa is adopted to evaluate the linear viscoelastic performance of bituminous binders, while the higher stress of 3.2 kPa is applied to characterize the nonlinear viscoelastic response of most bituminous binders [153]. In this study, the binders' responses at the lower stress of 0.1 kPa in the linear viscoelastic range were selected and modelled using the generalized Burgers model.

The generalized Burgers model (Figure 4.11), which consists of one Maxwell model and a number of Kelvin-Voigt model in series, has been widely used in modelling the viscoelastic behavior of bituminous materials [169, 170].

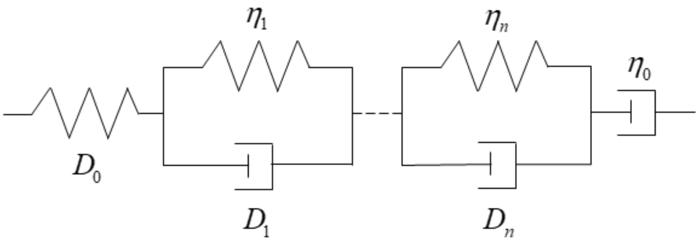

Figure 4.11 The generalized Burgers model

The creep strain response $\varepsilon(t)$ is given as,

$$\varepsilon_{(t)} = \sigma D_0 + \sum_{i=1}^{n} \sigma D_i (1 - e^{-t/\tau_i}) + \frac{\sigma}{\mu_0} t \tag{4-1}$$

where σ is the applied stress, kPa, t is the current time, D_0 is the creep compliance of the standalone spring, D_i is the creep compliance of the i^{th} Kevin series, τ_i is the retardation time of the i^{th} Kevin series, n is the number of Kevin series, t_0 is the time of creep phase, and μ_0 is the zero-shear viscosity [163, 171].

According to Bolzmann superposion principle, the strain in the recovery phase is given as,

$$\varepsilon_{(t)} = \sum_{i=1}^{n} \sigma D_i e^{-t/\tau_i} (e^{t_0/\tau_i} - 1) + \frac{\sigma}{\mu_0} t_0 \tag{4-2}$$

The least-squre curve fitting method in MATLAB® program was applied in both models to fit all creep and recovery data.

It was found that the original Burgers four element model, which contains one Kelvin model, was inadequate to fit the data well, especially for the recovery phase at higher temperature. When adding one more Kelvin model in series, it can be seen from Figure 4.12 that excellent fitting can be achieved. The fitting parameters are shown in Table 4.2, and the R^2 values are larger than 0.99 for all cases.

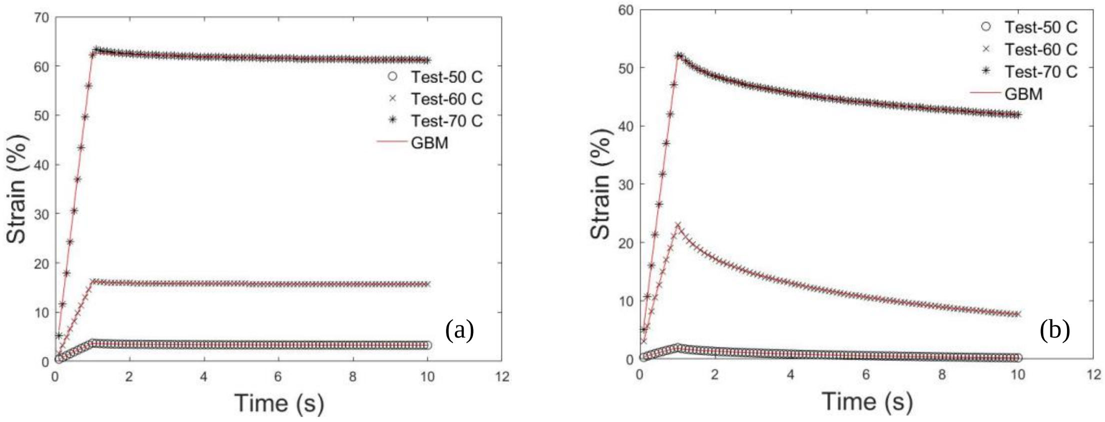

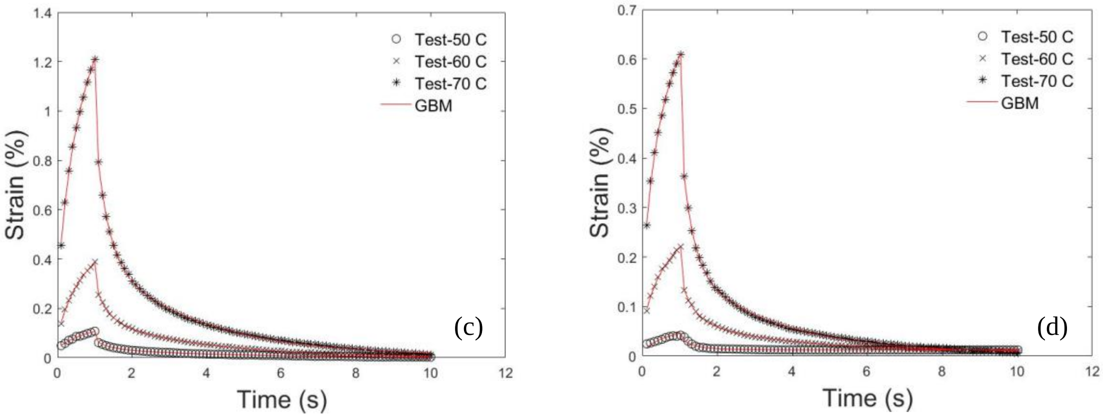

Figure 4.12 Generalized Burgers model (GBM) fitting: (a) WEBER-0, (b) WEBER-1, (c) WEBER-3, (d) WEBER-5

Table 4.2 Fitting parameters for the generalized Burgers model

Sample ID	Temperature (°C)	D_0	μ_0	D_1	τ_1	D_2	τ_2	R^2
WEBER-0	50	0.75	0.034	79.98	1.00	13.81	256.46	0.9999
	60	0.01	0.006	10.00	1.79	3.16	798.16	0.9983
	70	0.01	0.002	999.96	78.93	28.61	29.60	0.9925
WEBER-1	50	1.82	0.667	33.00	33.00	3.61	3.61	0.9998
	60	3.80	0.022	53.15	900.10	0.63	6.01	0.9993
	70	0.01	0.003	834.38	49.49	7.86	0.88	0.9969
WEBER-3	50	0.01	21.78	3.40	0.01	0.39	7.81E-07	0.9997
	60	0.02	6.10	2.80	0.05	0.33	2.23E-14	0.9998
	70	0.07	2.47	2.65	0.18	0.33	1.67E-03	0.9997
WEBER-5	50	2.28E-03	174.96	0.27	3.50E-03	0.78	3.88E-03	0.9999
	60	0.02	15.84	2.54	0.03	0.34	2.95E-03	0.9998
	70	0.05	6.17	2.35	0.09	0.30	1.82E-03	0.9998

In the generalized Burgers model, the viscosity parameter μ_0 of the single dashpot represents the zero-shear viscosity (ZSV). ZSV has been taken as an effective indicator for permanent deformation of bituminous binders by many researchers [172-174]. Larger values of ZSV indicate stronger resistance to permanent deformation. Table 4.2 shows that the values of ZSV generally increased with the increase of epoxy resin content and decreased with the increasing temperature. Similar results were reported in other studies [167, 171]. The possible mechanism is that the epoxy resin polymer networks within the bitumen matrix led to higher viscosity of the emulsion residues. These test results indicated that the temperature dependence of the bitumen emulsion residues was reduced by waterborne epoxy resin.

It can be found that the zero-shear viscosity μ_0 from the generalized Burgers model was closely related to bitumen viscosity, and was consistent with the respective material's performance, i.e., μ_0 increased with larger dosages of waterborne epoxy resin and decreased with higher temperatures.

4.2.6 Evaluation of aging resistance

Bitumen is subjected to short-term aging during construction of pavement, and long-term aging in service life as well [175]. In laboratory, the standard rolling thin film oven test (RTFOT) and the PAV test are recommended to simulate the short-term and long-term field aging, respectively [176]. However, aging of bitumen emulsion has not been explored in detail so far. Unlike traditional hot-mix asphalt, bitumen emulsion will not go through the short-term aging, as no high-temperature heating is performed during its construction. Nevertheless, the weathering will still lead to long-term aging of bitumen emulsion residues during service life. It is therefore reasonable to simulate the long-term aging of bitumen emulsion directly on the residues without short-term aging.

Aging of bitumen comes from both physical and chemical aspects. Physically, loss of volatiles leads to change of the bitumen structure. Regarding the chemical change, the oxidative reaction will cause an increase of the carbonyl and sulfoxide groups [177, 178]. The polar groups containing oxygen can further associate to form more complex and higher weight molecules. As a result, the bitumen become stiffer after aging, making the material more brittle and more sensitive to cracking and fracture [179].

4.2.6.1 Chemical analysis of aging

To evaluate the aging of bitumen using FTIR, the peaks located at 1700 cm^{-1} and 1030 cm^{-1} corresponding to carbonyl stretching vibration and sulfoxide stretching vibration are of particular interest. During the oxidative aging of bitumen binders, oxygen diffuses into bitumen and reacts with certain molecules and results in an increase of the peak intensity of carbonyl and sulfoxide functional groups. In an attempt to quantitatively evaluate the aging extent of bitumen binders, the indices of carbonyl and sulfoxide groups can be calculated as follows,

$$I_{C=O} = \frac{A_{C=O}}{\sum A} \tag{4-3}$$

$$I_{S=O} = \frac{A_{S=O}}{\sum A} \tag{4-4}$$

where $A_{C=O}$ and $A_{S=O}$ are the peak areas of carbonyl group and sulfoxide group, respectively, and $\sum A$ is the sum of peak areas which is represented by [180, 181],

$$\sum A = A_{724} + A_{743} + A_{814} + A_{864} + A_{1030} + A_{1367} + A_{1460} + A_{1600} + A_{1700} + A_{(2862,2923,2953)} \tag{4-5}$$

The use of $I_{C=O}$ as the index of bitumen oxidative aging is well established [182, 183], while $I_{S=O}$ is also used in some other studies [184, 185].

The FTIR spectra of WEBERs before and after PAV aging were presented in Figure 4.13. The peak around 1700 cm^{-1} ascribing to carbonyl functional group was not observed in the spectra of the unaged specimens but emerged after PAV aging. In addition, the sulfoxide peak at 1030 cm^{-1} shows an increase in peak intensity after PAV aging when compared with that of the unaged WEBERs. The indices of $I_{C=O}$ and $I_{S=O}$ were calculated to compare the aging extent of different WEBERs, which are presented in Figure 4.14 and Figure 4.15, respectively. The error bars represent the standard deviation of three measurements performed on each WEBER.

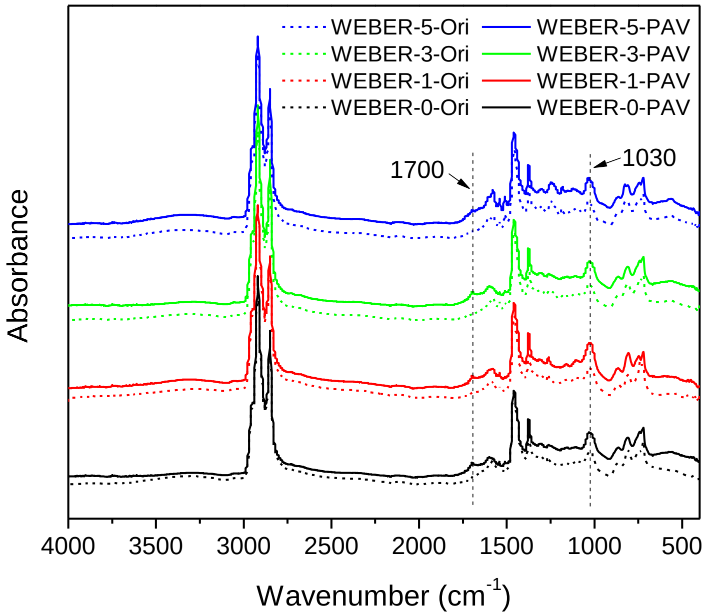

Figure 4.13 FTIR spectra of original and PAV aged WEBERs

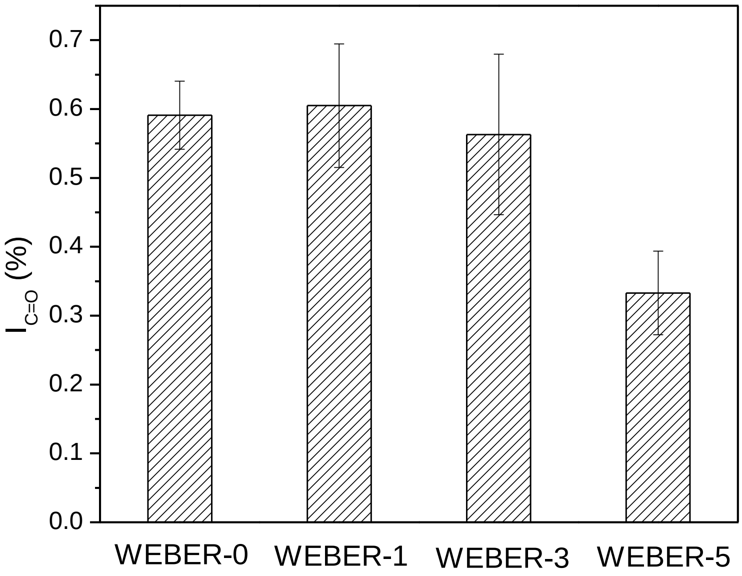

Figure 4.14 Aging indices $I_{C=O}$ of WEBERs

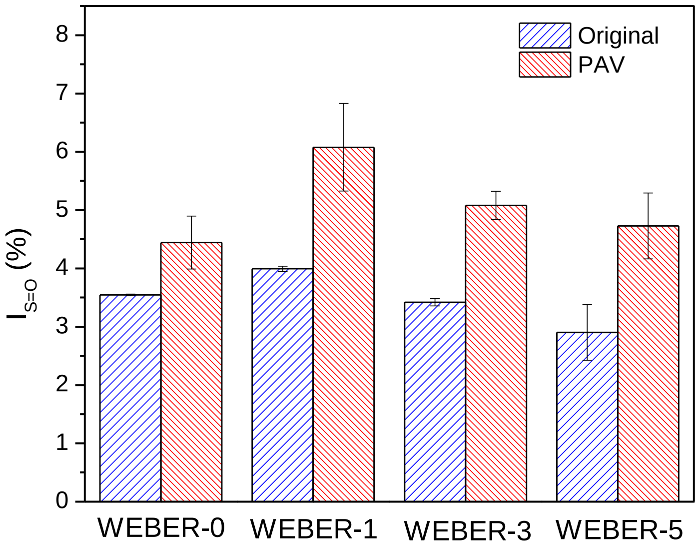

Figure 4.15 Aging indices $I_{S=O}$ of WEBERs

As can be seen from Figure 4.14, the $I_{C=O}$ of the aged WEBERs generally decreased with higher concentration of epoxy resin. On the other hand, the sulfoxide peak intensity was not very consistent even for the unaged binders (Figure 4.15). The scattering of the sulfoxide peak intensity may be due to the overlapping absorbance peaks of other functional groups like phosphate groups, certain alcohol or ether [186, 187]. Therefore, it is not very reliable to use $I_{S=O}$ as the oxidative aging index in this case, and consequently $I_{C=O}$ was selected in this study.

The decrease of $I_{C=O}$ indicates the incorporation of waterborne epoxy resin reduced the oxidative aging of the bitumen emulsion residues. As shown in the fluorescence microscopy of the WEBERs, the bitumen particles are encapsulated by the epoxy resin film. The polymer-rich film structure acts as a barrier between the bitumen and the air, thus significantly decreased the diffusion of oxygen to the bitumen phase, thereby reducing the oxidation of bitumen. The work by Apostolidis, et al. [188] also indicated that epoxy resin was able to decrease the oxidative aging level of the epoxy modified bitumen. Thus, it can be concluded that the addition of waterborne epoxy resin improved the emulsion residues' resistance to oxidative aging.

4.2.6.2 Effect of aging on rheological performance

To evaluate the aging effect on the complex modulus of WEBERs, the master curves of |G*| and phase angle were compared in Figure 4.16. It can be seen that the |G*| of the PAV aged WEBERs increased in comparison with their original counterparts, while the phase angle generally decreased, indicating that the WEBERs become stiffer after PAV aging. It is noticeable that the difference become more remarkable at the lower frequency domain. Taken a closer look at the phase angle, the phase angle trend of the PAV aged group for WEBER-0, WEBER-3, and WEBER-5 were similar compared with their original (unaged) counterparts. However, a peak was observed in the phase angle profile of the original WEBER-1, which disappeared in that of the PAV aged WEBER-1. Note that the epoxy networks were just lightly connected observed from the fluorescence microscopy of WEBER-1 in Figure 4.5, and such networks may have largely degraded during the PAV aging. On the other hand, the waterborne epoxy resin in WEBER-3 and WEBER-5 has formed stronger polymer-rich film, which was more robust and mostly preserved in the aging process. Thus, the phase angle profiles did not change much.

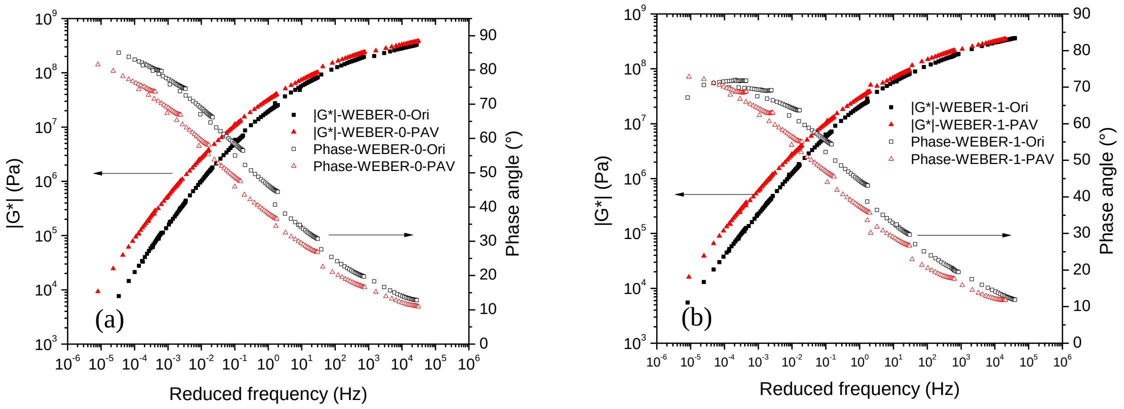

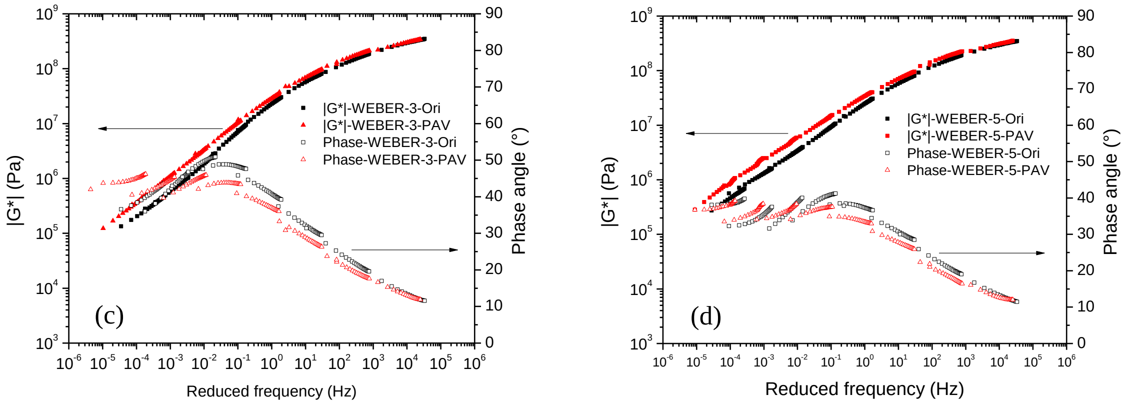

Figure 4.16 Comparison of complex modulus before and after PAV aging: (a) WEBER-0, (b) WEBER-1, (c) WEBER-3, and (d) WEBER-5 (reference temperature: 10 °C)

To quantitatively evaluate the PAV aging on the complex modulus, the difference of |G*| and phase angle at the frequency of 10 Hz were compared in Table 4.3. It can be seen that the difference of both the |G*| and phase angle difference generally decreased with the incorporation of waterborne epoxy resin, and the decreasing trend of phase angle is more consistent with the waterborne epoxy resin concentrations. Lower difference of |G*| and phase angle between the PAV aged specimens and their unaged counterparts indicates better resistance to aging. These results agree with that obtained from the FTIR outcome, which also demonstrates that the incorporation of waterborne epoxy resin can help improving the resistance to oxidative aging.

Table 4.3 Change of complex modulus comparison at 10 Hz

Sample-ID	|G*|-Ori (Pa)	δ-Ori (°)	|G*|-PAV (Pa)	δ-PAV (°)	|G*|-diff (%)	δ-diff (%)
WEBER-0	5.62E+07	34.2	7.31E+07	29.5	30.2	13.7
WEBER-1	5.64E+07	32.9	6.84E+07	29.0	21.3	11.6
WEBER-3	5.92E+07	31.9	7.15E+07	28.6	20.9	10.5
WEBER-5	5.98E+07	30.5	7.30E+07	27.6	22.0	9.5

Note: the |G*|-diff represents the percent difference of |G*|-Ori and |G*|-PAV for each specimen, and δ-diff represents the percent difference of δ-Ori and δ-PAV.

4.2.7 Fatigue of WEBERs

Fatigue damage represents one of the major distresses occurred in asphalt pavements, due to repeated vehicle loading and weathering. Because of the large difference in stiffness between the binder and aggregate in asphalt mixture, most of the bulk strain is concentrated in the binder domain [189]. It is found that the fatigue behavior of asphalt mixture is largely determined by the binders [161]. To evaluate the fatigue performance of bituminous binders, various testing methods have been developed. Bahia, et al. [161] proposed the repeated cyclic time sweep test using the dynamic shear rheometer (DSR), with stress-controlled or strain-controlled mode, to characterize the fatigue behavior of the binders. The damage accumulates faster in the stress-controlled time sweep test, whereas it accumulates much slower in the strain-controlled time sweep test. There is apparent failure at the end of the stress-controlled test, which is not observed for the strain-controlled mode. In fact, the stress becomes so small that it is difficult to break the sample in the strain-controlled mode. The fatigue life in the strain-controlled time sweep test is therefore defined as the repeated cycles when the modulus dropped to 50% of the initial modulus [190].

The criteria of determining the fatigue life mentioned above are arbitrary to some degree. To evaluate the fatigue life more accurately, the so-called dissipated energy concept was proposed [191, 192]. The dissipated energy can be obtained from Eq.(4-6). The dissipated energy is the energy lost in cyclic shear test, due to the mechanical work, heat generation, and damage done to the material [193]. The previous studies assumed that the all the dissipated energy contributes to the fatigue damage of the material, which is not correct, as only part of the dissipated energy is responsible for the damage done to the material [194, 195]. It is found that only the increment of the dissipated energy of one loading cycle in comparison with the previous loading cycle will produce further damage [194]. Thus, the ratio of dissipated energy change (RDEC), defined as the relative dissipate energy of two consecutive loading cycles (Eq.

(4-7)), was adopted as a failure indicator of the fatigue damage [194]. Moreover, the RDEC is independent of the loading mode, i.e., stress-controlled or strain-controlled, and provides a more fundamental indication of the fatigue damage. The failure is defined as the number of loading cycles at which the value of RDEC starts to rise rapidly. It is believed that significant damage has been done to the material at this point.

$$W_i = \pi\sigma_i\varepsilon_i \sin\delta_i \tag{4-6}$$

where W_i is the dissipated energy at load cycle *i*, σ_i is the stress amplitude at load cycle *i*, ε_i is the strain amplitude at load cycle *i*, and δ_i is the phase angle at load cycle *i*.

$$RDEC = \frac{DE_n - DE_m}{DE_m(n-m)} \tag{4-7}$$

where DE_m and DE_n represent the dissipated energy at load cycle *m* and *n*, respectively.

The time sweep test is recognized an effective method to evaluate the fatigue life of bituminous materials, however, it is time-consuming. In contrast, the linear amplitude sweep (LAS) test, developed by Bahia et al. [196], represents an accelerated fatigue test based on viscoelastic continuum damage (VECD) theory. It is found that the LAS test correlated fairly well with the pavement long-term fatigue performance [197]. The LAS test has been extensively employed to study the fatigue performance of bituminous materials by many researchers in recent years [197-201].

The epoxy resin can form an interconnected polymer structure within the binder, which turned the thermoplastic bitumen binder into a thermosetting composite. The crosslinks of the cured epoxy resin lead to increased stiffness of the binder, thereby decreasing the ductility and thus risks the reducing of the fatigue performance [202]. However, many studies found that the fatigue life of epoxy asphalt was increased compared with normal hot mix asphalt [131, 202-

204]. As a relatively new material, the fatigue of the waterborne epoxy resin modified bitumen emulsion residue has not been well understood. Thus, the fatigue performance of the waterborne epoxy resin modified bitumen emulsion residues will be evaluated after PAV aging in this study.

4.2.7.1 Time sweep fatigue test

The stress sweep tests were first conducted on the four emulsion residues at 20 °C, and the results are presented in Figure 4.17. The complex modulus |G*| was unstable at the initial stage because of the very small stress, which then kept almost unchanged until the shear stress reached around 100 kPa. With further increasing of the shear stress, the |G*| decreased rapidly, indicating that the response of the materials has become non-linear. The time sweep fatigue test was then conducted at the stress level larger than 100 kPa. It was found that too much time was needed with the stress smaller than 200 kPa. Thus, the stress levels were determined to be 300 kPa, 400 kPa, and 500 kPa.

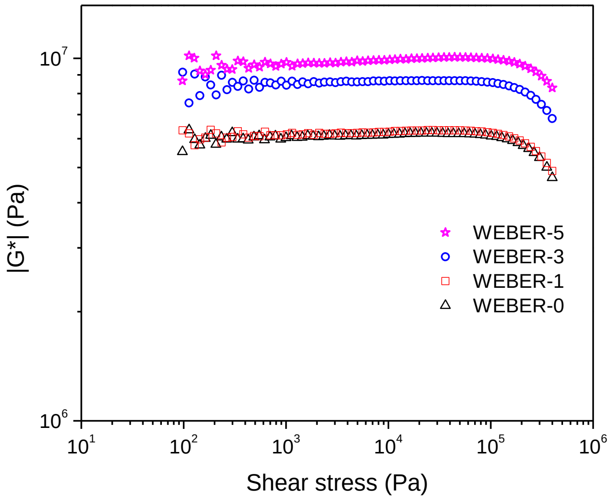

Figure 4.17 Stress sweep at 20 °C

Figure 4.18 depicts the time sweep tests at 300 kPa, 400 kPa, and 500 kPa, respectively. The initial shear strain values (average strain of the first 100 loading cycles) are presented in Table 4.4 for comparison. It is clear that the initial strain decreased with larger dosages of waterborne epoxy resin at each stress level, because of the increase of the modulus. A typical three-stage fatigue damage is observed from Figure 4.19. At the initial stage, the modulus decreased to some degree because of instability. In the second stage, the modulus decreased at a rate that is almost constant, and the damage accumulated gradually at this stage. The last stage shows that the modulus decreased sharply, indicating complete fracture of the materials. It is observed that the loading cycles increased apparently with increasing dosages of waterborne epoxy resin at all the three stress levels.

Table 4.4 Initial shear strain for the time sweep fatigue tests

Sample ID	Initial strain (%)		
	300 kPa	400 kPa	500 kPa
WEBER-0	1.55	2.48	3.04
WEBER-1	1.19	2.22	3.01
WEBER-3	1.15	2.20	2.53
WEBER-5	1.05	1.79	2.00

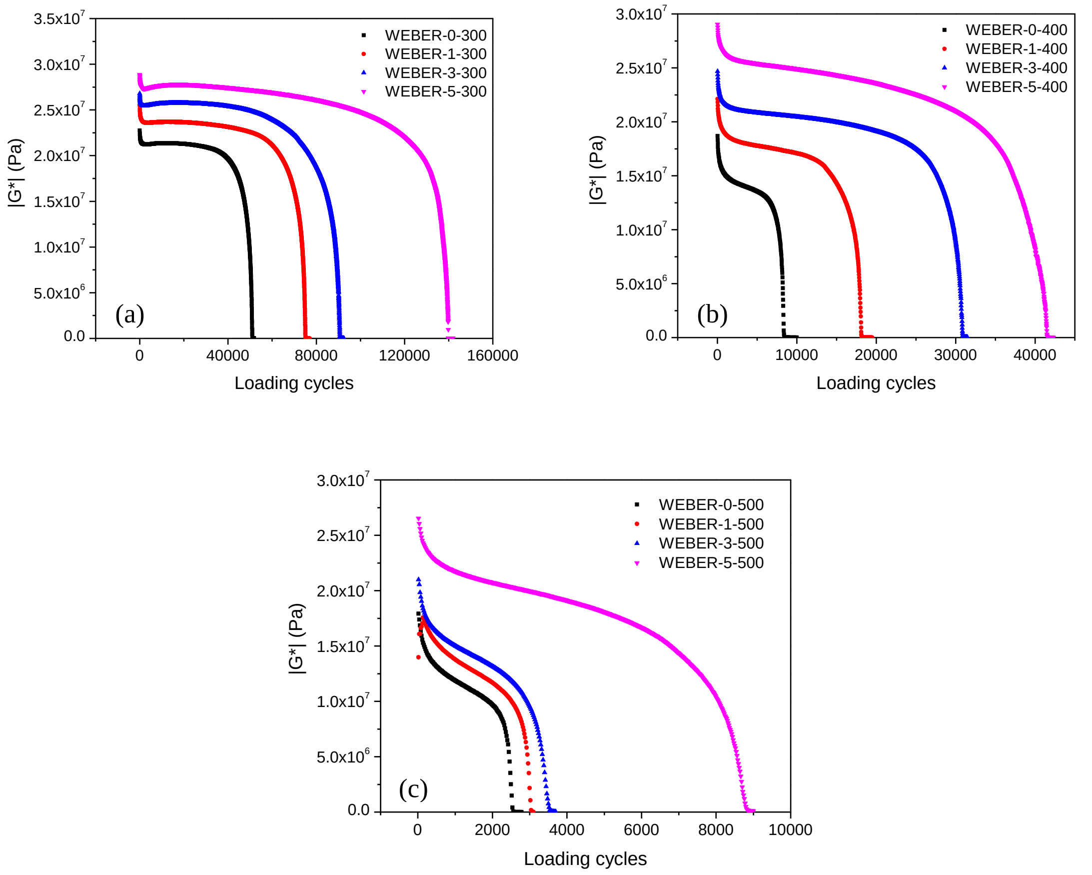

Figure 4.18 Stress-controlled time sweep tests at the stress level of: (a) 300 kPa, (b) 400 kPa, and (c) 500 kPa

The time sweep fatigue life was then analysed with the RDEC approach and presented in Figure 4.19. It can be seen that the RDEC first decreased, and then kept constant in the second stage, which increased rapidly at last. It clearly shows that a larger percentage of the dissipated energy was converted into damage to the material at the early stage. The damage done each cycle then decreased to a lower ratio and stabilized in the second stage. At the final stage, the damage rate increased sharply, indicating fracture of the material.

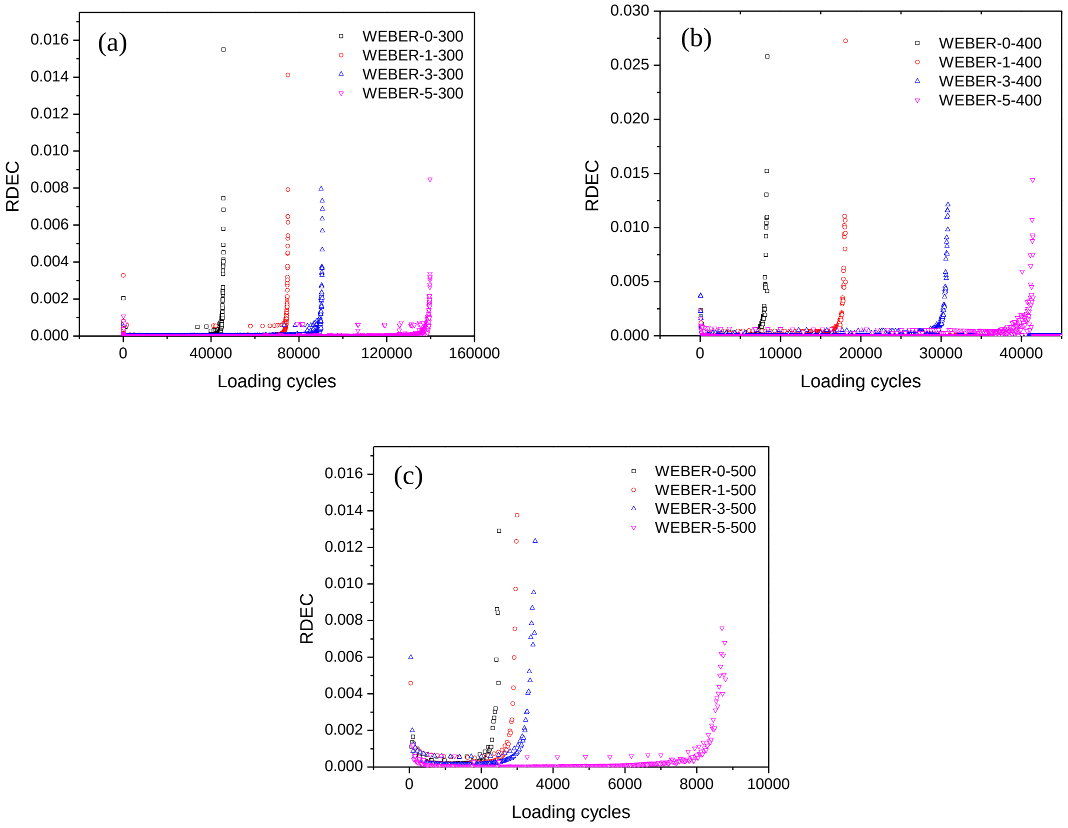

Figure 4.19 Rate of dissipated energy change (RDEC) at the stress level of: (a) 300 kPa, (b) 400 kPa, and (c) 500 kPa

The fatigue loading cycles of all the residues at the three stress levels are summarized in Table 4.5. It is clear that the fatigue life of the binders decreased dramatically with increasing of shear stress (Figure 4.20). On the other hand, it is noticeable that the fatigue life become larger with increasing contents of the waterborne epoxy resin at all the three tested stress levels, indicating the epoxy resin networks increased the emulsion residues resistance to fatigue damage. The incorporation of waterborne epoxy resin formed the inter-connected polymer structure, and the bitumen particles are encapsulated by the epoxy resin film, which increased the materials resistance to damage. Thus, the fatigue life of the emulsion residues containing waterborne epoxy resin increased compared with the pure bitumen emulsion residue in the tested stress levels.

Table 4.5 Fatigue life of WEBERs at different shearing stress

Shear stress (kPa)	Fatigue life (cycles)			
	WEBER-0	WEBER-1	WEBER-3	WEBER-5
300	44,240	73,860	88,200	135,240
400	7,540	16,900	28,620	38,580
500	2,060	2,620	3,020	7,220

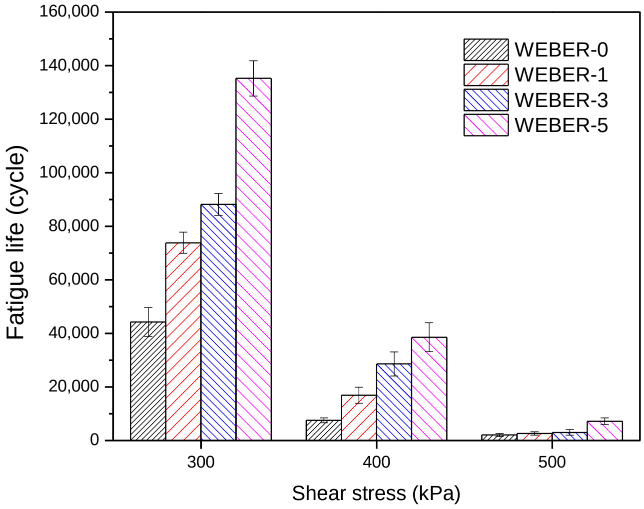

Figure 4.20 Fatigue life at different stress level

4.2.7.2 Linear amplitude sweep test

Despite many studies have employed the RDEC approach to evaluate the fatigue behavior of bituminous binders and mixes. It is still limited regarding the determination of the failure point. In addition, the time-sweep fatigue test is time consuming. The LAS test was then used to evaluate the fatigue life of the emulsion residues. Based on R.A.Schapery's work on crack growth of viscoelastic materials [205], the viscoelastic continuum damage (VECD) concept was employed to evaluated the fatigue performance conducted using the LAS test.

Figure 4.21 shows the relationships between the shear stress and shear strain for different WEBERs. It can be seen that the shear stresses first increased rapidly at the lower shear strain before reaching the peak, and then declined progressively with further increasing of the strain amplitude. What stands out in the figure is the significant difference regarding the stress drop rate in the large strain region (>10%) for different emulsion residues. It is clear that larger dosages of waterborne epoxy resin led to lower drop rate of the stress, indicating that the emulsion residue become more robust to damage with the formation of the epoxy polymer networks.

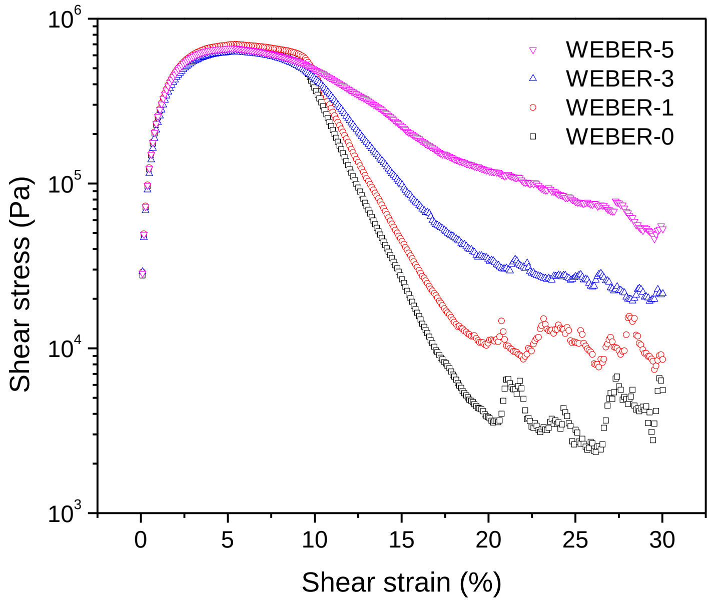

Figure 4.21 Stress-strain curves of different WEBERs (20 °C)

Table 4.6 presents the predicted of fatigue lives (N_f) at the strain levels of 2.5% and 5% based on the VECD model. The results indicate that with the increase of waterborne epoxy, the predicted fatigue life increased at both strain levels. The increase of fatigue life was more significant at the lower strain level (2.5%). The predicated fatigue life of WEBER-5 is more than double of the WEBER-0. However, it should be noted that at the higher strain of 5%, the predicated fatigue lives for the different WEBERs become very close. The predicated fatigue life versus shear strain (1%~20%) is shown in Figure 4.22. Based on the VECD model, the emulsion residues with waterborne epoxy resin had higher fatigue life compared with the pure bitumen emulsion residue at lower shear strain (<5%), however, the trend reversed with shear strain became larger than 5%. The embedded reason may be that the emulsion residues with waterborne epoxy resin forms a honeycomb-like composite structure, such structure is stronger than pure bitumen and is more robust under relatively small strain. However, the epoxy resin polymer structure is also stiffer and more rigid compared with bitumen. Thus, it is more sensitive to larger strain. Therefore, it is concluded that the WEBERs containing waterborne epoxy are more resistant to fatigue under smaller strain, while they are more sensitive to larger strain amplitude compared with the pure bitumen emulsion residue.

Table 4.6 Fatigue life prediction based on VECD model

Sample ID	A	B	$Nf_{2.5\%}$	$Nf_{5.0\%}$
WEBER-0	85,717.9	3.588	3,202	266
WEBER-1	112,330.5	3.784	3,506	255
WEBER-3	200,624.5	4.083	4,758	281
WEBER-5	747,132.9	4.955	7,972	257

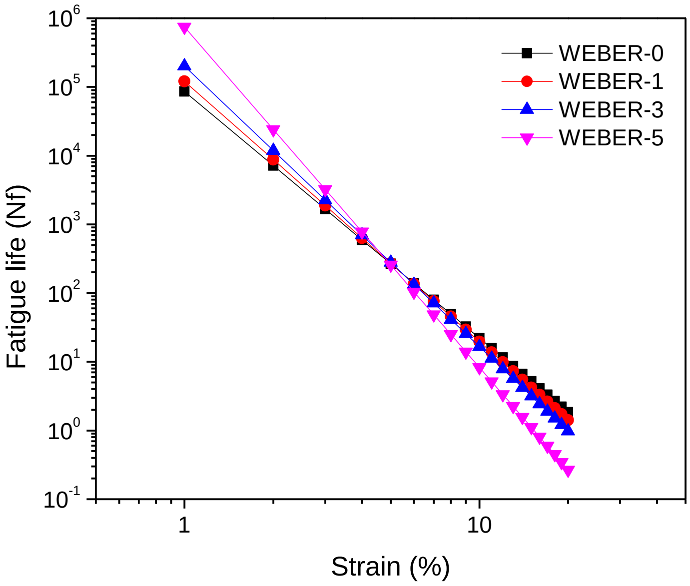

Figure 4.22 Fatigue life predication at different strain

4.2.8 Bond strength evaluation

Figure 4.23 compares the bond strength of different WEBERs at both 23 °C and 50°C. The specimens were conditioned at ambient room temperature for 24 h, plus 24 h of oven conditioning at 60 °C. It is clear that the addition of waterborne epoxy resin increased the bond strength with aggregate. The bond strength for WEBER-0 was close to 1.0 MPa at 23 °C, which increased to 3.7 MPa for WEBER-5 at the same testing temperature. It can be further noted that the bond strength of WEBER-1 (1.3 MPa) was not much different compared with that of WEBER-0. However, the bond strength of WEBER-3 reached 2.6 MPa, which was double of that of WEBER-1. However, one previous study [135] showed that the bond strength of bitumen emulsion was only 1.0 MPa at ambient temperature even with 40wt% of waterborne epoxy resin. Another study [206] found that the bond strength of the bitumen emulsion with 24wt% of waterborne epoxy resin was less than 2.0 MPa. In other words, the bond strengths in the previous studies are significantly lower than those obtained in this study. The possible reason for such difference is the improved compatibility between the waterborne epoxy resin and the bitumen emulsion in this study.

As shown in Figure 4.5, the waterborne epoxy resin content in WEBER-1 was not large enough to form a connected polymer structure. Thus, the bond strength of WEBER-1 did not improve much compared with WEBER-0. On the other hand, the connected polymer-rich phase has been formed in WEBER-3, and such structure contributes significantly to the strength improvement. The bond strength at 50 °C decreased in comparison with that at 23 °C. The bond strength of WEBER-0 and WEBER-5 at 50 °C were 0.16 MPa and 1.4 MPa, respectively, which dropped 83% and 62% compared with their counterparts at 23 °C. Yet, the bond strength drop rate was lower for the waterborne epoxy resin modified bitumen emulsion, which indicated that the waterborne epoxy resin reduced the temperature susceptibility of the emulsion residues.

The tensile force profiles at both 23 ºC and 50 °C against the displacement were plotted in Figure 4.24. It is clear that the elongation at break increased with larger concentration of waterborne epoxy resin, indicating that the waterborne epoxy resin increased the toughness of the emulsion residues.

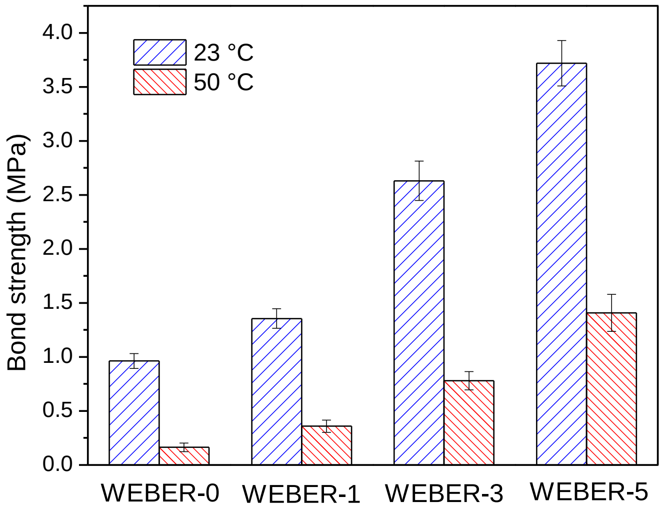

Figure 4.23 Bond strength of different WEBERs

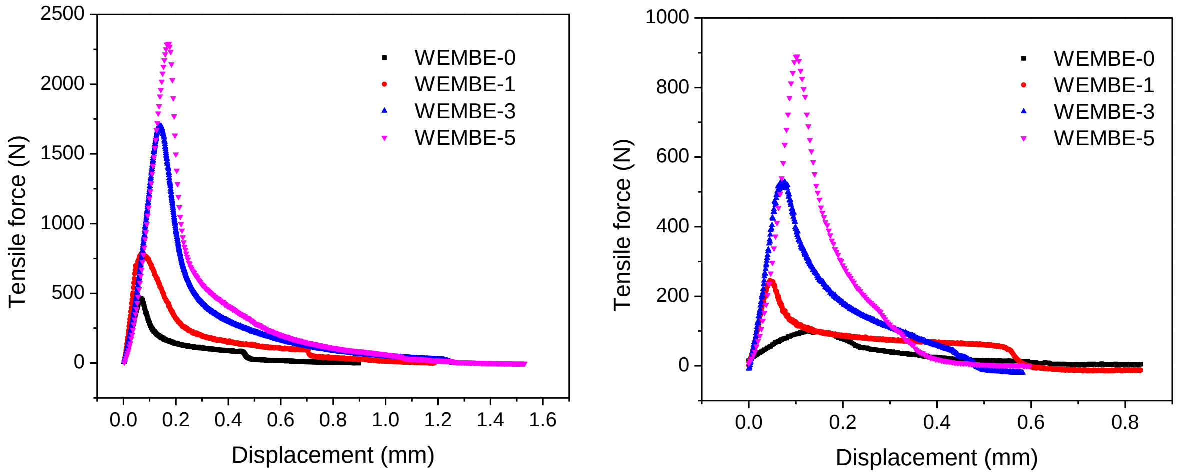

(a) (b)

Figure 4.24 Tensile force profile as a function of displacement at: (a) 23 °C, and (b) 50 °C

To evaluate the bond strength evolution with time under ambient temperature (23 ± 0.5 °C), the specimens of WEBER-0 and WEBER-5 were prepared and compared after conditioning for different days, and the results are presented in Figure 4.25. It is clear that the bond strength of both WEBER-0 and WEBER-5 kept increasing from day 1 to day 14. The bond strength of WEBER-5 was always larger than that of WEBER-0, and the difference between the two increased with increasing conditioning duration. On day 14, the bond strength of both WEBER-0 and WEBER-5 reached values close to their counterparts conditioned in oven as shown in Figure 4.23.

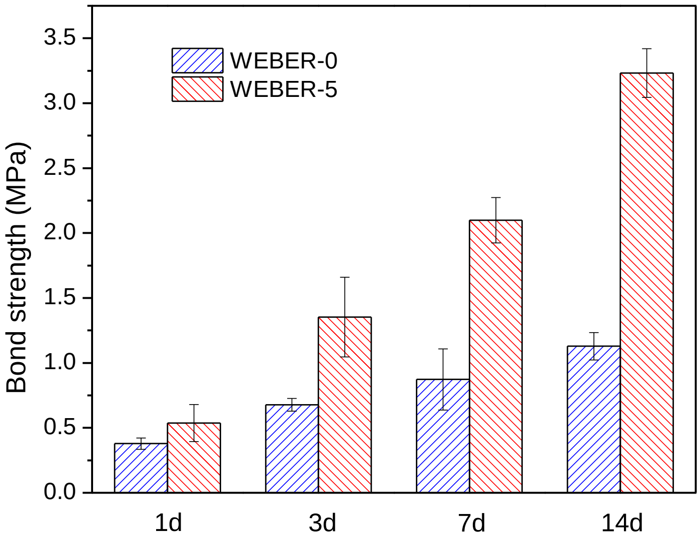

Figure 4.25 Bond strength evolution with time (23 °C)

4.2.9 Moisture susceptibility of WEMBE mixtures

The moisture susceptibilities of bitumen emulsion mixtures with different content of waterborne epoxy were characterized through the boiling tests. Figure 4.26 demonstrates the bitumen emulsion mixtures right after mixing and after emulsion breaking. It can be observed that all aggregates were well coated by bitumen emulsion, indicating good initial adhesion performance between bitumen emulsion and aggregate.

(a) (b)

Figure 4.26 Pictures of WEMBE mixture: (a) right after mixing, (b) after water evaporation

Figure 4.27 shows the pictures of 1 day-cured and 3 day-cured bitumen emulsion mixtures after the boiling tests. It is clear that the water stripping area declines with the increase of waterborne epoxy content for both curing periods. The control mixture (WEMBE-0) had the largest boiling loss area. In contrast, there was almost no apparent stripping when the waterborne epoxy content was 3wt% or above. Comparing the 1 day-cured and 3 day-cured cured mixtures, the stripping did not change much for WEMBE-0 mixture, which was substantially worse than the other three mixtures. However, the boiling loss of WEMBE-1 mixture decreased markedly after curing for 3 days in comparison with its 1 day-cured counterpart. Furthermore, no noticeable stripping was observed for the 3 day-cured mixtures of WEMBE-3 and WEMBE-5.

(a) 1 day-cured bitumen emulsion mixture (From left to right: WEMBE-0, WEMBE-1, WEMBE-3, WEMBE-5)

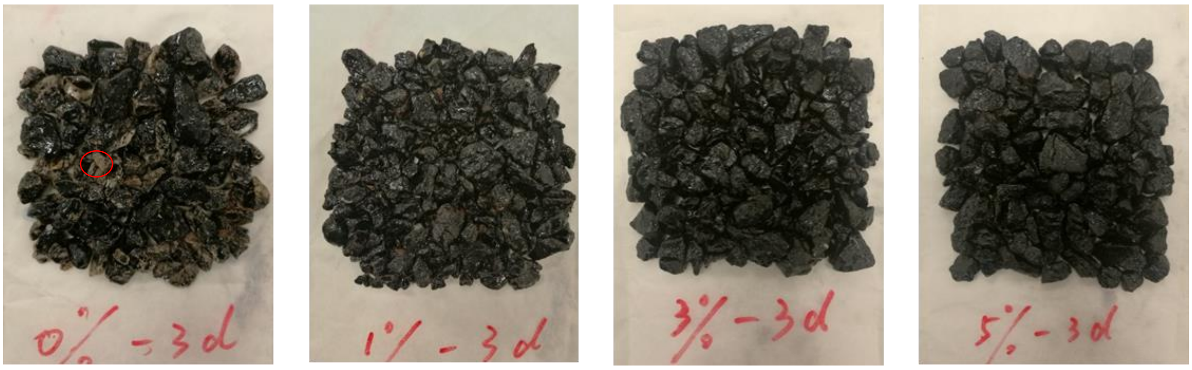

(b) 3 day-cured bitumen emulsion mixture (From left to right: WEMBE-0, WEMBE-1, WEMBE-3, WEMBE-5)

Figure 4.27 Images of bitumen emulsion mixtures after boiling (the red circles represent the stripped aggregates)

From the boiling test results, it can be inferred that waterborne epoxy can significantly improve the stripping resistance of bitumen emulsion mixture. The cross-linked epoxy networks strengthened the bonding between the bitumen emulsion and aggregate in the curing process.

Moreover, the polarity of epoxy resin is higher than bitumen, which further increased the bonding.

4.3 Cost comparison of WEMBE with traditional polymer modified bitumen

A cost comparison between the WEMBE in this study and traditional polymer modified bitumen was performed. WEMBE-5, which constitutes 5wt% of waterborne epoxy resin, was selected as the cold-paving binder in this study. The most commonly used polymer modified binder is the styrene-butadiene-styrene (SBS) modified bitumen that contains 5-6wt% of SBS. The price of pure bitumen emulsion and waterborne epoxy resin were around 2,500 RMB/t and 20,000 RMB/t, respectively. It is worth noting that the commercial bitumen emulsion generally has a solid content of 60wt%, and the rest is water. On the other hand, the price of SBS modified bitumen is about 4,900 RMB/t. The cost comparison of WEMBE-5 and SBS modified bitumen is summarized in Table 4.7.

Table 4.7 Direct cost comparison of WEMBE and traditional polymer modified bitumen

Item	Bitumen emulsion	Waterborne epoxy resin	WEMBE-5 (based on residue)	SBS modified bitumen
Cost (RMB/t)	2,500	20,000	5,550	4,900

The result shows that the cost of WEMBE-5 is approximately 13% higher than that of the traditional polymer modified bitumen. However, the traditional polymer modified bitumen must be heated to over 170 °C to ensure good workability, while the WEMBE can be used directly at ambient temperature without heating. The cost on the energy to heat the polymer modified bitumen should also be considered. In addition, during the production and construction of the traditional polymer modified bitumen, significant amounts of greenhouse gases and volatile organic compounds will be generated, affecting both human health and environment. Thus, a comprehensive life-cycle cost analysis should be conducted to compare the overall cost in the next stage.

4.4 Summary

In this chapter, the overall performances of WEBERs were evaluated, including the microstructure, the rheological properties, the resistance to aging and fatigue, the bond strength with aggregate, and the moisture susceptibility. The main findings of this chapter are summarized below:

(1) The cured waterborne epoxy resin forms an inter-connected polymer film that encapsulates the bitumen particles when the dosages of waterborne epoxy resin reached 3wt%. The distinct microstructure was first observed in this study with such a low concentration of waterborne epoxy resin.

(2) The addition of waterborne epoxy resin significantly improved the mechanical properties of bitumen emulsion. The complex shear moduli of emulsion residues containing waterborne epoxy resin were much larger than that of the pure bitumen emulsion residue, while the phase angles decreased markedly, indicating that waterborne epoxy resin changed the bitumen binder into a more elastic material.

(3) The MSCR results showed that with the increase of epoxy concentration, the percent recovery increased while the nonrecoverable creep compliance decreased, indicating improved resistance to permanent deformation. In addition, the generalized Burgers model can well describe the creep and recovery behavior of the emulsion residues, and the zero-shear viscosity can also be obtained from the model.

(4) The incorporation of waterborne epoxy resin into bitumen emulsion improved the resistance to oxidative aging of the residues, because of the formation of the polymer-rich film structure that decreased the diffusion of the oxygen into the bitumen phase.

(5) The WEBERs generally become stiffer after PAV aging, and the phase angle normally decreased. However, the difference of modulus |G*| and phase angle between the PAV

aged specimens and their unaged counterparts decreased with incorporation of waterborne epoxy resin, which also indicates that waterborne epoxy resin improved the resistance to oxidative aging of the emulsion residues.

(6) In all the time sweep tests at 300 kPa, 400 kPa, and 500 kPa, the fatigue life of the WEBERs increased with larger dosages of waterborne epoxy resin. On the other hand, it was concluded from the LAS tests results that the fatigue life of WEBERs containing waterborne epoxy resin was larger than that of the pure bitumen emulsion residue when the strain amplitude was lower than 5%. While the reverse was true when the strain amplitude become larger than 5%.

(7) The waterborne epoxy resin substantially increased the bond strength between the bitumen emulsion and aggregate, and the bond strength of waterborne epoxy resin modified bitumen emulsion was less affected by temperature. The bond strength of WEBER-5 was more than two times larger than that of WEBER-0 at ambient room temperature.

(8) The waterborne epoxy resin modified bitumen emulsion demonstrated good resistance to moisture damage. With only 1wt% of waterborne epoxy resin, the boiling loss area reduced dramatically compared with that of pure bitumen emulsion mix after 3 days of curing.

CHAPTER 5 CONSTITUTIVE MODELLING OF WEBERs

This chapter presents the constitutive modelling of the waterborne epoxy resin modified bitumen emulsion residues (WEBERs). Section 5.1 introduces different models that have been applied to simulate the responses of bituminous materials. Section 5.2 describes the models used in this study more detailly, including the "2S2P1D" model and the generalized Maxwell model. Section 5.3 presents the experiments conducted, including the frequency sweep test from -10 °C to 60 °C, and the relaxation test in the time domain at 0 °C. Section 5.4 describes the modelling results by the "2S2P1D" model, the Prony series was obtained from the data in both the frequency domain and the time domain.

5.1 Introduction

Bituminous materials are viscoelastic materials, which exhibit both viscous and elastic behaviors under loading. To simulate the viscoelastic properties of the bituminous materials, both empirical algebraic and analogical models have been developed and investigated extensively. Regarding the empirical algebraic approach, the mathematical formulations are adjusted to fit the experimental data, but the parameters may not represent any physical meanings. The Christensen and Anderson (CA) Model, one of the representative empirical algebraic models, was developed during the Strategic Highway Research Program (SHRP) study [207]. The CA model had been validated using the SHRP core bitumens, and the results indicated that this model can generally be used over a wide range of frequencies [207]. However, it is found that the CA model lacks the accuracy at low frequency or high temperature [208]. Another drawback of the CA model is its failure in describing the viscoelastic response of polymer modified bitumens [209]. In an attempt to resolve such limitations, the original CA model was modified by introducing one more parameter, which resulted the CAM

(Christensen-Anderson-Marasteanu) model. Yet, the CAM model still lacks the fitting accuracy at high temperature [208].

On the other hand, the analogical approach, a combination of elastic springs, the viscous dashpots and/or the parabolic elements, were constructed to simulate the viscoelastic performance of bitumens. Some common examples of the analogical models include the generalized Maxwell model, the generalized Kelvin-Voigt model, the Huet-Sayegh (HS) model, the "2S2P1D" (two springs, two parabolic dashpots, and one linear dashpot) model, and the modified Huet-Sayegh (MHS) model [210]. The generalized Maxwell model is constituted by a number of Maxwell model in parallel, while the generalized Kelvin-Voigt model is constituted by a number of Kelvin-Voigt model in series. These two models can generally describe the viscoelastic properties of bitumen binders and mixtures fairly well as long as sufficient numbers of elements are implemented. However, the limitations are that too many parameters are needed to fit the models, and the models are discrete. In contrast, the Huet model [211], constituted by a spring and two parabolic dashpots in series, has a continuous spectrum ((i.e., can be represented by an infinity number of Maxwell elements in parallel or Kelvin-Voigt elements in series). The original Huet model, however, lacks the ability to model polymer modified bitumen correctly. To solve this limitation, Sayegh modified the Huet model by placing a spring in parallel with the Huet model [212]. Since the linear dashpot is not included in the HS model, the accuracy of this model in fitting the data at very low frequency is still limited [210]. In this regard, Olard and Di Benedetto [210] developed the "2S2P1D" model by placing a linear dashpot in series with the two parabolic elements and the spring of rigidity in the original Huet-Sayegh (HS) model. It is found that the "2S2P1D" model can simulate the viscoelastic response of both bituminous binders and mixtures with high accuracy in a wide spectrum of frequency. In addition, the "2S2P1D" model has only 7 parameters, which is significantly less than that of the generalized Maxwell model and the generalized Kevin-Voigt model. Alternatively, Woldekidan, et al. [213] added a linear dashpot in series with the HS model, which was named the modified Huet-Sayegh (MHS) model. Like the “2S2P1D” model, the MHS model agrees well with the viscoelastic responses of most bituminous binders, either the unmodified or the polymer modified binders [214, 215].

However, no analytical forms exist in the time domain for the HS, the “2S2P1D” and the MHS models [210]. To describe the material response in the time domain, the “Prony” series representation of the generalized Maxwell model or the generalized Kevin-Voigt model is more commonly used. The Prony series can well describe the viscoelastic behavior of bituminous materials, and it is computational efficiency in the numerical environment because of the exponential-based formulations [216].

Bituminous materials demonstrate strong time-dependent properties, and such properties are commonly evaluated using the relaxation test and/or the creep test [217]. In this study, the relaxation test was applied to capture such properties. During the relaxation test, the specimen is held with a constant strain, and the stress response is recorded in this process. Given the fact that the material response in the frequency domain and the time domain are intrinsically related if the response stays in the linear viscoelastic region, the constitutive relation in the time domain can be derived if the relation is known in the frequency domain, and vice versa.

The distinct microstructures of the WEBERs may lead to significant viscoelastic change to this novel material, which has not been well investigated. This research aims to constitutively model the response of WEBERs. To achieve such objective, the frequency sweep from 0.1Hz to 30Hz in the temperature of -10 °C to 60 °C was first conducted, followed by the relaxation test at 0 °C. Because of its accuracy in simulating the viscoelastic behavior of bituminous materials in a wide spectrum of frequency, the “2S2P1D” model was employed to simulate the data in the frequency domain. The Prony series based on the generalized Maxwell model was then obtained from the data in both the frequency domain and the time domain.

5.2 Model description

5.2.1 The “2S2P1D” model

Figure 5.1 depicts the “2S2P1D” model [210].

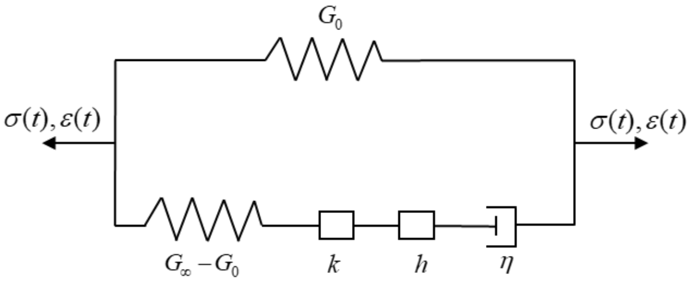

Figure 5.1 The “2S2P1D” model

The complex modulus of the “2S2P1D” model is given as,

$$G^*(\omega) = G_0 + \frac{G_g - G_0}{1 + \alpha(i\omega\tau)^{-k} + (i\omega\tau)^{-h} + (i\omega\beta\tau)^{-1}} \tag{5-1}$$

where ω is the frequency, k and h are exponents with 0 < k, h < 1 (The parabolic element behaves more like an elastic spring with a smaller value, while it behaves more like a viscous dashpot with a larger value), α is a constant, G_0 is the static modulus when $\omega=0$, G_g is the glassy modulus when $\omega=\infty$, τ is the characteristic time that influenced only by the temperature for a specific material, and β is a constant defined as,

$$\eta = (G_g - G_0)\beta\tau \tag{5-2}$$

in which η is the Newtonian viscosity.

5.2.2 The generalized Maxwell model

Figure 5.2 depicts the generalized Maxwell model.

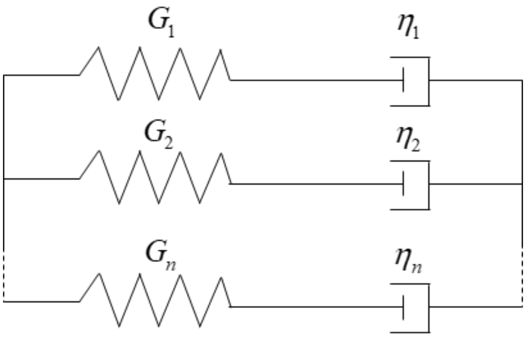

Figure 5.2 The generalized Maxwell model

The storage modulus $G^{'}$ and loss modulus $G^{''}$ are given as,

$$G^{'}(\omega)=\sum_{i=1}^{n}\frac{G_i\omega^2\tau_i^2}{1+\omega^2\tau_i^2}\text{, and } G^{''}(\omega)=\sum_{i=1}^{n}\frac{G_i\omega\tau_i}{1+\omega^2\tau_i^2} \tag{5-3}$$

where G_i and τ_i are the *i*th relaxation modulus and the *i*th relaxation time, respectively.

The relaxation modulus $G(t)$ based on the generalized Maxwell model is given as,

$$G(t)=\frac{\sigma(t)}{\varepsilon_0}=\sum_{i=1}^{n}G_i\exp(-t/\tau_i) \tag{5-4}$$

where ε_0 is the constant strain, t is the relaxation time, $\sigma(t)$ is the stress at time t.

To construct a master curve of the complex modulus, the data obtained at different temperatures are shifted to a reference temperature according to the time-temperature superposition principle (TTSP). The shift factor $\alpha(T)$ is normally calculated using the Williams-Landel-Ferry (WLF) equation [218],

$$\log a(T)=\frac{-C_1(T-T_r)}{C_2+T-T_r} \tag{5-5}$$

where C_1 and C_2 are parameters, T is the testing temperature (°C), and T_r is the reference temperature (°C).

The reduced frequency ω_r at the reference temperature can then be obtained from the following equation,

$$\omega_r = \omega \times 10^{\log a(T)} \tag{5-6}$$

5.3 Experiments

Frequency sweep from 0.1Hz to 30Hz was conducted at -10 °C, 0 °C, 10 °C, 20 °C, 30 °C, 40 °C, 50 °C, and 60 °C in the linear viscoelastic region. Furthermore, the relaxation test at 0 °C was performed at a step strain of 0.1% for 15 min. It should be noted that the both the frequency sweep and the relaxation test used the same specimen to reduce testing errors.

5.4 Results and discussions

5.4.1 Modelling outcome by “2S2P1D” model

The master curves of the complex modulus fitted by the “2S2P1D” model were obtained employing the regression analysis in the Excel spreadsheet, and the objective function in Eq.(5-7) was used. Table 5.1 and Table 5.2 present the fitting parameters for the WLF function that determines the horizontal shifting factors, as well as the parameters for the “2S2P1D” model, respectively. Figure 5.3 depicts the master curves of the modulus |G*| and the phase angle for WEBER-0, WEBER-1, WEBER-3, and WEBER-5, respectively. It can be seen that both the modulus and the phase angle are well fitted with the “2S2P1D” model, and the fitting quality R^2 are larger than 0.96 for all cases as shown in Table 5.3.

$$f_{\min} = \sum \frac{|G'_M - G'_T|}{G'_T} + \sum \frac{|G''_M - G''_T|}{G''_T} + \sum \frac{|G^*_M - G^*_T|}{G^*_T} + \sum \frac{|\delta_M - \delta_T|}{\delta_T} \tag{5-7}$$

where G', G'', G^*, and δ denote the storage modulus, loss modulus, complex modulus, and phase angle, respectively. The subscripts of *M* and *T* indicate the data obtained from model and test, respectively.

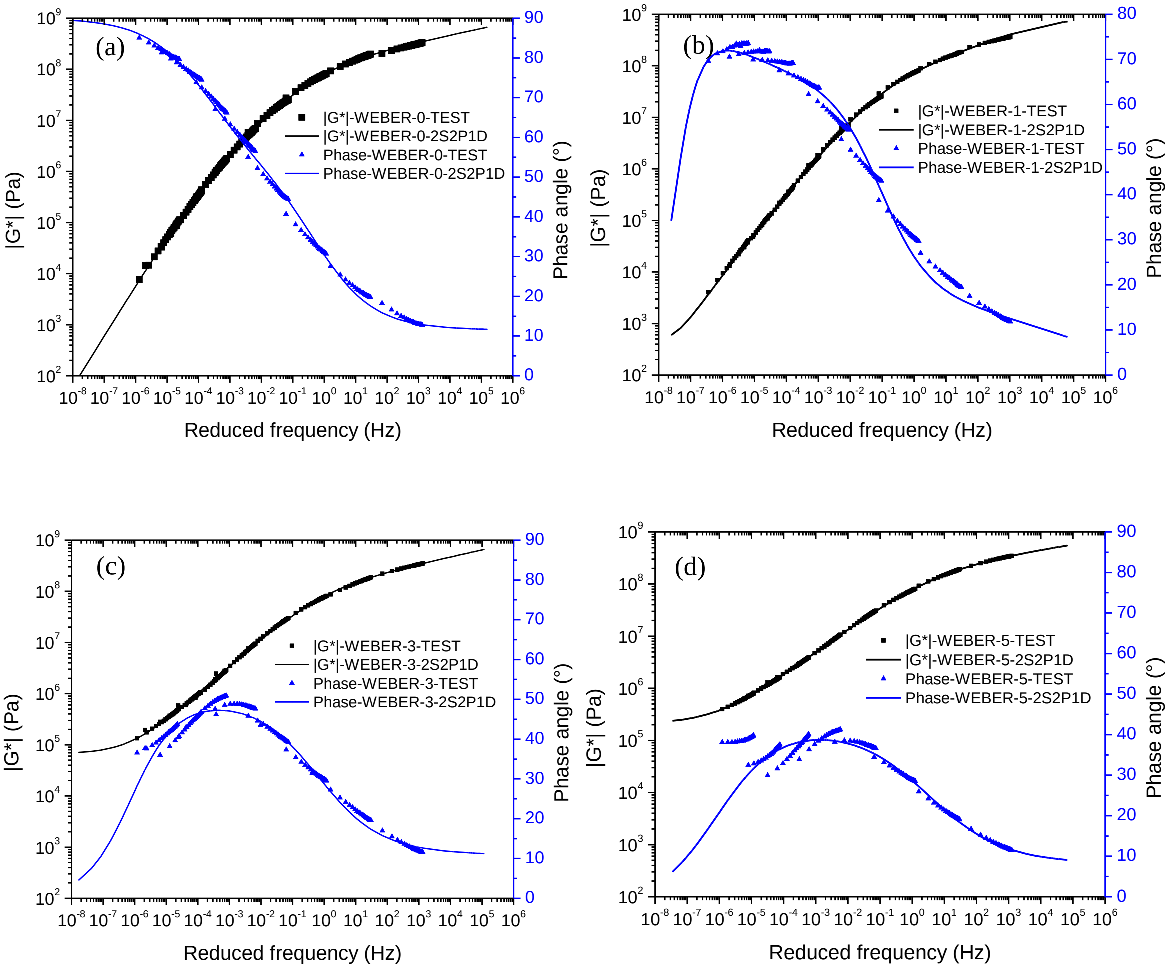

Figure 5.3 Master curves of complex moduli and phase angle: (a) WEBER-0, (b) WEBER-1, (c) WEBER-3, (d) WEBER-5 (reference temperature: 0 °C)

Table 5.1 Parameters for WLF equation

Sample ID	C_1	C_2 (K)
WEBER-0	18.52	119.64
WEBER-1	20.60	136.45
WEBER-3	18.06	118.99
WEBER-5	23.10	155.12

Table 5.2 The “2S2P1D” model parameters for WEBERs

Sample ID	k	h	α	β	τ (s)	G_0 (Pa)	G_g(Pa)
WEBER-0	0.131	0.581	66.3	1.53E+03	1.39E-04	7.50E-9	2.91E+10
WEBER-1	0.205	0.717	6.3	1.04E+02	2.87E-01	4.42E+02	6.78E+08
WEBER-3	0.131	0.556	26.8	3.59E+05	6.82E-04	6.70E+04	9.46E+09
WEBER-5	0.095	0.464	32.8	5.50E+06	2.37E-05	2.20E+05	1.71E+10

Table 5.3 Fitting quality of the experiment data (R^2 values)

Sample ID	R^2-Complex modulus	R^2-Phase angle
WEBER-0	0.984	0.987
WEBER-1	0.997	0.991
WEBER-3	0.999	0.972
WEBER-5	0.999	0.969

It is noticed from Table 5.2 that the parameter G_0 of the pure bitumen emulsion residue WEBER-0 was close to 0, indicating that the stand-alone spring can be removed. Comparing the parameters for the three emulsion residues that containing waterborne epoxy resin, i.e., WEBER-1, WEBER-3, and WEBER-5, it is observed that they demonstrated certain trend with increasing dosages of waterborne epoxy resin. Both the glassy spring parameter G_g and the static stand-alone spring parameter G_0 increased with larger concentration of waterborne epoxy resin, indicating increased elasticity of the binder. In contrast, the parabolic element parameters k and h decreased with larger concentration of waterborne epoxy resin, suggesting enhanced interaction between the bitumen particles and the epoxy resin networks. In addition, the values of h were over three times larger than those of k for each specimen, which revealed that the first parabolic element performed more like an elastic spring, while the second parabolic element performed more like a viscous dashpot. It is further observed that the parameter α increased with increasing concentration of waterborne epoxy resin. Previous studies [214, 219] have shown that α generally becomes larger for stiffer materials. This is also consistent from this study, as larger concentration of waterborne epoxy resin leads to higher stiffness. Furthermore, the parameter β is related to the viscous character of the linear dashpot, which demonstrated an increasing tendency with the increase concentration of waterborne epoxy resin, because of the increment of viscosity.

Figure 5.4 depicts the schematic relation between the WEBER’s microstructure and the ‘2S2P1D” model. The cured epoxy resin film forms the skeleton structure of the material, and the bitumen particles are encapsulated by the epoxy resin film. The epoxy resin film represents the stand-alone static spring, which provides the elasticity to the material. On the other hand, the interaction between the bitumen particles with epoxy resin and the bitumen particles are equivalent to the parabolic dashpots and the viscous dashpot, respectively, and they provide the viscoelasticity and the viscous properties to the material. When a stress in the linear viscoelastic domain is applied on the material, an instant deformation will occur because of the elasticity, which increases with time due to the viscoelasticity of the material. Upon removing of this stress, there is an instant elastic recovery, followed by a slow deformation recovery with increasing of time. Given the viscous character of the bitumen particles, part of the deformation may not recover.

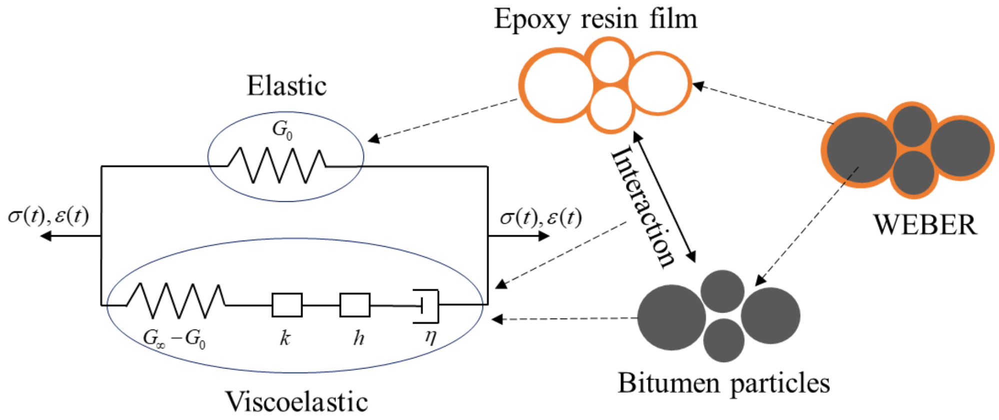

Figure 5.4 Schematic relation between the microstructure of WEBER and the “2S2P1D” model

5.4.2 Modelling outcome by the generalized Maxwell model

It has been shown that the scatter of the experimental data can affect the fitting outcome of the Prony series, and they may also lead to negative coefficients, which is physically unrealistic [216]. It is therefore desirable that the experimental data be pre-smoothed in advance, which can generally result in better fitting quality. Various models, such as the CA model, the power law model, the “2S2P1D” model, and the MHS model, have been employed to perform the pre-smoothing of the data [217, 220]. In this study, the response data pre-smoothed by the

"2S2P1D" model were then fitted employing the generalized Maxwell model to obtain the Prony series.

Previous research has shown that the optimization based only on the data from the frequency domain or the time domain alone cannot obtain precise fitting outcome [221], thus the data from both the frequency domain and the time domain are considered in the optimization in this study. The objective function in Eq.(5-8) was used for the optimization,

$$f_{\min} = \sum \frac{|G'_M - G'_T|}{G'_T} + \sum \frac{|G''_M - G''_T|}{G''_T} + \sum \frac{|G^*_M - G^*_T|}{G^*_T} + \sum \frac{|\delta_M - \delta_T|}{\delta_T} + \sum \frac{|G(t)_M - G(t)_T|}{G(t)_T} \tag{5-8}$$

where $G(t)_M$ and $G(t)_T$ are the relaxation modulus obtained from model and test, respectively.

Figure 5.5 shows that the generalized Maxwell model can describe the complex modulus |G*| with high accuracy. While the fitting quality of phase angel was not as good, which showed oscillatory deviation. It was found that 12 Maxwell terms were suitable for the modelling in this study. The parameters and the fitting quality are presented in Table 5.4 and Table 5.5, respectively. The discrepancy for the phase angel results mainly form the discrete nature of the generalized Maxwell model.

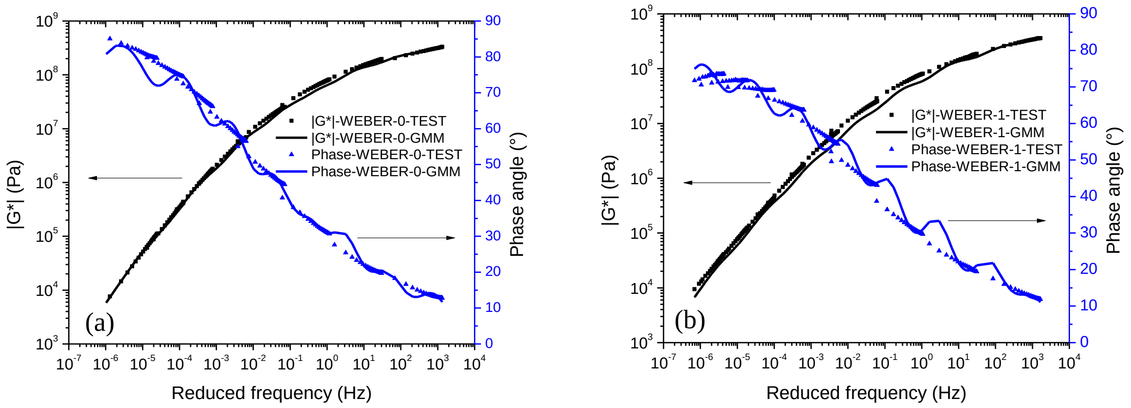

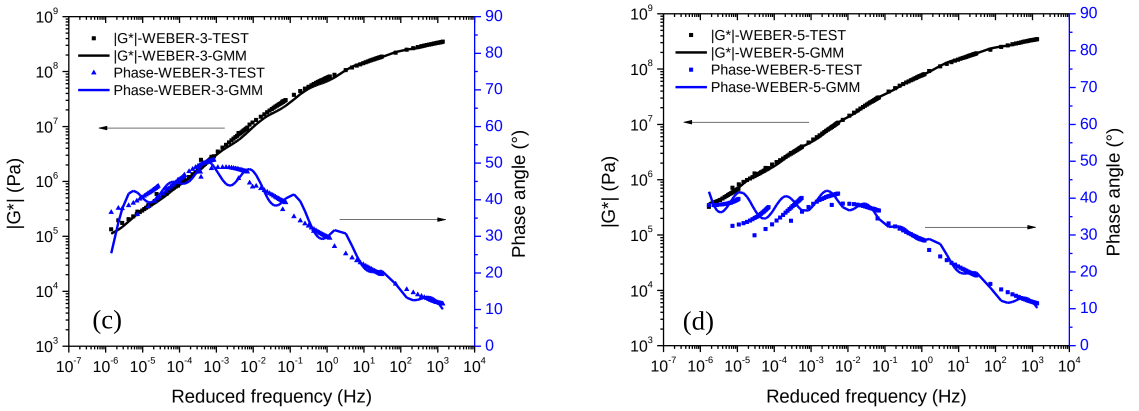

Figure 5.5 Generalized Maxwell model fitting: (a) WEBER-0, (b) WEBER-1, (c) WEBER-3, and (d) WEBER-5 (reference temperature: 0 °C)

Table 5.4 Fitting parameters of the generalized Maxwell model

	WEBER-0		WEBER-1		WEBER-3		WEBER-5	
n	G_n	τ_n	G_n	τ_n	G_n	τ_n	G_n	τ_n
1	1.15E+08	9.86E-03	1.17E+08	1.01E-02	1.26E+08	1.41E-02	1.25E+08	1.15E-02
2	1.23E+08	7.93E-04	1.07E+08	8.60E-04	1.23E+08	9.55E-04	1.16E+08	8.95E-04
3	6.44E+07	1.07E-01	9.21E+07	1.81E-01	9.42E+07	2.30E-01	9.45E+07	1.95E-01
4	4.97E+07	1.07E+00	2.92E+07	3.33E+00	3.85E+07	4.11E+00	3.51E+07	3.07E+00
5	2.38E+07	1.20E+01	7.96E+06	2.57E+01	1.06E+07	7.52E+01	1.08E+07	2.48E+01
6	6.74E+06	1.43E+02	4.21E+06	1.44E+02	2.42E+06	1.14E+03	1.96E+06	2.07E+03
7	9.15E+05	2.17E+03	1.03E+06	2.53E+03	4.76E+05	1.73E+04	5.70E+06	1.76E+02
8	4.36E+04	6.07E+04	1.11E+05	4.29E+04	1.62E+05	1.89E+05	7.82E+05	2.77E+04
9	2.99E+01	1.57E+08	1.12E+04	1.01E+06	8.41E+04	1.39E+10	4.64E+05	1.38E+06
10	3.36E-02	1.58E+00	3.36E-02	1.58E+00	3.36E-02	1.58E+00	3.36E-02	1.58E+00
11	2.99E-10	2.85E+00	3.09E-10	2.85E+00	2.93E-10	2.85E+00	4.39E-10	2.85E+00
12	6.76E-11	4.52E-04	7.17E-11	4.52E-04	6.77E-11	4.52E-04	1.39E-10	4.52E-04

Table 5.5 Fitting quality of experiment data to GMM

Sample ID	R^2-Complex moduli	R^2-Phase angle
WEBER-0	0.997	0.997
WEBER-1	0.998	0.964
WEBER-3	0.997	0.961
WEBER-5	0.995	0.931

Since the constitutive relation in the LVE region is inter-convertible for the response in the frequency domain and the time domain, the relation in the time domain can be obtained given the relation in the frequency domain.

In the relaxation test, a constant shear strain is applied on the specimen, and the stress response is recorded during this process. Figure 5.6 depicts the strain profile in the test. It can be seen that the strain increased to the target strain (0.1%) within 0.1 s and kept constant for the next 15 min.

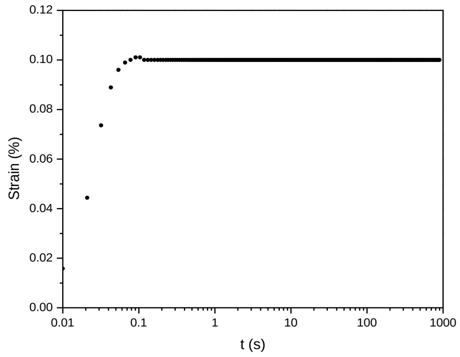

Figure 5.6 Strain profile in the relaxation test

Figure 5.7 depicts the relaxation modulus profile from both test and model prediction for all WEBERs, and Table 5.6 presents the fitting quality. It is observed the predicted values fit the experiment data fairly well, indicating that the Prony series can also describe the emulsion residues response in the time domain in an acceptable accuracy.

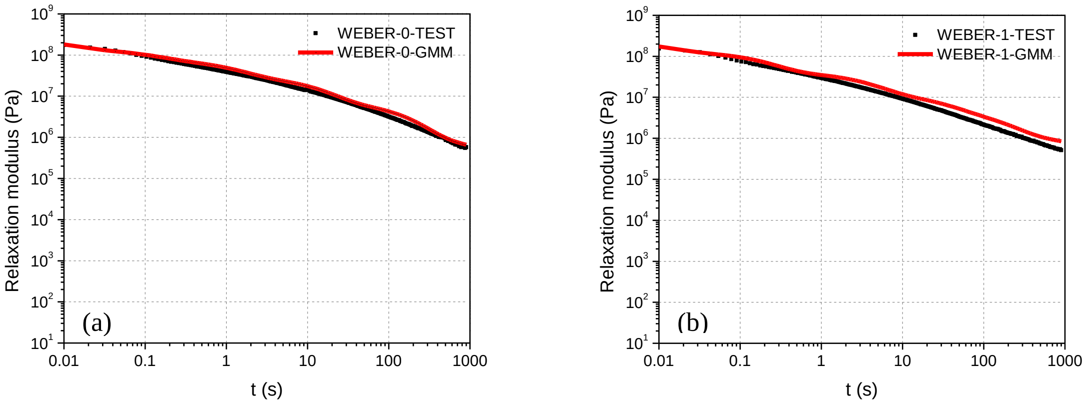

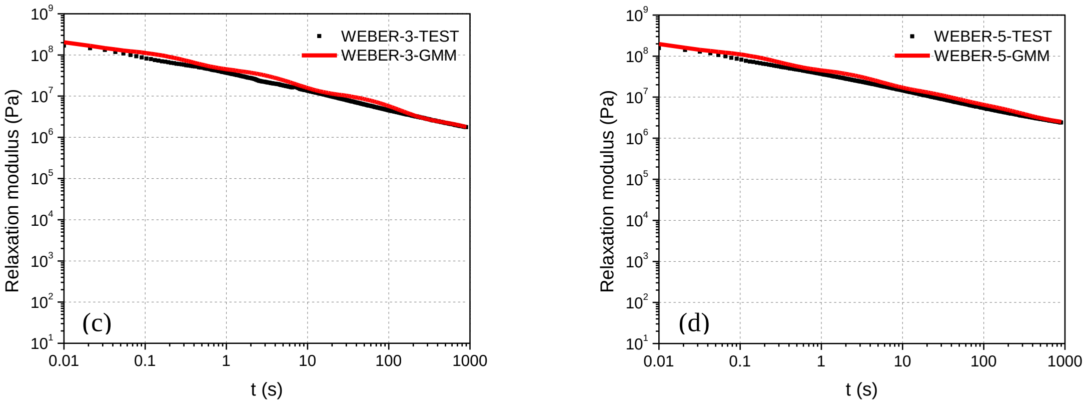

Figure 5.7 Tested and predicted relaxation modulus: (a) WEBER-0, (b) WEBER-1, (c) WEBER-3, and (d) WEBER-5

Table 5.6 Quality of fitting to experiment data

Sample ID	WEBER-0	WEBER-1	WEBER-3	WEBER-5
R^2	0.962	0.890	0.885	0.887

Additionally, it can be seen that the relaxation modulus decreased with extension of time from Figure 5.6. However, the decreasing rate of the relaxation moduli varies for different WEBERs. With the increase of the waterborne epoxy resin dosages, the decreasing rate of the relaxation modulus lowered. Table 5.7 presents the ratios of the final relaxation modulus G_{final} to that of the initial relaxation modulus G_{ini}. This result indicates that the stress relaxed slower under strain for the waterborne epoxy resin modified bitumen emulsion residues in comparison with the unmodified emulsion residue. The faster relaxation of the unmodified emulsion residue WEBER-0 results mainly from the fact that the smaller molecules have better mobility and can relocate themselves more efficiently, and thus the stress or relaxation moduli decreased faster. On the other hand, the presence of the inter-connected epoxy structure in the WEBERs significantly decreased the molecule mobility. As a result, the stress relaxation of the waterborne epoxy bitumen emulsion residues is largely reduced.

Table 5.7 Percentage of G_{final} to G_{ini}

Sample ID	WEBER-0	WEBER-1	WEBER-3	WEBER-5
G_{final}/ G_{ini} (%)	0.328	0.329	1.04	1.54

5.5 Summary

The “2S2P1D” model has been used to describe the frequency domain response of WEBERs. The results show that the model is capable in describing the response over a wide frequency window, both the pure bitumen emulsion residue as well as the waterborne epoxy resin modified bitumen emulsion residues. In addition, the microstructure of the WEBERs is closely related with the parameters of the “2S2P1D” model. Both the glassy modulus parameter G_g and the static modulus G_0 increased with increasing of waterborne epoxy resin dosages, while the parabolic parameters k and h decreased.

After the pre-smoothing of the experimental data in the frequency domain, the generalized Maxwell model was utilized to fit the data and generate the Prony series. However, in comparison to the “2S2P1D” model the phase angle description of the generalized Maxwell model has been found to be less accurate. This behavior is mainly related to the discrete nature of the analytical expression that is used to describe the material functions.

In order to establish the relation between the frequency domain response and the time domain response, the Prony series was obtained from the data in both the frequency domain and the time domain. The results of the simulations have been compared with experimental data, which showed good agreement between the experimental data and the predicted data. The obtained Prony series can be used for future studies like the finite element analysis of this material.

CHAPTER 6 APPLICATION OF WEMBE AS A TACK COAT MATERIAL

This chapter presents a case study of using the waterborne epoxy resin modified bitumen emulsion as the material for tack coat application. Section 6.1 gives the background and significance of this work. Section 6.2 describes the direct shear test conducted to evaluate the shear strength of a double-layer asphalt mixture prepared with a Superpave gyratory compactor (SGC). Section 6.3 presents the findings.

6.1 Introduction

Pavements are constructed by several layers, and the interlayer bonding is crucial to improve the integrity of the pavement structure. Effective bonding between the layers guarantees the proper distribution and transfer of the stress between different layers. Many previous studies have shown that inadequate interlayer bonding may lead to premature failures of pavement like slippage, cracking and potholes, thereby decreasing the pavement service life [222-224]. Pavement failures caused by bond problems have been frequently found in locations subjected to high braking and turning forces [75]. It was reported that the pavement service life may reduce 40% to 80% for lack of sufficient interlayer bonding [225]. To increase the pavement interlayer bonding, tack coat is commonly applied. Tack coat is defined as a light "application of bituminous material to an existing relatively nonabsorptive surface to provide a thorough bond between old and new surfacing", according to the American Society for Testing and Materials (ASTM) D8-20. Conventionally, hot asphalt cement, cutback asphalt and bitumen emulsion have been used as tack coat materials. However, the cutback asphalt is rarely used now because of safety and environmental concerns [226]. The application of hot asphalt cement as tack coat material is also limited due to the need of heating, and the difficulty in ensuring uniform spraying especially at low application rate [227]. On the other hand, the bitumen emulsion-based tack coat offers many additional advantages, such as ease of handling, reduced energy consumption, and environmental impacts [228]. Thus, bitumen emulsion is more preferred as tack coat material.

Different types of bitumen emulsions are used based on considerations of existing pavement surface conditions, weather, and construction window, etc. However, it is reported that the cationic emulsions are the most commonly used tack coat materials [229]. Additionally, a survey by Paul and Scherocman [230] indicated that most projects of tack coat in the US used the slow-setting bitumen emulsions, and the residual application rates of the emulsions generally varied between 0.06 L/m^2 and 0.26 L/m^2 depending on the surface conditions of the existing layer. The reasons for selecting the slow-setting bitumen emulsion includes: 1) they allow sufficient time for the distributor to function at normal speed when lower application rates are used, and 2) they flow easily from the distributor at ambient temperatures that ensures a more uniform application [231, 232]. The application rate of the tack coat depends on many factors, including type of tack coat, pavement surface texture, and type of pavement (cement concrete or asphalt concrete) [73].

A series of testing methods, including torsion, tensile and shear tests, have been developed to evaluate the interlayer bonding strength of different pavement layers. Nevertheless, previous research indicated that the interface failure of the pavement is mainly caused by shear stress [233]. As a result, the shear test is the most widely used testing method for evaluating the pavement interlayer bonding [234, 235]. The Leutner shear test, developed in Germany to characterize the shear bond strength of asphalt mixture without normal force [236], is now frequently used. This test is performed on a 150 mm diameter two-layer asphalt mixture prepared in the laboratory or taken from the field, and the testing temperature is typically 20 °C. A constant loading rate of 50 mm/min is applied on the two-layer structure, and the shear force is monitored until failure.

This chapter presents a case study on investigating the influence of WEMBE to the interlayer bond strength of asphalt mixture. To achieve this objective, the bitumen emulsions containing different amounts of waterborne epoxy resin (1wt%, 3wt%, and 5wt%, denoted as WEMBE-1, WEMBE-3, and WEMBE-5, respectively) were prepared and evaluated as tack coat materials, and the bitumen emulsion without waterborne epoxy resin was considered as the control group (WEMBE-0). A two-layer cylindrical asphalt mixture structure was fabricated using the Superpave gyratory compactor (SGC), and the direct shear strength was then measured and compared with a dynamic testing system (DTS-30, PAVETEST) after proper conditioning.

6.2 Methods

A bottom layer asphalt mixture with the gradation of BC28 (base course dense-graded mixture with a nominal maximum aggregate size of 28mm) and a wearing course asphalt mixture with the gradation of WC20 (wearing course dense-graded mixture with a nominal maximum aggregate size of 20mm) were used for the two-layer specimen fabrication. Figure 6.1 depicts the gradations of both BC28 and WC20. The Superpave gyratory compactor was employed to prepare the specimens with a diameter of 150 mm. The thicknesses of the bottom and the upper layer were 60 mm and 40 mm, respectively, which were determined in accordance with typical pavement design in Hong Kong. The air void of the mixture was determined to be 6% ± 1% according to the specification AASHTO T 312 [237].

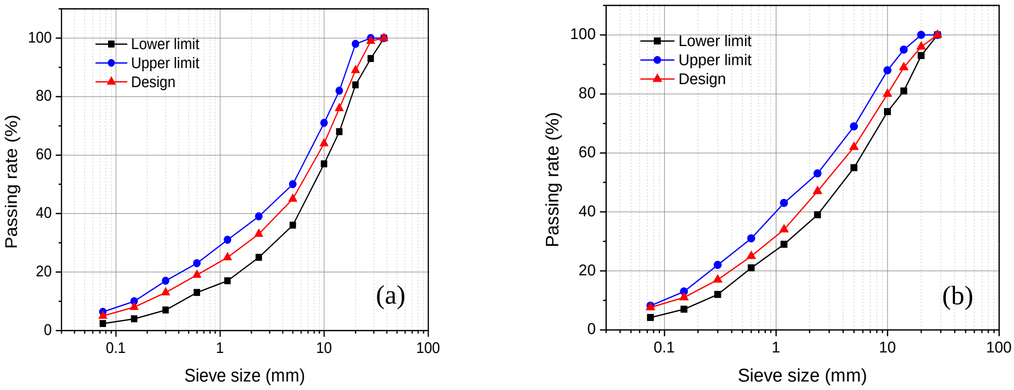

Figure 6.1 Aggregate gradation of: (a) BC28 and (b) WC20

The bottom layer was compacted first and extruded from the mold, which was then placed at the room temperature (23 ± 0.5 °C) for 24 h. To measure the mean texture depth (MTD) of the bottom layer surface, the sand-patch method was employed according to BS EN 13036 [238] (Figure 6.2). The MTD was determined to be 0.337 mm, with a coefficient of variation (CV) of 5.4% based on three measurements. The bitumen emulsion was then uniformly applied on the surface using a brush, which was then maintained for approximately 2 hours to allow the breaking of the emulsion (Figure 6.3). The bottom layer was subsequently put back into the SGC mold, and the loose mixture of the upper layer was then placed and compacted on top of the bottom layer. The two-layer structure was then taken out form the mold and cured in an oven for 4 days at the temperature of 40 °C (Figure 6.4). The specimens were then conditioned in the chamber for at least 4 hours prior to testing. Two temperatures were considered during the direct shear test, 25 °C and 50 °C. A loading rate of 50 mm/min was applied during the direct shear test, and the shear force was recorded in the process.

The optimum amount of bitumen emulsion was first determined in this study. Note that the newly constructed pavement normally requires less amount of tack coat because of the smoother surface. Three different application rates of residual bitumen emulsion were compared in the first stage: 0.12 kg/m^2, 0.24 kg/m^2, and 0.36 kg/m^2. In the second stage, the influence of different WEMBEs was evaluated at the optimum application rate. A custom-designed shear device was applied for the shear strength test (Figure 6.5). Two specimens were fabricated and measured for each sample test.

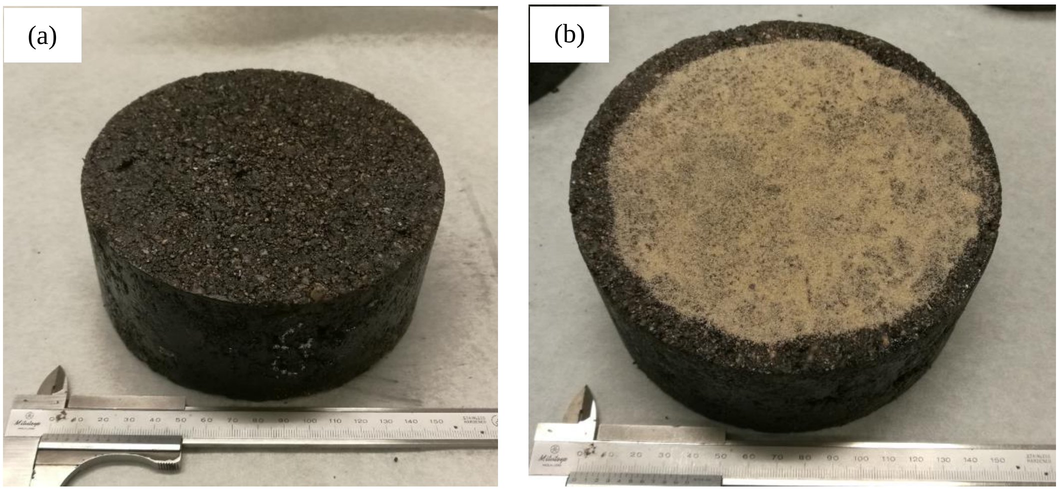

Figure 6.2 Determination of mean texture depth (MTD) using the sand patch method: (a) the bottom layer asphalt mixture, (b) sand patch method

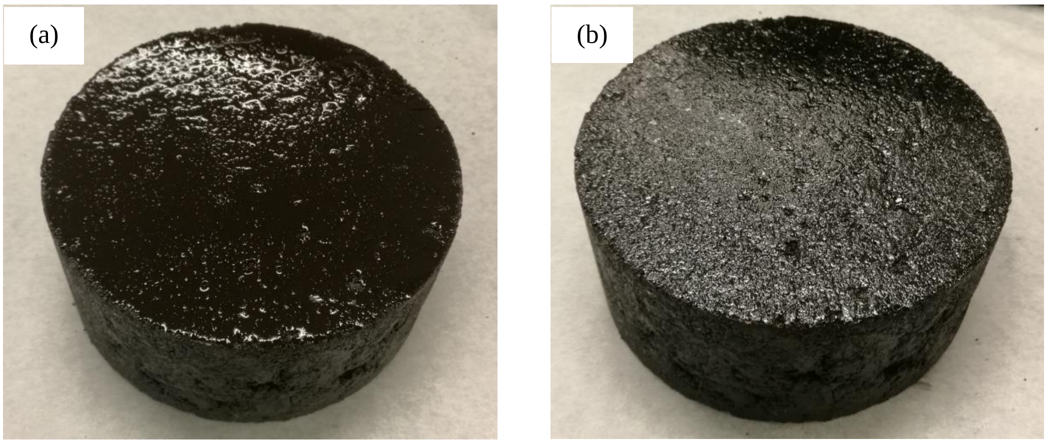

Figure 6.3 Application of the bitumen emulsion: (a) before breaking, (b) after breaking

Figure 6.4 The two-layer asphalt mixture structure

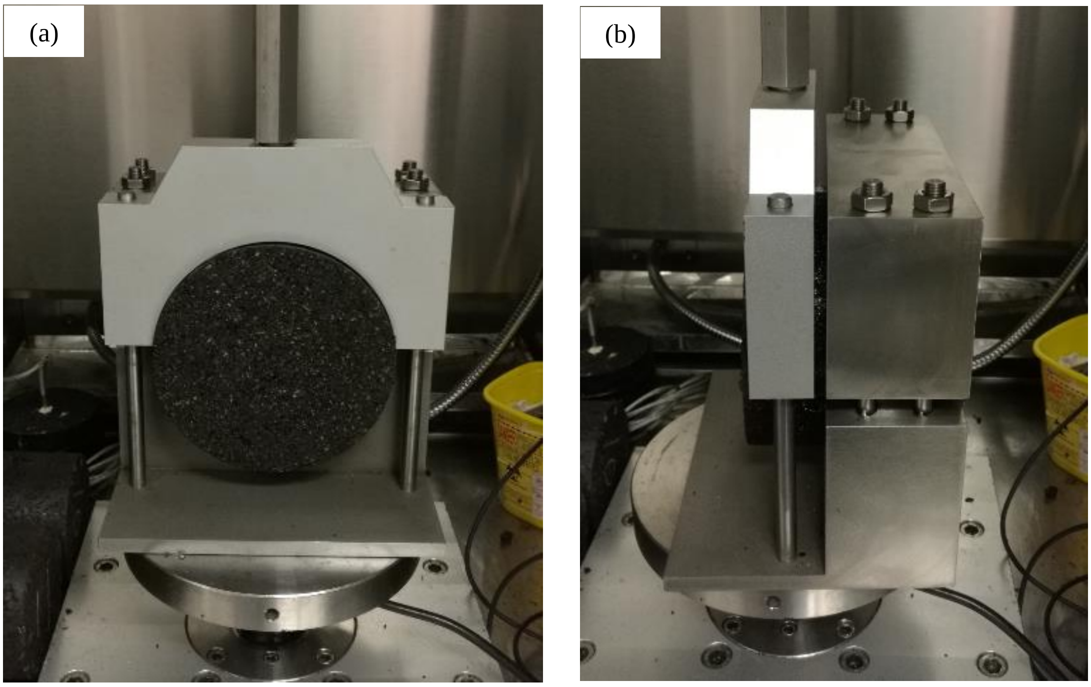

Figure 6.5 Direct shear testing set-up: (a) front view, (b) side view

6.3 Results and discussions

6.3.1 Optimum application rate

Figure 6.6 depicts the shear strength of the two-layer structure for different application rates of the bitumen emulsion at the temperature of 20 °C. The shear strength for the application of 0.12 kg/m^2 and 0.24 kg/m^2 were very close (1.59 MPa and 1.58 MPa, respectively), which dropped to 1.48 MPa at the higher application rate of 0.36 kg/m^2. The lower shear strength for 0.36 kg/m^2 indicates that an excess of the tack coat may decrease the interlayer bonding and promote shear slippage. In fact, too much tack coat can act as a lubricating material between the layer, thereby decreasing the interlocking between the layers. As a result, the application rate of 0.12 kg/m^2 tack coat was selected for further study based on the shear strength and cost considerations. It should be noted that the maximum shear force was larger than 28 kN at the temperature of 20 °C, which was close to the upper limit (30 kN) of the equipment. Hence, the following tests were performed at 25 °C and 50 °C, to represent normal ambient temperature and high service temperature in hot seasons, respectively.

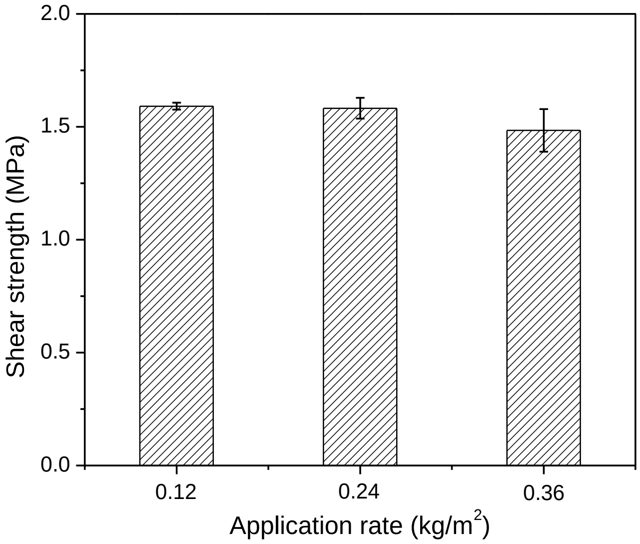

Figure 6.6 Effect of application rate of the bitumen emulsion on shear strength

6.3.2 Influence of waterborne epoxy resin contents

Figure 6.7 depicts the shear strength of different WEMBEs with different dosages of waterborne epoxy resin at both 25 °C and 50 °C. It is observed that the shear strength of the two-layer structure increased with increasing of waterborne epoxy resin contents at both temperatures. The shear strength values of WEBME-3 and WEBME-5 were 1.10 MPa and 1.13 MPa at 25 °C, respectively, representing an increase of 15.3% and 18.0% compared with that of the control bitumen emulsion. It is noticeable that temperature plays a significant role on the shear strength of the two-layer structure. For example, the shear strength of WEMBE-0 and WEMBE-5 at 50 °C dropped 77% and 73% compared with their counterparts at 25 °C. However, the shear strength of the waterborne epoxy resin modified bitumen emulsions are still larger than that of the pure bitumen emulsion at 50 °C.

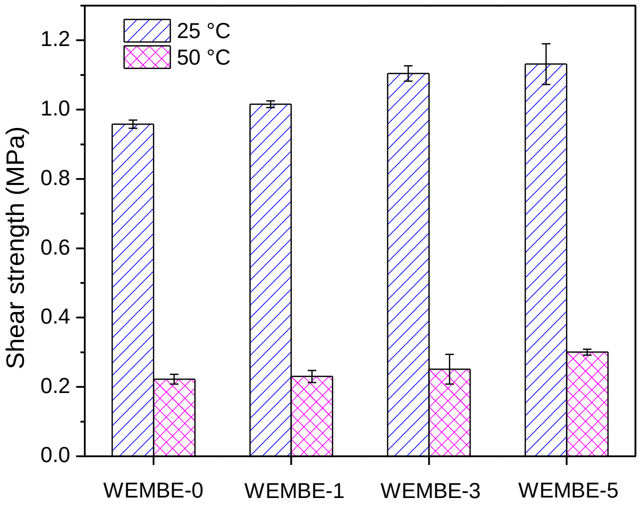

Figure 6.7 Shear strength of different WEMBEs

Figure 6.8 depicts the shear force profile against the displacement during the shear test at both 25 °C and 50 °C. It can be seen that shear force increased linearly at first, and decreased after the peak. The peak force at 25 °C is 4-5 times larger than that of the values at 50 °C. However, the force dropped more rapidly after the peak value at 25 °C in comparison with that of the 50 °C. Such phenomenon indicates that the failure is more brittle at the lower temperature, and the higher temperature failure is more ductile. This finding is similar with that reported by Recasens, et al. [239]. Nevertheless, it is clear that the peak force increased with larger contents of waterborne epoxy resin at both testing temperatures.

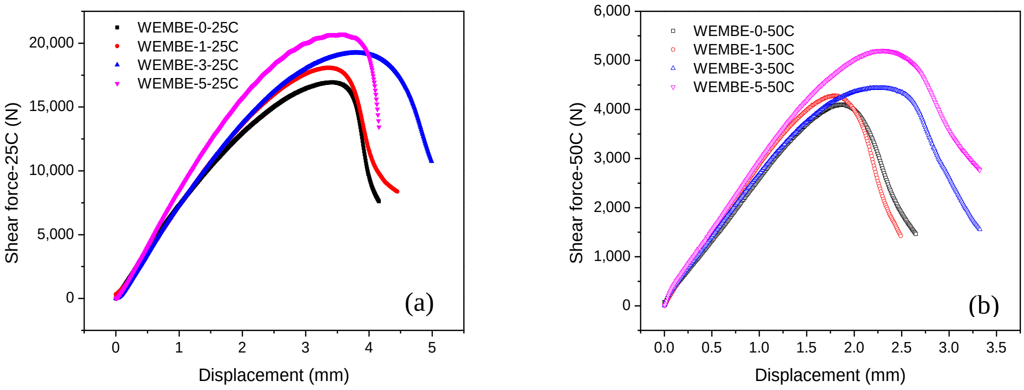

Figure 6.8 Plot of shear force-displacement curves at: (a) 25 °C and (b) 50 °C

6.4 Summary

In this chapter, the influence of waterborne epoxy resin modified bitumen emulsion on the bond strength of the two-layer asphalt mixture structure was evaluated through direct shear test. A two-layer asphalt mixture structure was fabricated in the lab using the Superpave gyratory compactor, and the bitumen emulsions containing 0wt%, 1wt%, 3wt%, and 5wt% of waterborne epoxy resin were evaluated. The following conclusions can be drawn from this study:

(1) The optimum application rate of the bitumen emulsion was determined to be 0.12 kg/m^2 based on the residue. Because of the smooth surface of the newly compacted dense-graded bottom layer, the application rate of the bitumen emulsion is relatively low.

(2) The shear strength increased with increasing of the waterborne epoxy resin dosages. The shear strength values of WEBME-3 and WEBME-5 reached 1.10 MPa and 1.13 MPa at 25 °C, respectively, representing an increase of 15.3% and 18.0% compared with that of the control bitumen emulsion.

(3) The shear failure is more brittle at the lower temperature, and the higher temperature failure is more ductile.

The results from this chapter indicates that the application of waterborne epoxy resin modified bitumen emulsion as a tack coat material can increase the shear strength between different asphalt mixture layers. Such performance is desirable to reduce the asphalt pavement premature distresses caused by poor bonding strength, or in the sections where high interlayer shear stress is expected, such as bus station, road slopes and corners.

CHAPTER 7 CONCLUSIONS AND RECOMMENDATIONS

Modification of bitumen emulsion with waterborne epoxy resin represents a green and sustainable technology for producing the high-performance polymer modified bituminous materials. It can be potentially applied in pavement surface treatment (chip seal, micro-surfacing, slurry seal), tack coat, cold recycling, and cold mixes. The overall objective of this study is to investigate the influence of waterborne epoxy resin on the microstructure and mechanical performance of bitumen emulsion. To achieve this objective, the following research tasks were performed: 1) evaluation of the effect of waterborne epoxy resin on the performance of bitumen emulsion, including microstructure, stability and rheological properties; 2) investigation of the effect of waterborne epoxy resin on the performance of emulsion residues, including microstructure, rheology, high temperature performance, aging, fatigue, bond strength with aggregate, and moisture susceptibility; 3) development of the constitutive models of the waterborne epoxy resin modified bitumen emulsion residues (WEBERs) based on frequency sweep and relaxation measurements; and 4) characterization of the performance of waterborne epoxy resin modified bitumen emulsion (WEMBE) as a tack coat material.

7.1 Findings and conclusions

Based on the outcomes of this study, the following major findings have been obtained:

1. The waterborne curing agent (WCA) synthesized in this study was dispersed in water with a very small mean particle size of 55 nm, indicating strong self-emulsifying ability. In addition, the WCA can effectively emulsify the epoxy resin, and the average diameter of the obtained epoxy resin droplets was 247 nm.

2. Most of the bitumen particles in the bitumen emulsion were smaller than 10 μm, and became larger after storing for 5 days. However, the sizes of the bitumen particles in

bitumen emulsion with waterborne epoxy resin were not so large as those of the pure bitumen emulsion, indicating that the waterborne epoxy resin acted as a barrier between bitumen particles, thus hindered the bitumen particles from coalescence.

3. All the bitumen emulsions showed significant shear-thinning behavior at the lower shear rate region (0-10 s^{-1}). The pure bitumen emulsion behaved as a Newtonian fluid at the higher shear rate (10-200 s^{-1}), while the waterborne epoxy resin modified bitumen emulsion showed shear-thickening behavior. The difference may be caused by the waterborne epoxy resin, which could become entangled with each other at higher shear rate, thereby increasing the viscosity.

4. Bitumen emulsion demonstrated strong thixotropy behavior. The bitumen particles are closely packed in bitumen emulsion, and their interaction can be disrupted by shear stress. However, such interaction can reform again with the decrease of shear rate.

5. The cured waterborne epoxy resin formed a polymer-rich film when the dosages of waterborne epoxy resin reached 3wt%. Such polymer structure is beneficial for the improvement of the mechanical performance of the emulsion residue.

6. The addition of waterborne epoxy resin significantly improved the mechanical properties of bitumen emulsion. The complex shear moduli of WEBERs were much larger than that of the pure bitumen emulsion residue, while the phase angles decreased markedly, indicating that the waterborne epoxy resin changed the base bitumen binder into a more elastic material.

7. The MSCR results showed that with the increase of waterborne epoxy concentration, the percent recovery increased while the nonrecoverable creep compliance decreased, indicating that the resistance to permanent deformation was dramatically improved by waterborne epoxy resin.

8. The incorporation of waterborne epoxy resin into bitumen emulsion improved the resistance to oxidative aging of the residues. This effect is attributed to the formation of the polymer-rich film that encapsulated the bitumen particles, which reduced the diffusion of oxygen into the bitumen phase.

9. The time sweep test results at the stresses of 300 kPa to 500 kPa indicated that the fatigue life of the emulsion residue was increased by incorporation of waterborne epoxy resin. Yet, from the LAS tests, it was concluded that the fatigue life of WEBERs containing waterborne epoxy resin was larger than that of the pure bitumen emulsion residue when the strain amplitude was lower than 5%. While the reverse was true when the strain amplitude become larger than 5%.

10. The waterborne epoxy resin substantially increased the bond strength between the bitumen emulsion and aggregate, and the bond strength of waterborne epoxy resin modified bitumen emulsion was less affected by temperature.

11. The waterborne epoxy resin modified bitumen emulsion demonstrated better resistance to moisture damage by boiling test. With only 1wt% of waterborne epoxy resin, the boiling loss area reduced dramatically compared with that of pure bitumen emulsion mix after 3 days of maintenance.

12. The “2S2P1D” model was capable of describing the response of the waterborne epoxy resin bitumen emulsion residues over a wide frequency window. In addition, the Prony series can describe the material’s response in both the frequency domain and the time domain fairly well.

13. The shear strength between different asphalt mixture layers was increased with the increase of the waterborne epoxy resin contents, indicating the feasibility of using the waterborne epoxy resin modified bitumen emulsion as a tack coat material.

Correspondingly, the following general conclusions have been drawn:

1. The cured waterborne epoxy resin forms an inter-connected structure in the emulsion residue when the dosages of waterborne epoxy resin reached 3wt%. Such structure changes the viscoelasticity of the base bitumen substantially, which is beneficial for the improvement of the mechanical performance of the emulsion residue.

2. The incorporation of waterborne epoxy resin can significantly increase the performances of the bitumen emulsion residues, including the high-temperature performance, fatigue performance, and adhesion with aggregate, while the moisture susceptibility was decreased.

3. The incorporation of waterborne epoxy resin into bitumen emulsion can improve the resistance to oxidative aging and fatigue of the residues, because of the formation of the polymer-rich film structure.

4. The “2S2P1D” model can describe the dynamic response of the waterborne epoxy resin bitumen emulsion residues with high accuracy.

5. When the waterborne epoxy resin bitumen emulsion is used as a tack coat material, it can improve the interface bonding between the asphalt layers.

7.2 Recommendations for future research

Since WEMBE is a relatively new research topic, more research is still required to more extensively explore its properties and applications. Based on the findings and conclusions of this research, future research is recommended on the following aspects:

- Effect of storage time on the microstructure and performance of WEMBE should be further investigated.

- The performance of WEMBE in different applications, such as pavement surface treatment, cold recycling, and cold mixes, should be further evaluated.
- Comparative life cycle assessment should be conducted between WEMBE and normal polymer modified bitumen to quantify its overall sustainability performance.

REFERENCES

[1] S. E. E. Khay, J. Neji, and A. Loulizi, Shrinkage properties of compacted sand concrete used in pavements, *Construction and Building materials,* vol. 24, no. 9, pp. 1790-1795, 2010.

[2] M. García-Morales, P. Partal, F. J. Navarro, and C. Gallegos, Effect of waste polymer addition on the rheology of modified bitumen, *Fuel,* vol. 85, no. 7, pp. 936-943, 2006.

[3] M. A. Rodríguez-Valverde, P. Ramón-Torregrosa, A. Páez-Dueñas, M. A. Cabrerizo-Vílchez, and R. Hidalgo-Álvarez, Imaging techniques applied to characterize bitumen and bituminous emulsions, *Advances in Colloid and Interface Science,* vol. 136, no. 1, pp. 93-108, 2008.

[4] D. Lesueur, The colloidal structure of bitumen: Consequences on the rheology and on the mechanisms of bitumen modification, *Advances in Colloid and Interface Science,* vol. 145, no. 1, pp. 42-82, 2009.

[5] G. Polacco, S. Filippi, F. Merusi, and G. Stastna, A review of the fundamentals of polymer-modified asphalts: Asphalt/polymer interactions and principles of compatibility, *Advances in Colloid and Interface Science,* vol. 224, pp. 72-112, 2015/10/01/ 2015.

[6] J. Zhu, B. Birgisson, and N. Kringos, Polymer modification of bitumen: Advances and challenges, *European Polymer Journal,* vol. 54, pp. 18-38, 2014/05/01/ 2014.

[7] Y. Yildirim, Polymer modified asphalt binders, *Construction and Building Materials,* vol. 21, no. 1, pp. 66-72, 2007/01/01/ 2007.

[8] A. Calabi-Floody and G. Thenoux, Controlling asphalt aging by inclusion of byproducts from red wine industry, *Construction and Building Materials,* vol. 28, no. 1, pp. 616-623, 2012/03/01/ 2012.

[9] S. D. Capitão, L. G. Picado-Santos, and F. Martinho, Pavement engineering materials: Review on the use of warm-mix asphalt, *Construction and Building Materials,* vol. 36, pp. 1016-1024, 2012.

[10] J.-P. Gingras, P. A. Tanguy, S. Mariotti, and P. Chaverot, Effect of process parameters on bitumen emulsions, *Chemical Engineering & Processing: Process Intensification,* vol. 44, no. 9, pp. 979-986, 2005.

[11] A. Yuliestyan, M. García-Morales, E. Moreno, V. Carrera, and P. Partal, Assessment of modified lignin cationic emulsifier for bitumen emulsions used in road paving, *Materials & Design,* vol. 131, pp. 242-251, 2017.

[12] A. K. Todd Thomas, "Performance – related tests and specifications for cold in-place recycling; lab and field experience," presented at the TRB, 2002.

[13] H. Al Nageim, S. F. Al-Busaltan, W. Atherton, and G. Sharples, A comparative study for improving the mechanical properties of cold bituminous emulsion mixtures with cement and waste materials, *Construction and Building Materials,* vol. 36, pp. 743-748, 2012.

[14] S. Oruc, F. Celik, and M. Akpinar, Effect of Cement on Emulsified Asphalt Mixtures, *Journal of Materials Engineering and Performance,* vol. 16, no. 5, pp. 578-583, 2007.

[15] B. Gómez-Meijide and I. Pérez, A proposed methodology for the global study of the mechanical properties of cold asphalt mixtures, *Materials & Design,* vol. 57, pp. 520-527, 2014/05/01/ 2014.

[16] C. S. Ruggles, The efficient use of environmentally-friendly NR latex (NRL) in road construction–Past, present and the future, *Natuurrubber,* vol. 37, pp. 2-4, 2005.

[17] H. M. Cai, T. Wang, J. Y. Zhang, and Y. Z. Zhang, Preparation of an SBS Latex–Modified Bitumen Emulsion and Performance Assessment, *Petroleum Science and Technology,* vol. 28, no. 10, pp. 987-996, 2010/05/17 2010.

[18] A. Khadivar and A. Kavussi, Rheological characteristics of SBR and NR polymer modified bitumen emulsions at average pavement temperatures, *Construction and Building Materials,* vol. 47, pp. 1099-1105, 2013/10/01/ 2013.

[19] J. Jiang, F. Ni, J. Zheng, Y. Han, and X. Zhao, Improving the high-temperature performance of cold recycled mixtures by polymer-modified asphalt emulsion, *International Journal of Pavement Engineering,* vol. 21, no. 1, pp. 41-48, 2020/01/02 2020.

[20] R. Zhang, Y. He, and Z. Ao, An asphalt emulsion modified by compound of epoxy resin and styrene-butadiene rubber emulsion, *International Journal of Mathematical Models Methods in Applied Sciense,* vol. 4, 2007.

[21] R. Li, Z. Leng, Y. Zhang, and X. Ma, Preparation and characterization of waterborne epoxy modified bitumen emulsion as a potential high-performance cold binder, *Journal of Cleaner Production,* 2019.

[22] C. Hu, J. Zhao, Z. Leng, M. N. Partl, and R. Li, Laboratory evaluation of waterborne epoxy bitumen emulsion for pavement preventative maintenance application, *Construction and Building Materials,* vol. 197, pp. 220-227, 2019/02/10/ 2019.

[23] Y. Kim, S. Im, and H. D. Lee, Impacts of curing time and moisture content on engineering properties of cold in-place recycling mixtures using foamed or emulsified asphalt, *Journal of Materials in Civil Engineering,* vol. 23, no. 5, pp. 542-553, 2010.

[24] A. Raposeiras, J. Rojas-Mora, E. Piffaut, D. Movilla-Quesada, and D. Castro-Fresno, Development of an estimative model for the optimal tack coat dosage based on aggregate gradation of hot mix asphalt pavements, *Construction and Building Materials,* vol. 118, pp. 1-10, 2016.

[25] M.-C. Liao, C.-C. Luo, T.-Y. Wang, and X. Xie, Developing effective test methods for evaluating cold-mix asphalt patching materials, *Journal of Materials in Civil Engineering,* vol. 28, no. 10, p. 04016108, 2016.

[26] A. Behnood and M. Modiri Gharehveran, Morphology, rheology, and physical properties of polymer-modified asphalt binders, *European Polymer Journal,* vol. 112, pp. 766-791, 2019/03/01/ 2019.

[27] G. Airey, Styrene butadiene styrene polymer modification of road bitumens, *Journal of Materials Science,* vol. 39, no. 3, pp. 951-959, 2004.

[28] F. J. Navarro *et al.*, Bitumen modification with reactive and non-reactive (virgin and recycled) polymers: A comparative analysis, *Journal of Industrial and Engineering Chemistry,* vol. 15, no. 4, pp. 458-464, 2009.

[29] M. C. Rubio, G. Martínez, L. Baena, and F. Moreno, Warm mix asphalt: an overview, *Journal of Cleaner Production,* vol. 24, pp. 76-84, 2012.

[30] Z. Leng, H. Yu, Z. Zhang, and Z. Tan, Optimizing the mixing procedure of warm asphalt rubber with wax-based additives through mechanism investigation and performance characterization, *Construction and Building Materials,* vol. 144, pp. 291-299, 2017/07/30/ 2017.

[31] A. Jamshidi, M. O. Hamzah, K. Kurumisawa, T. Nawa, and B. Samali, Evaluation of sustainable technologies that upgrade the binder performance grade in asphalt pavement construction, *Materials & Design,* vol. 95, pp. 9-20, 2016.

[32] A. Jamshidi, M. O. Hamzah, and Z. You, Performance of Warm Mix Asphalt containing Sasobit®: State-of-the-art, *Construction and Building Materials,* vol. 38, pp. 530-553, 2013.

[33] T. A. Doyle, C. McNally, A. Gibney, and A. Tabaković, Developing maturity methods for the assessment of cold-mix bituminous materials, *Construction and Building Materials,* vol. 38, pp. 524-529, 2013.

[34] J. Wang, F. Xiao, Z. Chen, X. Li, and S. Amirkhanian, Application of tack coat in pavement engineering, *Construction and Building Materials,* vol. 152, pp. 856-871, 2017.

[35] Y. Wang, Z. Leng, X. Li, and C. Hu, Cold recycling of reclaimed asphalt pavement towards improved engineering performance, *Journal of Cleaner Production,* vol. 171, pp. 1031-1038, 2018.

[36] M. Rodrıguez-Valverde, M. Cabrerizo-Vılchez, A. Paez-Duenas, and R. Hidalgo-Alvarez, Stability of highly charged particles: bitumen-in-water dispersions, *Colloids and Surfaces A: Physicochemical and Engineering Aspects,* vol. 222, no. 1, pp. 233-251, 2003.

[37] F. L. Calderon, J. Biais, and J. Bibette, Asphalt emulsions: Flocculation induced by a cationic surfactant and application to size partitioning, *Colloids and Surfaces A: Physicochemical and Engineering Aspects,* vol. 74, no. 2, pp. 303-309, 1993/07/23/ 1993.

[38] L. W. Corbett, Composition of asphalt based on generic fractionation, using solvent deasphaltening, elution-adsorption chromatography, and densimetric characterization, *Analytical Chemistry,* vol. 41, no. 4, pp. 576-579, 1969.

[39] M. Salou, B. Siffert, and A. Jada, Study of the stability of bitumen emulsions by application of DLVO theory, *Colloids and Surfaces A: Physicochemical and Engineering Aspects,* vol. 142, no. 1, pp. 9-16, 1998/11/30/ 1998.

[40] J. P. Pfeiffer and R. Saal, Asphaltic bitumen as colloid system, *The Journal of Physical Chemistry,* vol. 44, no. 2, pp. 139-149, 1940.

[41] J. P. Gingras, L. Fradette, P. Tanguy, and J. Bousquet, Inline bitumen emulsification using static mixers, *Ind. Eng. Chem. Res.,* vol. 46, no. 8, pp. 2618-2627, 2007.

[42] E. Arenas-Calderon, V. Sadtler, P. Marchal, L. Choplin, F. Delfosse, and M. Maze, Preparation of highly concentrated bitumen emulsions by catastrophic phase inversion: Follow-up of the emulsification process, *Colloids and Surfaces A: Physicochemical and Engineering Aspects,* vol. 458, pp. 25-31, 2014.

[43] S. H. Firoozifar, S. Foroutan, and S. Foroutan, The effect of pH and bituminous density on stabilization of bitumen-in-water emulsion, *Petroleum & Coal,* vol. 52, no. 1, pp. 31-34, 2010.

[44] F. Wang, Y. Liu, Y. Zhang, and S. Hu, Experimental study on the stability of asphalt emulsion for CA mortar by laser diffraction technique, *Construction and Building Materials,* vol. 28, no. 1, pp. 117-121, 2012/03/01/ 2012.

[45] X. Fang, A. Garcia-Hernandez, F. Winnefeld, and P. Lura, Influence of Cement on Rheology and Stability of Rosin Emulsified Anionic Bitumen Emulsion, *Journal of Materials in Civil Engineering,* vol. 28, no. 5, p. 04015199, 2016.

[46] E.-H. Liu and K. M. McGrath, Emulsion microstructure and energy input, roles in emulsion stability, *Colloids and Surfaces A: Physicochemical and Engineering Aspects,* vol. 262, no. 1, pp. 101-112, 2005.

[47] A. Jada, C. Florentin, and S. Mariotti, Study of the electrical properties of cationic bitumen emulsions by microelectrophoresis, *Advances in Colloid and Interface Science,* vol. 108, pp. 127-132, 2004.

[48] J. Gorman, R. Crawford, and I. Harding, Bitumen emulsions in road construction - A review, *Road & Transport Research,* vol. 13, no. 1, pp. 25-38, 2004.

[49] M. Ronald and F. P. Luis, Asphalt emulsions formulation: State-of-the-art and dependency of formulation on emulsions properties, *Construction and Building Materials,* vol. 123, pp. 162-173, 2016.

[50] D. R. Mallawarachchi, A. D. U. S. Amarasinghe, and M. A. B. Prashantha, Suitability of Chitosan as an emulsifier for cationic bitumen emulsions and its behaviour as an additive to bitumen emulsion, *Construction and Building Materials,* vol. 102, pp. 1-6, 2016.

[51] L. Loeber, S. Alexandre, G. Muller, J.-C. Triquigneaux, Y. Jolivet, and M. Malot, Bituminous emulsions and their characterization by atomic force microscopy, *Journal of microscopy,* vol. 198, pp. 10-16, 2000.

[52] D. Mallawarachchi, A. Amarasinghe, and M. Prashantha, Suitability of Chitosan as an emulsifier for cationic bitumen emulsions and its behaviour as an additive to bitumen emulsion, *Construction and Building Materials,* vol. 102, pp. 1-6, 2016.

[53] A. Banerjee, A. de Fortier Smit, and J. A. Prozzi, Modeling the effect of environmental factors on evaporative water loss in asphalt emulsions for chip seal applications, *Construction and Building Materials,* 2011.

[54] A. M. Al-Sabagh, N. N. Zaki, and A. F. M. Badawi, Effect of binary surfactant mixtures on the stability of asphalt emulsions, *Journal of Chemical Technology & Biotechnology: International Research in Process, Environmental AND Clean Technology,* vol. 69, no. 3, pp. 350-356, 1997.

[55] L. Ziyani, V. Gaudefroy, V. Ferber, and F. Hammoum, A predictive and experimental method to assess bitumen emulsion wetting on mineral substrates, *Colloids and Surfaces A: Physicochemical and Engineering Aspects,* vol. 489, pp. 322-335, 2016.

[56] X. Fang, A. Garcia-Hernandez, F. Winnefeld, and P. Lura, Influence of cement on rheology and stability of rosin emulsified anionic bitumen emulsion, *Journal of Materials in Civil Engineering,* vol. 28, no. 5, p. 04015199, 2015.

[57] J. Weiss and D. McClements, Influence of Ostwald ripening on rheology of oil-in-water emulsions containing electrostatically stabilized droplets, *Langmuir,* vol. 16, no. 5, pp. 2145-2150, 2000.

[58] L. Bonakdar *et al.*, Rupturing of bitumen-in-water emulsions: experimental evidence for viscous sintering phenomena, *Colloids and Surfaces A: Physicochemical and Engineering Aspects,* vol. 176, no. 2, pp. 185-194, 2001.

[59] T. F. Tadros, Fundamental principles of emulsion rheology and their applications, *Colloids and Surfaces A: Physicochemical and Engineering Aspects*, vol. 91, pp. 39-55, 1994.

[60] P. Izquierdo *et al.*, Formation and stability of nano-emulsions prepared using the phase inversion temperature method, *Langmuir,* vol. 18, no. 1, pp. 26-30, 2002.

[61] T. Tadros, Application of rheology for assessment and prediction of the long-term physical stability of emulsions, *Adv Colloid Interface Sci*, vol. 108-109, pp. 227-58, May 20 2004.

[62] J. F. Kennedy and T. A. Norris, "Modern Aspects of Emulsion Science," vol. 40, ed. London: The Royal Society of Chemistry, 1999, pp. 159-159.

[63] A. Håkansson, Experimental methods for measuring coalescence during emulsification – A critical review, *Journal of Food Engineering,* vol. 178, pp. 47-59, 2016.

[64] J. Moore and E. Cerasoli, "Particle Light Scattering Methods and Applications," in *Encyclopedia of Spectroscopy and Spectrometry (Third Edition)*, J. C. Lindon, G. E. Tranter, and D. W. Koppenaal, Eds. Oxford: Academic Press, 2017, pp. 543-553.

[65] I. Pinto and A. Buss, ζ Potential as a Measure of Asphalt Emulsion Stability, *Energy & Fuels,* vol. 34, no. 2, pp. 2143-2151, 2020/02/20 2020.

[66] T. Tadros, "Chapter 2 - Colloid and interface aspects of pharmaceutical science," in *Colloid and Interface Science in Pharmaceutical Research and Development*, H. Ohshima and K. Makino, Eds. Amsterdam: Elsevier, 2014, pp. 29-54.

[67] P. Esmaeili, F. Lin, and A. Yeung, Stability of Emulsified Heavy Oil: The Combined Effects of Deterministic DLVO Forces and Random Surface Charges, *Langmuir,* vol. 28, no. 11, pp. 4948-4954, 2012/03/20 2012.

[68] J. Lee and H. Ahn, Effect of Electrical Surface Charge on Seal Coat Curing and Aggregate Loss Performance, *Journal of Testing and Evaluation,* vol. 44, no. 4, pp. 1661-1670, 07/01 2016.

[69] A. Jada, C. Florentin, and S. Mariotti, Study of the electrical properties of cationic bitumen emulsions by microelectrophoresis, *Advances in Colloid and Interface Science,* vol. 108-109, pp. 127-132, 2004/05/20/ 2004.

[70] A. Jada and H. Debih, Hydrophobation of Clay Particles by Asphaltenes Adsorption, *Composite Interfaces,* vol. 16, no. 2-3, pp. 219-235, 2009/01/01 2009.

[71] R. Zhang and P. Somasundaran, Advances in adsorption of surfactants and their mixtures at solid/solution interfaces, *Advances in Colloid and Interface Science,* vol. 123, pp. 213-229, 2006.

[72] K. Takamura and A. James, "Paving with asphalt emulsions," in *Advances in Asphalt Materials*: Elsevier, 2015, pp. 393-426.

[73] W. Zhang, Effect of tack coat application on interlayer shear strength of asphalt pavement: A state-of-the-art review based on application in the United States, *International Journal of Pavement Research and Technology,* vol. 10, no. 5, pp. 434-445, 2017/09/01/ 2017.

[74] M. Kruntcheva, A. Collop, and N. Thom, Theoretical and practical aspects of the importance of bonding in a pavement structure, *Project report PGR,* vol. 8, 2000.

[75] Y. Hachiya, S. Umeno, and K. Sato, Effect of tack coat on bonding characteristics at interface between asphalt concrete layers, *Doboku Gakkai Ronbunshu,* vol. 1997, no. 571, pp. 199-209, 1997.

[76] A. C. Raposeiras, D. Castro-Fresno, A. Vega-Zamanillo, and J. Rodriguez-Hernandez, Test methods and influential factors for analysis of bonding between bituminous pavement layers, *Construction and Building Materials,* vol. 43, pp. 372-381, 2013/06/01/ 2013.

[77] L. Mohammad, S. Saadeh, Y. Qi, J. W. Button, and J. Scherocman, Worldwide state of practice on the use of tack coats: a survey, *Journal of the Association of Asphalt Paving Technologists,* vol. 77, 2008.

[78] A. C. Collop, M. H. Sutanto, G. D. Airey, and R. C. Elliott, Development of an automatic torque test to measure the shear bond strength between asphalt, *Construction and Building Materials,* vol. 25, no. 2, pp. 623-629, 2011/02/01/ 2011.

[79] M. Diakhaté, A. Millien, C. Petit, A. Phelipot-Mardelé, and B. Pouteau, Experimental investigation of tack coat fatigue performance: Towards an improved lifetime assessment of

pavement structure interfaces, *Construction and Building Materials,* vol. 25, no. 2, pp. 1123-1133, 2011/02/01/ 2011.

[80] A. Cuadri, C. Roman, M. García-Morales, F. Guisado, E. Moreno, and P. Partal, Formulation and processing of recycled-low-density-polyethylene-modified bitumen emulsions for reduced-temperature asphalt technologies, *Chemical Engineering Science,* vol. 156, pp. 197-205, 2016.

[81] J.-S. Chou and T.-S. Le, Reliability-based performance simulation for optimized pavement maintenance, *Reliability Engineering & System Safety,* vol. 96, no. 10, pp. 1402-1410, 2011/10/01/ 2011.

[82] H. Wang and Z. Wang, Evaluation of pavement surface friction subject to various pavement preservation treatments, *Construction and Building Materials,* vol. 48, pp. 194-202, 2013/11/01/ 2013.

[83] H. Gong, Q. Dong, B. Huang, and X. Jia, Effectiveness analyses of flexible pavement preventive maintenance treatments with LTPP SPS-3 experiment data, *Journal of Transportation Engineering,* vol. 142, no. 2, p. 04015045, 2015.

[84] F. Giustozzi, M. Crispino, and G. Flintsch, Multi-attribute life cycle assessment of preventive maintenance treatments on road pavements for achieving environmental sustainability, *The International Journal of Life Cycle Assessment,* vol. 17, no. 4, pp. 409-419, 2012.

[85] B. Broughton, S.-J. Lee, and Y.-J. Kim, 30 Years of Microsurfacing: A Review, *ISRN Civil Engineering,* vol. 2012, 2012.

[86] L. Pellecuer, G. J. Assaf, and M. St-Jacques, Life cycle environmental benefits of pavement surface maintenance, *Canadian Journal of Civil Engineering,* vol. 41, no. 8, pp. 695-702, 2014.

[87] M. S. Mamlouk and M. Dosa, Verification of effectiveness of chip seal as a pavement preventive maintenance treatment using LTPP data, *International Journal of Pavement Engineering,* vol. 15, no. 10, pp. 879-888, 2014.

[88] J.-P. Gingras, P. A. Tanguy, S. Mariotti, and P. Chaverot, Effect of process parameters on bitumen emulsions, *Chemical Engineering and Processing: Process Intensification,* vol. 44, no. 9, pp. 979-986, 2005.

[89] M. J. Khattak and M. Alrashidi, Performance of preventive maintenance treatments of flexible pavements, *International Journal of Pavement Research and Technology,* vol. 6, no. 3, pp. 184-196, 2013.

[90] D. Simões, A. Almeida-Costa, and A. Benta, Preventive maintenance of road pavement with microsurfacing—an economic and sustainable strategy, *International Journal of Sustainable Transportation,* vol. 11, no. 9, pp. 670-680, 2017.

[91] H. Gong, Q. Dong, B. Huang, and X. Jia, Effectiveness Analyses of Flexible Pavement Preventive Maintenance Treatments with LTPP SPS-3 Experiment Data, *Journal of Transportation Engineering,* vol. 142, no. 2, p. 1, 2016.

[92] R. Hicks, J. Moulthrop, and J. Daleiden, Selecting a preventive maintenance treatment for flexible pavements, *Transportation Research Record: Journal of the Transportation Research Board,* no. 1680, pp. 1-12, 1999.

[93] R. Yang, S. Kang, H. Ozer, and I. L. Al-Qadi, Environmental and economic analyses of recycled asphalt concrete mixtures based on material production and potential performance, *Resources, Conservation and Recycling,* vol. 104, pp. 141-151, 2015.

[94] Q. Aurangzeb, I. L. Al-Qadi, H. Ozer, and R. Yang, Hybrid life cycle assessment for asphalt mixtures with high RAP content, *Resources, Conservation and Recycling,* vol. 83, pp. 77-86, 2014/02/01/ 2014.

[95] Y. Huang, R. Bird, and O. Heidrich, Development of a life cycle assessment tool for construction and maintenance of asphalt pavements, *Journal of Cleaner Production,* vol. 17, no. 2, pp. 283-296, 2009/01/01/ 2009.

[96] T. Miller and H. Bahia, Sustainable asphalt pavements: Technologies, knowledge gaps and opportunities, *Modified Asphalt Research Center, Univ. of Wisconsin, Madison, WI,* 2009.

[97] S. A. Cross, W. H. Chesner, H. G. Justus, and E. R. Kearney, Life-Cycle Environmental Analysis for Evaluation of Pavement Rehabilitation Options, *Transportation Research Record,* vol. 2227, no. 1, pp. 43-52, 2011/01/01 2011.

[98] A. Modarres, M. Rahimzadeh, and M. Zarrabi, Field investigation of pavement rehabilitation utilizing cold in-place recycling, *Resources, Conservation and Recycling,* vol. 83, pp. 112-120, 2014.

[99] M. I. Giani, G. Dotelli, N. Brandini, and L. Zampori, Comparative life cycle assessment of asphalt pavements using reclaimed asphalt, warm mix technology and cold in-place recycling, *Resources, Conservation and Recycling,* vol. 104, pp. 224-238, 2015.

[100] T. Thomas, A. Kadrmas, and J. Huffman, Cold in-place recycling on US-283 in Kansas, *Transportation Research Record: Journal of the Transportation Research Board,* no. 1723, pp. 53-56, 2000.

[101] A.-A.-A. J. C. Committee and A.-A.-A. J. C. C. T. F. No., *Report on cold recycling of asphalt pavements*. American Association of State Highway and Transportation Officials, 1998.

[102] Y. Kim, S. Im, and H. D. Lee, Impacts of Curing Time and Moisture Content on Engineering Properties of Cold In-Place Recycling Mixtures Using Foamed or Emulsified Asphalt, *Journal of Materials in Civil Engineering,* vol. 23, no. 5, pp. 542-553, 2011.

[103] J. Mills-Beale and Z. You, The mechanical properties of asphalt mixtures with recycled concrete aggregates, *Construction and Building Materials,* vol. 24, no. 3, pp. 230-235, 2010.

[104] K. Takamura, "Pavement Preservation Using the SBR Latex Modified Asphalt Emulsion, BASF Corporation," in *International Latex Conference, Charlotte, NC*, 2005.

[105] A. Forbes, R. G. Haverkamp, T. Robertson, J. Bryant, and S. Bearsley, Studies of the microstructure of polymer-modified bitumen emulsions using confocal laser scanning microscopy, *Journal of Microscopy,* vol. 204, no. 3, pp. 252-257, 2001.

[106] K. Takamura, "Microsurfacing with SBR latex modified asphalt emulsion," Charlotte, NC, BASF, 2002.

[107] K. Takamura and W. Heckmann, "Polymer network formation in the emulsion residue recovered by forced air drying," in *Proc. Int. Symp. Asphalt Emulsion Technology,* 1999, pp. 185-194.

[108] J. B. Johnston and G. King, Using Polymer Modified Asphalt Emulsions in Surface Treatments A Federal Lands Highway Interim Report, *Federal Highway Administration, New Jersey Avenue, Washington DC, USA,* 2008.

[109] M. Abedini, A. Hassani, M. R. Kaymanesh, and A. A. Yousefi, Low-temperature adhesion performance of polymer-modified Bitumen emulsion in chip seals using different SBR latexes, *Petroleum Science and Technology,* vol. 35, no. 1, pp. 59-65, 2017/01/02 2017.

[110] L. E. Chávez-Valencia, E. Alonso, A. Manzano, J. Pérez, M. E. Contreras, and C. Signoret, Improving the compressive strengths of cold-mix asphalt using asphalt emulsion modified by polyvinyl acetate, *Construction and Building Materials,* vol. 21, no. 3, pp. 583-589, 2007/03/01/ 2007.

[111] A. James, Overview of asphalt emulsion, *Transportation research circular,* pp. 1-15, 2006.

[112] M. Abedini, A. Hassani, M. R. Kaymanesh, and A. A. Yousefi, The rheological properties of a bitumen emulsion modified with two types of SBR latex, *Petroleum Science and Technology,* vol. 34, no. 17-18, pp. 1589-1594, 2016/09/16 2016.

[113] B. Shirkavand Hadavand, B. Ghobadi Jola, K. Didehban, and A. Mirshokraie, Modified bitumen emulsion by anionic polyurethane dispersion nanocomposites, *Road Materials and Pavement Design,* vol. 21, no. 6, pp. 1763-1774, 2020/08/17 2020.

[114] C. Xia and Y. Luo, Modification of bitumen emulsion via heterocoagulation with SIS triblock copolymer latex, *Journal of Applied Polymer Science,* vol. 134, no. 48, p. 45510, 2017.

[115] R. Zhang, Y. He, and Z. Ao, An asphalt emulsion modified by compound of epoxy resin and styrene-butadiene rubber emulsion, *International Journal of Mathematical Models and Methods in Applied Sciense,* no. 4, 2007.

[116] A. Catalani and M. G. Bonicelli, Kinetics of the curing reaction of a diglycidyl ether of bisphenol A with a modified polyamine, *Thermochimica Acta,* vol. 438, no. 1, pp. 126-129, 2005.

[117] T. Maity, B. C. Samanta, S. Dalai, and A. K. Banthia, Curing study of epoxy resin by new aromatic amine functional curing agents along with mechanical and thermal evaluation, *Materials Science & Engineering A,* vol. 464, no. 1, pp. 38-46, 2007.

[118] M. F. Mustafa, W. D. Cook, T. L. Schiller, and H. M. Siddiqi, Curing behavior and thermal properties of TGDDM copolymerized with a new pyridine-containing diamine and with DDM or DDS, *Thermochimica Acta,* vol. 575, pp. 21-28, 2014.

[119] M. Ghaemy, M. Barghamadi, and H. Behmadi, Cure kinetics of epoxy resin and aromatic diamines, *Journal of Applied Polymer Science,* vol. 94, no. 3, pp. 1049-1056, 2004.

[120] N. Sbirrazzuoli, S. Vyazovkin, A. Mititelu, C. Sladic, and L. Vincent, A Study of Epoxy-Amine Cure Kinetics by Combining Isoconversional Analysis with Temperature Modulated DSC and Dynamic Rheometry, *Macromolecular Chemistry and Physics,* vol. 204, no. 15, pp. 1815-1821, 2003.

[121] H. Yamasaki and S. Morita, Identification of the epoxy curing mechanism under isothermal conditions by thermal analysis and infrared spectroscopy, *Journal of Molecular Structure,* vol. 1069, pp. 164-170, 2014.

[122] B. Dębska and L. Lichołai, The effect of the type of curing agent on selected properties of epoxy mortar modified with PET glycolisate, *Construction and Building Materials,* vol. 124, pp. 11-19, 2016.

[123] C. Ramírez, M. Rico, A. Torres, L. Barral, J. López, and B. Montero, Epoxy/POSS organic–inorganic hybrids: ATR-FTIR and DSC studies, *European Polymer Journal,* vol. 44, no. 10, pp. 3035-3045, 2008.

[124] W. C. Simpson, Sommer H.J., Griffin R.L., Miles T. K., Epoxy Asphalt Concrete for Airfield Pavements, *Journal of the Air Transport Division, Proceedings of the American Society of Civil Engineer,* vol. 86, pp. 57-71, 1960.

[125] G. R.W, "Epoxy asphalt concrete: a polymer concrete with 25 years experience," presented at the Polymer Concrete Overlays, American Concrete Institute Technical Session Conference, Minnesota, 1993.

[126] Y. Xiao, M. F. C. van de Ven, A. A. A. Molenaar, Z. Su, and F. Zandvoort, Characteristics of two-component epoxy modified bitumen, *Materials and Structures,* journal article vol. 44, no. 3, pp. 611-622, 2011.

[127] J. Yu, P. Cong, and S. Wu, Laboratory investigation of the properties of asphalt modified with epoxy resin, *Journal of Applied Polymer Science,* vol. 113, no. 6, pp. 3557-3563, 2009.

[128] L. J, "Orthotropic Deck Wear Surface System Selection - Lions Gate Bridge North Approach Viaduct, Vancouver BC," presented at the 2013 Conference of the Transportation Association of Canada, Winnipeg, Manitoba, Canada, 2013.

[129] S. A. Bagshaw, P. R. Herrington, and J. P. Wu, Preliminary examination of chipseals prepared with epoxy-modified bitumen, *Construction and Building Materials,* vol. 88, pp. 232-240, 2015.

[130] Z. Qian and Q. Lu, Design and laboratory evaluation of small particle porous epoxy asphalt surface mixture for roadway pavements, *Construction and Building Materials,* vol. 77, pp. 110-116, 2015.

[131] Q. Lu and J. Bors, Alternate uses of epoxy asphalt on bridge decks and roadways, *Construction and Building Materials,* vol. 78, pp. 18-25, 2015.

[132] M. Huang, X. Wen, and L. Wang, Influence of foaming effect, operation time and health preserving properties of foam epoxy asphalt mixtures, *Construction and Building Materials,* vol. 151, pp. 931-938, 2017/10/01/ 2017.

[133] Z. Zhaoying, H. Yuhui, L. Bing, and C. Guangming, Studies on particle size of waterborne emulsions derived from epoxy resin, *European Polymer Journal,* vol. 37, no. 6, pp. 1207-1211, 2001.

[134] X. Yuan, B. Zhu, X. Cai, J. Liu, K. Qiao, and J. Yu, Improved interfacial adhesion in carbon fiber/epoxy composites through a waterborne epoxy resin sizing agent, *Journal of Applied Polymer Science,* vol. 134, no. 17, pp. n/a-n/a, 2017.

[135] M. Liu, S. Han, J. Pan, and W. Ren, Study on cohesion performance of waterborne epoxy resin emulsified asphalt as interlayer materials, *Construction and Building Materials,* vol. 177, pp. 72-82, 2018/07/20/ 2018.

[136] Q. Zhang, Y.-h. Xu, and Z.-g. Wen, Influence of water-borne epoxy resin content on performance of waterborne epoxy resin compound SBR modified emulsified asphalt for tack coat, *Construction and Building Materials,* vol. 153, pp. 774-782, 2017.

[137] L. Guangqi, S. Jianzhong, and Z. Qiyun, Synthesis and characterization of waterborne epoxy curing agent modified by silane, *Chinese Journal of Chemical Engineering,* vol. 15, no. 6, pp. 899-905, 2007.

[138] B. Sengoz and G. Isikyakar, Analysis of styrene-butadiene-styrene polymer modified bitumen using fluorescent microscopy and conventional test methods, *Journal of Hazardous Materials,* vol. 150, no. 2, pp. 424-432, 2008/01/31/ 2008.

[139] B. Sengoz and G. Isikyakar, Evaluation of the properties and microstructure of SBS and EVA polymer modified bitumen, *Construction and Building Materials,* vol. 22, no. 9, pp. 1897-1905, 2008/09/01/ 2008.

[140] H. Soenen, X. Lu, and P. Redelius, The Morphology of Bitumen-SBS Blends by UV Microscopy, *Road Materials and Pavement Design,* vol. 9, no. 1, pp. 97-110, 2008/01/01 2008.

[141] A. Schaur, S. Unterberger, and R. Lackner, Impact of molecular structure of SBS on thermomechanical properties of polymer modified bitumen, *European Polymer Journal,* vol. 96, pp. 256-265, 2017/11/01/ 2017.

[142] A. Topal, Evaluation of the properties and microstructure of plastomeric polymer modified bitumens, *Fuel Processing Technology,* vol. 91, no. 1, pp. 45-51, 2010/01/01/ 2010.

[143] S. BEARSLEY, A. FORBES, and R. G. HAVERKAMP, Direct observation of the asphaltene structure in paving-grade bitumen using confocal laser-scanning microscopy, *Journal of Microscopy,* vol. 215, no. 2, pp. 149-155, 2004.

[144] F. Handle, H. Grothe, and S. Neudl, "Confocal laser scanning microscopy—observation of the microstructure of bitumen and asphalt concrete," in *5th Eurasphalt & Eurobitume Congress, Istanbul*, 2012, pp. 13-15.

[145] D. Kaya, A. Topal, and T. McNally, Correlation of processing parameters and ageing with the phase morphology of styrene-butadiene-styrene block co-polymer modified bitumen, *Materials Research Express,* vol. 6, no. 10, p. 105309, 2019/08/07 2019.

[146] T. Tadros, Application of rheology for assessment and prediction of the long-term physical stability of emulsions, *Advances in Colloid and Interface Science,* vol. 108-109, pp. 227-258, 2004/05/20/ 2004.

[147] B. Binks, Modern Aspects of Emulsion Science, Royal Soc, *Chem., Cambridge,* 1998.

[148] R. Mercado and L. Fuentes, Measure of asphalt emulsions stability by oscillatory rheology, *Construction and Building Materials,* vol. 155, pp. 838-845, 2017/11/30/ 2017.

[149] Y. Otsubo and R. K. Prud'homme, Rheology of oil-in-water emulsions, *Rheologica acta,* vol. 33, no. 1, pp. 29-37, 1994.

[150] J. Koszkul and J. Nabialek, Viscosity models in simulation of the filling stage of the injection molding process, *Journal of Materials Processing Technology,* vol. 157, no. 158, pp. 183-187, 2004.

[151] R. B. Bird, G. Dai, and B. J. Yarusso, The rheology and flow of viscoplastic materials, *Reviews in Chemical Engineering,* vol. 1, no. 1, pp. 1-70, 1983.

[152] J. Mewis and N. J. Wagner, Thixotropy, *Advances in Colloid and Interface Science,* vol. 147-148, pp. 214-227, 2009/03/01/ 2009.

[153] A. Behnood and J. Olek, Rheological properties of asphalt binders modified with styrene-butadiene-styrene (SBS), ground tire rubber (GTR), or polyphosphoric acid (PPA), *Construction and Building Materials,* vol. 151, pp. 464-478, 2017.

[154] *Estimating Damage Tolerance of Asphalt Binders Using the Linear Amplitude Sweep*, TP101, 2014.

[155] Y. Gu, B. Tang, L. He, F. Yang, H. Wang, and J. Ling, Compatibility of cured phase-inversion waterborne epoxy resin emulsified asphalt, *Construction and Building Materials,* vol. 229, p. 116942, 2019/12/30/ 2019.

[156] C. Ouyang, S. Wang, Y. Zhang, and Y. Zhang, Thermo-rheological properties and storage stability of SEBS/kaolinite clay compound modified asphalts, *European Polymer Journal,* vol. 42, no. 2, pp. 446-457, 2006.

[157] G. Wen, Y. Zhang, Y. Zhang, K. Sun, and Y. Fan, Rheological characterization of storage-stable SBS-modified asphalts, *Polymer Testing,* vol. 21, no. 3, pp. 295-302, 2002/01/01/ 2002.

[158] G. Polacco, J. Stastna, D. Biondi, and L. Zanzotto, Relation between polymer architecture and nonlinear viscoelastic behavior of modified asphalts, *Current Opinion in Colloid & Interface Science,* vol. 11, no. 4, pp. 230-245, 2006/10/01/ 2006.

[159] T. Xia *et al.*, Viscoelastic phase behavior in SBS modified bitumen studied by morphology evolution and viscoelasticity change, *Construction and Building Materials,* vol. 105, pp. 589-594, 2016/02/15/ 2016.

[160] K. D. Stuart, W. S. Mogawer, and P. Romero, "Evaluation of the Superpave asphalt binder specification for high-temperature pavement performance," in *Association of Asphalt Paving Technologists Proc,* 2000, vol. 69.

[161] H. U. Bahia, D. Hanson, M. Zeng, H. Zhai, M. Khatri, and R. Anderson, *Characterization of modified asphalt binders in superpave mix design* (no. Project 9-10 FY'96). 2001.

[162] J. D'Angelo and R. Dongre, "Superpave binder specifications and their performance relationship to modified binders," in *Proceedings of the Forty-Seventh Annual Conference of the Canadian Technical Asphalt Association (CTAA): Calgary, Alberta,* 2002.

[163] S. Biro, T. Gandhi, and S. Amirkhanian, Determination of zero shear viscosity of warm asphalt binders, *Construction and Building Materials,* vol. 23, no. 5, pp. 2080-2086, 2009/05/01/ 2009.

[164] J. D'Angelo, Current status of Superpave binder specification, *Road Materials and Pavement Design,* vol. 10, no. sup1, pp. 13-24, 2009.

[165] J. A. D'Angelo, The Relationship of the MSCR Test to Rutting, *Road Materials and Pavement Design,* vol. 10, no. sup1, pp. 61-80, 2009/01/01 2009.

[166] E. DuBois, D. Y. Mehta, and A. Nolan, Correlation between multiple stress creep recovery (MSCR) results and polymer modification of binder, *Construction and Building Materials,* vol. 65, pp. 184-190, 2014/08/29/ 2014.

[167] O.-V. Laukkanen, H. Soenen, T. Pellinen, S. Heyrman, and G. Lemoine, Creep-recovery behavior of bituminous binders and its relation to asphalt mixture rutting, *Materials and Structures,* journal article vol. 48, no. 12, pp. 4039-4053, December 01 2015.

[168] J. Zhang, L. F. Walubita, A. N. M. Faruk, P. Karki, and G. S. Simate, Use of the MSCR test to characterize the asphalt binder properties relative to HMA rutting performance – A laboratory study, *Construction and Building Materials,* vol. 94, pp. 218-227, 2015/09/30/ 2015.

[169] M. F. Woldekidan, "Response modelling of bitumen, bituminous mastic and mortar," Road and Railway Engineering, Delft University of Technology, 2011.

[170] C. Celauro, C. Fecarotti, A. Pirrotta, and A. C. Collop, Experimental validation of a fractional model for creep/recovery testing of asphalt mixtures, *Construction and Building Materials,* vol. 36, pp. 458-466, 2012/11/01/ 2012.

[171] F. Giuliani, F. Merusi, and I. Antunes, "Creep flow behavior of asphalt rubber binder—The zero shear viscosity analysis," in *Proceedings of the Asphalt rubber,* 2006.

[172] M. Phillips and C. Robertus, "Binder rheology and asphaltic pavement permanent deformation; the zero-shear-viscosity," in *EURASPHALT & EUROBITUME CONGRESS, STRASBOURG, 7-10 MAY 1996. VOLUME 3. PAPER E&E. 5.134,* 1996.

[173] C. Binard, D. Anderson, L. Lapalu, and J. Planche, "Zero shear viscosity of modified and unmodified binders," in *PROCEEDINGS OF THE 3RD EURASPHALT AND EUROBITUME CONGRESS HELD VIENNA, MAY 2004,* 2004, vol. 2.

[174] F. Morea, J. O. Agnusdei, and R. Zerbino, Comparison of methods for measuring zero shear viscosity in asphalts, *Materials and Structures,* journal article vol. 43, no. 4, pp. 499-507, May 01 2010.

[175] X. Lu and U. Isacsson, Artificial aging of polymer modified bitumens, vol. 76, no. 12, pp. 1811-1824, 2000.

[176] Y. Wang, L. Sun, and Y. Qin, Aging mechanism of SBS modified asphalt based on chemical reaction kinetics, *Construction and Building Materials,* vol. 91, pp. 47-56, 2015/08/30/ 2015.

[177] J. C. Petersen, Quantitative functional group analysis of asphalts using differential infrared spectrometry and selective chemical reactions--theory and application, *Transportation Research Record,* no. 1096, 1986.

[178] M. R. Nivitha, E. Prasad, and J. M. Krishnan, Ageing in modified bitumen using FTIR spectroscopy, *International Journal of Pavement Engineering,* vol. 17, no. 7, pp. 565-577, 2016/08/08 2016.

[179] J. C. Petersen, A review of the fundamentals of asphalt oxidation: chemical, physicochemical, physical property, and durability relationships, *Transportation Research Circular,* no. E-C140, 2009.

[180] J. Lamontagne, P. Dumas, V. Mouillet, and J. Kister, Comparison by Fourier transform infrared (FTIR) spectroscopy of different ageing techniques: application to road bitumens, *Fuel,* vol. 80, no. 4, pp. 483-488, 2001.

[181] F. Durrieu, F. Farcas, and V. Mouillet, The influence of UV aging of a Styrene/Butadiene/Styrene modified bitumen: Comparison between laboratory and on site aging, *Fuel,* vol. 86, no. 10, pp. 1446-1451, 2007/07/01/ 2007.

[182] X. Lu and U. Isacsson, Artificial aging of polymer modified bitumens, *Journal of Applied Polymer Science,* vol. 76, no. 12, pp. 1811-1824, 2000.

[183] I. Menapace, W. Yiming, and E. Masad, Chemical analysis of surface and bulk of asphalt binders aged with accelerated weathering tester and standard aging methods, *Fuel,* vol. 202, pp. 366-379, 2017.

[184] M. C. Cavalli, M. Zaumanis, E. Mazza, M. N. Partl, and L. D. Poulikakos, Effect of ageing on the mechanical and chemical properties of binder from RAP treated with bio-based rejuvenators, *Composites Part B: Engineering,* vol. 141, pp. 174-181, 2018/05/15/ 2018.

[185] D. Kaya, A. Topal, J. Gupta, and T. McNally, Aging effects on the composition and thermal properties of styrene-butadiene-styrene (SBS) modified bitumen, *Construction and Building Materials,* vol. 235, p. 117450, 2020/02/28/ 2020.

[186] J. B. Lambert, *Organic structural spectroscopy*. Pearson College Division, 1998.

[187] A. M. Hung and E. H. Fini, Absorption spectroscopy to determine the extent and mechanisms of aging in bitumen and asphaltenes, *Fuel,* vol. 242, pp. 408-415, 2019/04/15/ 2019.

[188] P. Apostolidis, X. Liu, S. Erkens, and A. Scarpas, Evaluation of epoxy modification in bitumen, *Construction and Building Materials,* vol. 208, pp. 361-368, 2019/05/30/ 2019.

[189] H. U. Bahia, H. Zhai, K. Onnetti, and S. Kose, Non-linear viscoelastic and fatigue properties of asphalt binders, *Journal of the Association of Asphalt Paving Technologists,* vol. 68, 1999.

[190] A. A. Tayebali, G. M. Rowe, and J. B. Sousa, Fatigue response of asphalt-aggregate mixtures (with discussion), *Journal of the Association of Asphalt Paving Technologists,* vol. 61, 1992.

[191] W. Van Dijk, Practical fatigue characterization of bituminous mixes, *Journal of the Association of Asphalt Paving Technologists,* vol. 44, pp. 38-72, 1975.

[192] W. Van Dijk and V. W, The energy approach to fatigue for pavement design, *Journal of the Association of Asphalt Paving Technologists,* vol. 46, pp. 1-40, 1977.

[193] K. A. Ghuzlan and S. H. Carpenter, Fatigue damage analysis in asphalt concrete mixtures using the dissipated energy approach, *Canadian Journal of Civil Engineering,* vol. 33, no. 7, pp. 890-901, 2006.

[194] K. A. Ghuzlan and S. H. Carpenter, Energy-Derived, Damage-Based Failure Criterion for Fatigue Testing, *Transportation Research Record,* vol. 1723, no. 1, pp. 141-149, 2000.

[195] S. Shen, G. D. Airey, S. H. Carpenter, and H. Huang, A Dissipated Energy Approach to Fatigue Evaluation, *Road Materials and Pavement Design,* vol. 7, no. 1, pp. 47-69, 2006/01/01 2006.

[196] C. Johnson and H. U. Bahia, Evaluation of an accelerated procedure for fatigue characterization of asphalt binders, *Submitted for publication in Road Materials and Pavement Design,* 2010.

[197] C. Hintz, R. Velasquez, C. Johnson, and H. Bahia, Modification and Validation of Linear Amplitude Sweep Test for Binder Fatigue Specification, *Transportation Research Record,* vol. 2207, no. 1, pp. 99-106, 2011.

[198] M. Sabouri, D. Mirzaiyan, and A. Moniri, Effectiveness of Linear Amplitude Sweep (LAS) asphalt binder test in predicting asphalt mixtures fatigue performance, *Construction and Building Materials,* vol. 171, pp. 281-290, 2018/05/20/ 2018.

[199] W. Cao and C. Wang, A new comprehensive analysis framework for fatigue characterization of asphalt binder using the Linear Amplitude Sweep test, *Construction and Building Materials,* vol. 171, pp. 1-12, 2018/05/20/ 2018.

[200] M. A. Notani, F. Moghadas Nejad, A. Khodaii, and P. Hajikarimi, Evaluating fatigue resistance of toner-modified asphalt binders using the linear amplitude sweep test, *Road Materials and Pavement Design,* vol. 20, no. 8, pp. 1927-1940, 2019/11/17 2019.

[201] R. Li, Z. Leng, Y. Zhang, and X. Ma, Preparation and characterization of waterborne epoxy modified bitumen emulsion as a potential high-performance cold binder, *Journal of Cleaner Production,* vol. 235, pp. 1265-1275, 2019/10/20/ 2019.

[202] S. Luo, Z. Qian, X. Yang, and Q. Lu, Fatigue behavior of epoxy asphalt concrete and its moisture susceptibility from flexural stiffness and phase angle, *Construction and Building Materials,* vol. 145, pp. 506-517, 2017/08/01/ 2017.

[203] P. Cong, S. Chen, and J. Yu, Investigation of the properties of epoxy resin-modified asphalt mixtures for application to orthotropic bridge decks, *Journal of Applied Polymer Science,* vol. 121, no. 4, pp. 2310-2316, 2011.

[204] C. Chen, W. O. Eisenhut, K. Lau, A. Buss, and J. Bors, Performance characteristics of epoxy asphalt paving material for thin orthotropic steel plate decks, *International Journal of Pavement Engineering,* vol. 21, no. 3, pp. 397-407, 2020/02/23 2020.

[205] R. A. Schapery, Correspondence principles and a generalizedJ integral for large deformation and fracture analysis of viscoelastic media, *International Journal of Fracture,* vol. 25, no. 3, pp. 195-223, 1984.

[206] C. Pan, D. Liang, L. Mo, M. Riara, and J. Lin, Influence of Different Modifiers on Bonding Strength and Rheological Performance of Bitumen Emulsion, *Materials,* vol. 12, no. 15, p. 2414, 2019.

[207] D. W. Christensen and D. A. Anderson, Interpretation of dynamic mechanical test data for paving grade asphalt cements (with discussion), *Journal of the Association of Asphalt Paving Technologists*, vol. 61, 1992.

[208] L. Socal da Silva, M. M. de Camargo Forte, L. de Alencastro Vignol, and N. S. M. Cardozo, Study of rheological properties of pure and polymer-modified Brazilian asphalt binders, *Journal of Materials Science*, vol. 39, no. 2, pp. 539-546, 2004/01/01 2004.

[209] G. D. Airey, "Rheological characteristics of polymer modified and aged bitumens," University of Nottingham, 1997.

[210] F. Olard and H. Di Benedetto, General "2S2P1D" Model and Relation Between the Linear Viscoelastic Behaviours of Bituminous Binders and Mixes, *Road Materials and Pavement Design,* vol. 4, no. 2, pp. 185-224, 2003/01/01 2003.

[211] C. Huet, "Etude par une méthode d'impédance du comportement viscoélastique des matériaux hydrocarbonés," 1965.

[212] G. Sayegh, "Viscoelastic properties of bituminous mixtures," in *Intl Conf Struct Design Asphalt Pvmts*, 1967.

[213] M. F. Woldekidan, M. Huurman, and A. C. Pronk, A modified HS model: Numerical applications in modeling the response of bituminous materials, *Finite Elements in Analysis and Design,* vol. 53, pp. 37-47, 2012/06/01/ 2012.

[214] N. I. Md. Yusoff, D. Mounier, G. Marc-Stéphane, M. Rosli Hainin, G. D. Airey, and H. Di Benedetto, Modelling the rheological properties of bituminous binders using the 2S2P1D Model, *Construction and Building Materials,* vol. 38, pp. 395-406, 2013/01/01/ 2013.

[215] M. Yusoff and G. Airey, The 2S2P1D: An excellent linear viscoelastic model, *Journal of Civil Engineering, Science and Technology,* vol. 1, no. 2, pp. 1-7, 2010.

[216] S. W. Park and Y. R. Kim, Fitting Prony-Series Viscoelastic Models with Power-Law Presmoothing, *Journal of Materials in Civil Engineering*, vol. 13, no. 1, pp. 26-32, 2001.

[217] M. F. Woldekidan, Response modelling of bitumen, bituminous mastic and mortar, 2011.

[218] M. L. Williams, R. F. Landel, and J. D. Ferry, The temperature dependence of relaxation mechanisms in amorphous polymers and other glass-forming liquids, *Journal of the American Chemical society,* vol. 77, no. 14, pp. 3701-3707, 1955.

[219] F. Olard, H. Di Benedetto, B. Eckmann, and J.-P. Triquigneaux, Linear Viscoelastic Properties of Bituminous Binders and Mixtures at Low and Intermediate Temperatures, *Road Materials and Pavement Design*, vol. 4, no. 1, pp. 77-107, 2003/01/01 2003.

[220] H. Di Benedetto, N. Mondher, C. Sauzéat, and F. Olard, Three-dimensional Thermo-viscoplastic Behaviour of Bituminous Materials: The DBN Model, *Road Materials and Pavement Design,* vol. 8, no. 2, pp. 285-315, 2007/01/01 2007.

[221] L. Shan, Y. Xu, H. He, and N. Ren, Optimization criterion of viscoelastic response model for asphalt binders, *Construction and Building Materials,* vol. 113, pp. 553-560, 2016.

[222] J. Uzan, M. Livneh, and Y. Eshed, "Investigation of adhesion properties between asphaltic-concrete layers," in *Association of Asphalt Paving Technologists Proc*, 1978, vol. 47.

[223] A. Vanelstraete and L. Francken, *Prevention of reflective cracking in pavements*. CRC Press, 2004.

[224] L. Tashman, K. Nam, and A. Papagiannakis, "Evaluation of the influence of tack coat construction factors on the bond strength between pavement layers," Washington State Department of Transportation Olympia2006.

[225] K. Khweir and D. Fordyce, Influence of layer bonding on the prediction of pavement life, *Proceedings of the Institution of Civil Engineers - Transport*, vol. 156, no. 2, pp. 73-83, 2003.

[226] L. N. Mohammad, *Optimization of tack coat for HMA placement*. Transportation Research Board, 2012.

[227] E. R. Brown, S. L. Brandau, H. H. Bush, A. A. o. S. Highway, T. Officials, and F. A. Administration, *Hot-mix Asphalt Paving Handbook 2000*. US Army Corps of Engineers, 2000.

[228] L. N. Mohammad, A. Bae, M. A. Elseifi, J. Button, and N. Patel, Effects of Pavement Surface Type and Sample Preparation Method on Tack Coat Interface Shear Strength, *Transportation Research Record*, vol. 2180, no. 1, pp. 93-101, 2010.

[229] J.-C. Roffe and F. CHAIGNON, "Characterisation tests on bond coats: worldwide study, impact, tests, recommendations," in *PROCEEDINGS OF THE 3RD INTERNATIONAL CONFERENCE ON BITUMINOUS MIXTURES AND PAVEMENTS, HELD THESSALONIKI, GREECE, NOVEMBER 2002.*, 2002, vol. 1.

[230] H. R. Paul and J. A. Scherocman, Friction Testing of Tack Coat Surfaces, *Transportation Research Record*, vol. 1616, no. 1, pp. 6-12, 1998.

[231] S. A. Cross and P. P. Shrestha, Guidelines for Using Prime and Tack Coats, (in English), Tech Report 2005.

[232] L. Tashman, K. Nam, T. Papagiannakis, K. Willoughby, L. Pierce, and T. Baker, Evaluation of Construction Practices That Influence the Bond Strength at the Interface between Pavement Layers, *Journal of Performance of Constructed Facilities*, vol. 22, no. 3, pp. 154-161, 2008.

[233] A. Mahmoud, E. Coleri, J. Batti, and D. Covey, Development of a field torque test to evaluate in-situ tack coat performance, *Construction and Building Materials*, vol. 135, pp. 377-385, 2017/03/15/ 2017.

[234] C. Raab and M. N. Partl, Interlayer bonding of binder, base and subbase layers of asphalt pavements: Long-term performance, *Construction and Building Materials*, vol. 23, no. 8, pp. 2926-2931, 2009/08/01/ 2009.

[235] C. Guo, F. Wang, and Y. Zhong, Assessing pavement interfacial bonding condition, *Construction and Building Materials*, vol. 124, pp. 85-94, 2016/10/15/ 2016.

[236] A. C. Collop, N. H. Thom, and C. Sangiorgi, Assessment of bond condition using the Leutner shear test, *Proceedings of the Institution of Civil Engineers - Transport*, vol. 156, no. 4, pp. 211-217, 2003.

[237] *Preparing and determining the density of hot-mix asphalt (HMA) specimens by means of the superpave gyratory compactor*, 2004.

[238] BSI, "BS EN 13036-1: 2010. Road and airfield surface characteristics. Test methods. Measurement of pavement surface macrotexture depth using a volumetric patch technique," ed: BSI London, UK, 2010.

[239] R. M. Recasens, F. P. Jiménez, J. B. González, and M. Partl, "Evaluation of the effect of tack coats. LCB shear test," in *Sixth International RILEM Symposium on Performance Testing and Evaluation of Bituminous Materials*, 2003, pp. 550-556: RILEM Publications SARL.